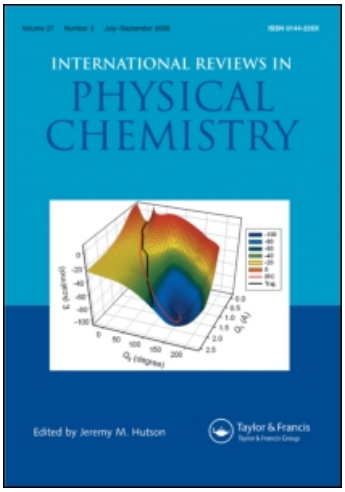

International Reviews in Physical Chemistry
Publication details, including instructions for authors and subscription information:
http://www.informaworld.com/smpp/title~content=t713724383

Quantitative insights about molecules exhibiting Jahn-Teller and related effects

Timothy A. Barckholtz

Online publication date: 26 November 2010

To cite this Article Barckholtz, Timothy A.(1998) 'Quantitative insights about molecules exhibiting Jahn-Teller and related effects', International Reviews in Physical Chemistry, 17: 4, 435 — 524
To link to this Article: DOI: 10.1080/014423598230036
URL: http://dx.doi.org/10.1080/014423598230036

INTERNATIONAL REVIEWS IN PHYSICAL CHEMISTRY, 1998, VOL. 17, NO. 4, 435–524

Quantitative insights about molecules exhibiting Jahn–Teller and related effects

by TIMOTHY A. BARCKHOLTZ and TERRY A. MILLER

Department of Chemistry, Ohio State University, 120 West 18th Avenue, Columbus, Ohio 43210–1173, USA

Open-shell states of molecules undergo a variety of phenomena different from closed-shell states. Two such effects, with which this paper is concerned, are Jahn–Teller coupling and spin–orbit coupling. We first develop a generalized Hamiltonian for the Jahn–Teller coupling of the electronic and vibrational motion and include the effects of spin–orbit coupling, we then consider the symmetry properties of the Hamiltonian in detail. The potential energy surfaces for various combinations of Jahn–Teller and spin–orbit coupling are also presented. The vibronic and spin–vibronic energy levels for a C_{3v} molecule are discussed in depth, with particular attention paid to the results of our rigorous numerical calculations of the eigenvalues and eigenfunctions. The results of these calculations are compared and contrasted with many assumptions about the energy levels that have been made in the past. While Jahn–Teller coupling has its largest effects on the vibronic energy levels, it also has non-negligible effects on the rotational energy levels. The rotational structure of Jahn–Teller states is developed, with special emphasis on the coupling of the vibronic, rotational and spin angular momenta. We discuss at length the relationship between Coriolis coupling and the spin–rotation interaction and show how these effects are related to the spin–vibronic Jahn–Teller and spin–orbit parameters of the state. Because most of the experimental investigations of Jahn–Teller states have been via electronic spectroscopy, we derive formulae for the intensities of these transitions in the presence of Jahn–Teller and spin–orbit coupling. The final portion of this article is a review of the application of the theory to the analysis of the spin–vibronic structure of the lowest excited states of several organometallic monomethyl radicals and the ground states of the methoxy family of radicals. These examples illustrate the diversity of signatures that Jahn–Teller active molecules display in their electronic spectra, and the different ways in which the Jahn–Teller and spin–orbit coupling can be elucidated from these signatures.

Contents

0144-235X/98 $12·00

1. Introduction

The original paper of Jahn and Teller [1] in 1936 that described the spontaneous symmetry breaking of molecules in degenerate electronic states is one of the most seminal in chemical physics. Indeed, about 50 years later, Bersuker [2] published a bibliography of papers on the Jahn–Teller effect with over 3200 references. Moreover, a number of excellent overviews of the subject have been published, both before and contemporaneous with the bibliography [3–9]. Why then is there a need today for yet another review on the subject?

The simplest answer to that question is that in the little more than 10 years since the publication of Bersuker's bibliography, very significant progress, both experimentally and computationally, has been made towards quantitatively understanding this effect in real molecules, isolated from environmental influences. Much of the earlier experimental work was performed on condensed-phase systems where inherent molecular distortions were very difficult to separate from environmentally induced distortions. Recently, the coupling of high-resolution laser spectroscopy with supersonic free jet cooling [10] has yielded, for the first time, detailed spectra revealing various characteristics attributable to, and quantifying, the Jahn–Teller effect in isolated molecules.

During that same period of time, computational capabilities have grown by orders of magnitude. As we shall see, these computational capabilities are often necessary to extract quantitative information from the spectra. Similarly, the growth in computational power has made possible meaningful *ab initio* calculations for the open-shell molecular systems where experimental observations of Jahn–Teller effects are possible.

The principal purpose of this review is to describe much of the combined theoretical and experimental progress of the last few years. Our aim is to describe the necessary theory underlying the spectral analyses and their interpretation in a manner easily applicable to the increasing number of experiments requiring such treatments. We shall illustrate our approach with several examples of Jahn–Teller active molecules observed recently in our laboratory. The examples focus on some simple, nominally C_{3v} molecules, the lowest order symmetry group for which orbitally degenerate states can occur and give rise to Jahn–Teller effects. These examples include the ^{2}E lowest excited electronic states of the metal methyl radicals MCH_3 (M = Mg, Ca, Zn or Cd), and the ^{2}E ground states of the methoxy family of radicals CH_3O, CH_3S, CF_3O and CF_3S. Numerous other Jahn–Teller active molecules have

also been studied as isolated species, a partial list of which includes C_5H_5 [11–15], $C_6H_6^+$ [16–20], the substituted benzene cations *sym*-$C_6H_3F_3^+$, $C_6F_6^+$, *sym*-$C_6H_3Cl_3^+$, *sym*-$C_6Cl_3F_3^+$ and *sym*-$C_6Br_3F_3^+$ [7], and the alkali and coinage metal trimers M_3 (M = Na [21], Cu [22], Ag [23] or Au [24]). However, we shall restrict our examples to the methoxy and metal methyl families because of the abundance of data for them and their similarities, and also because they are simple and light enough for meaningful *ab initio* calculations.

In analysing the Jahn–Teller induced effects in the spectra of these molecules, we have recognized that several 'complications' that in the past were typically treated as small perturbations or simply ignored often held the key to truly understanding these spectra. With the present state of computational techniques, many approximations are often no longer necessary and some quite interesting insights are now possible. The original Jahn–Teller paper considered only the linear Jahn–Teller effect and all early calculations focused on a single active mode. For a number of years now, it has been realized that multimode calculations are necessary [7, 25], but only recently have they become computationally routine. Similarly, quadratic and other higher order Jahn–Teller interactions have been theoretically recognized to be present but generally hoped to be negligibly small for the molecules studied. This assumption is no longer necessary.

Most importantly, the ramifications of simultaneous Jahn–Teller effects and spin–orbit coupling have largely been ignored, except for various perturbation approaches, some group-theoretical arguments, and in a few isolated papers [24, 26–30]. The orbital degeneracy requirement of the Jahn–Teller theorem necessitates non-zero electronic orbital angular momentum. It also requires an open-shell electronic configuration, which, while possibly giving rise to singlet electronic states, has resulted in non-zero electronic spin states in most of the Jahn–Teller active molecules so far observed in the gas phase. This combination of electronic orbital angular momentum and non-zero spin guarantees first-order spin–orbit coupling interactions in the molecules. Only in special cases is the spin–orbit coupling small enough to be neglected. Generally speaking, both spin–orbit coupling and multimode Jahn–Teller effects must be included to describe real molecules.

The remainder of this review is accordingly organized as follows. The existing Jahn–Teller theory is reviewed and comprehensively formulated in section 2 to include all the above-mentioned effects. Attention is given to symmetry properties and the concept of a potential energy surface (PES). In the following section, the results of accurate computations of the vibronic and spin–vibronic levels, including all these effects, are compared with various approximations that have frequently been adopted in the past. In section 4, the rotational structure of the vibronic Jahn–Teller states is presented. Thereafter, the selection rules and intensities for electronic transitions between a ^2E state and a $^2A_1$ or a $^2A_2$ state under C_{3v} symmetry are developed, which are appropriate for the methoxy family of radicals and the metal monomethyl radicals. The final section gives examples of the analysis of the electronic spectra of those Jahn–Teller active molecules. These examples illustrate several different ways in which information about the Jahn–Teller and spin–orbit coupling can be extracted from electronic spectra, as well as some of the pitfalls to beware.

This review article is intended, in part, as an experimentalist's handbook for the analysis of spectra of Jahn–Teller active molecules. Unfortunately, there has been a great proliferation in the variety of notations for the various quantities involved in Jahn–Teller and related interactions, leading to some confusion for both

experimentalists and theoreticians alike. For this reason, we include in appendix A a brief glossary of the symbols used in this paper.

2. The quantum mechanics of Jahn–Teller and spin–orbit coupling

In our initial development, we shall consider a general treatment of the theory, although we shall restrict ourselves to those point groups that have at most doubly degenerate irreducible representations. This approach, while excluding the cubic point groups, greatly simplifies the notation and resulting expressions. Should the need arise, extension to the cubic symmetries should be fairly straightforward. Later in our development, we shall provide specific expositions corresponding to the C_{3v} symmetry of the molecules that we discuss as examples.

Hopefully this account will be a comprehensive guide, particularly for the experimentalist, however, it is important to recognize that it is, for the most part, not original, although we believe in some parts to have made significant extensions or clarifications of existing theory. Our exposition is based upon the seminal works in the field, first by Longuet-Higgins and co-workers [31–33], and later by Brown [34], Hougen [35], and Watson [36], among others.

2.1. *The basis set*

Jahn–Teller coupling involves the interaction of the electronic motion in a degenerate electronic state with the nuclear motion of degenerate vibrational modes, while spin–orbit coupling is the interaction of the electron spin angular momentum with the electronic orbital angular momentum. The complete basis set is therefore the product of electronic, vibrational and electron spin basis functions:

$$|\text{spin–vibronic}\rangle = |\text{electronic}\rangle\,|\text{vibrational}\rangle\,|\text{electron spin}\rangle. \tag{1}$$

(In section 4 we shall consider the rotation of the molecule. In this review we shall not concern ourselves with nuclear spin.)

We take as the electronic portion of the basis set the two components of the electronic state, denoted

$$|\text{electronic}\rangle = |\Lambda\rangle. \tag{2}$$

The label Λ, which takes on the values $+1$ or -1, distinguishes between the two complex electronic functions that make up the basis. Even though for nonlinear molecules Λ is not an eigenfunction of L_z, as it is for linear molecules, we can still treat it as a good quantum number, as it distinguishes the angular momentum properties of the two components of the degenerate state [36, 37].

We can also distinguish the two electronic components by their symmetry properties with respect to the $\hat{C}_n$ operation:

$$\hat{C}_n\,|\Lambda\rangle = \exp\left(-\frac{2\pi_i}{n} s_e \Lambda\right)|\Lambda\rangle, \tag{3}$$

where s_e denotes which degenerate representation E_{s_e} of the point group the electronic wavefunction transforms as. For those point groups with $n \leqslant 4$, there is only one degenerate representation, denoted E, for which $s_e = 1$. While $|\Lambda\rangle$ may actually have a rather complicated angular dependence, involving a linear combination of functions of the form $\exp(ix\theta)$ with different values of x, each must obey equation (3) in order that the overall function $|\Lambda\rangle$ transforms according to the E_{s_e} representation.

To the electronic basis set we add a set of vibrational quantum numbers. The

complete vibrational basis set is a product of all $3N - 6$ vibrational modes, where N is the number of atoms in the molecule. However, we are interested only in those vibrational modes that exhibit Jahn–Teller activity and shall consider explicitly only these modes in the vibrational portion of the basis set. The vibrational basis set is then the product of p two-dimensional harmonic oscillator wavefunctions [37], each with the usual vibrational quantum numbers v_i and l_i, the principal vibrational quantum number and the vibrational angular momentum quantum number, respectively. The vibrational portion of the basis set is therefore

$$|\text{vibrational}\rangle = \prod_{i=1}^{p} |v_i, vl_i\rangle . \tag{4}$$

The vibrational basis functions $|v_i, l_i\rangle$ can be taken to be proportional to $\exp(+is_v l\phi)$ and transform as the symmetry species e_{s_v}. The transformation properties, with respect to the $\hat{C}_n$ operation, of the vibrational part of the basis set that is relevant to the Jahn–Teller problem is

$$\hat{C}_n \prod_{i=1}^{p} |v_i, l_i\rangle = \exp\left(\frac{2\pi i}{n} s_v l_t\right) \prod_{i=1}^{p} |v_i, l_i\rangle , \tag{5}$$

where $l_t = \sum_i l_i$. When more than one symmetry of vibrational mode is included, the quantity $s_v l_t$ should be replaced by a summation over the individual vibronic angular momenta contributions.†

The relative signs in the exponentials of equations (3) and (5) warrant additional comments. We assume the same phase convention for the electronic basis function as given above for the vibrational basis function. We have then chosen to follow the transformation conventions of Longuet-Higgins and co-workers [31–33]. They accomplished these conventions by defining opposite senses of the rotations for the electronic and vibrational phase angles, respectively θ and ϕ. We therefore define the $\hat{C}_n$ operation to have the following effects on θ and ϕ, that is $\theta \rightarrow \theta - 2\pi/n$ and $\phi \rightarrow \phi + 2\pi/n$. While this might seem to be a peculiar choice by today's standards, it is the predominant phase convention in the Jahn–Teller literature. In later sections, we shall draw special attention to those places where this phase convention may introduce confusion.

When spin–orbit coupling is included, the projection Σ of the electron spin S on the C_n axis is added to the basis set:

$$|\text{electron spin}\rangle = |S, \Sigma\rangle . \tag{6}$$

Because S is conserved for all the terms in the Hamiltonian that we shall consider, we do not explicitly include it in the basis set from here on. Under the $\hat{C}_n$ operation,

† For those point groups with C_4 axes, the Jahn–Teller active modes are non-degenerate and a slightly modified basis set is required [38–41]. In the C_{4v} case, as well as any case when one is considering the properties of the complete vibrational basis function, a more general transformation relation was given by Hougen [38], $\hat{C}_n |\text{vibrational}\rangle = \exp[+(2\pi i/n)G_s] |\text{vibrational}\rangle$, with the present phase convention. If modes of only symmetry e_{s_v} are considered, G_s reduces to $s_v l_t$, as in equation (5). As mentioned earlier, we do not explicitly consider the cubic point groups, for which degeneracies higher than two are possible.

the spin portion of the basis set transforms as

$$\hat{C}_n |\Sigma\rangle = \exp\left(-\frac{2\pi \mathrm{i}}{n}\Sigma\right)|\Sigma\rangle. \tag{7}$$

The final spin–vibronic basis set can therefore be written as

$$|\Lambda\rangle \prod_{i=1}^{p} |v_i, l_i\rangle |\Sigma\rangle, \tag{8}$$

with

$$\begin{aligned} \Lambda &= \pm 1, \\ v_i &= 0, 1, 2, \ldots, \\ l_i &= v_i, v_i - 2, v_i - 4, \ldots, -v_i + 2, -v_i, \\ \Sigma &= -S, -S + 1, \ldots, S - 1, S \end{aligned}$$

Under the harmonic oscillator approximation, each of the v_i can take any positive integer value, which makes the basis set infinitely large. Therefore, the basis set for each Jahn–Teller active mode must be truncated to a manageable level. In general, the larger the Jahn–Teller coupling constants are for each mode, the larger the basis set must be for that mode. In practice, a relatively small basis set is typically used to do some initial calculations. The basis set is then expanded until additional basis functions have a negligible effect on the eigenvalues. We have not included the totally symmetric modes, or any other vibrational modes that are not Jahn–Teller active, in the basis set because they are not coupled into the calculation of the Jahn–Teller vibronic energy levels using the approximate Hamiltonian developed in the next section. In section 2.3, we shall place further restrictions on which vibrational modes are explicitly included in the basis set, depending upon the electronic state's symmetry.

2.2. *The Hamiltonian*

The general Hamiltonian for any polyatomic system is

$$\hat{\mathscr{H}} = \hat{\mathscr{H}}_{\mathrm{T}} + \hat{\mathrm{V}} + \hat{\mathscr{H}}_{\mathrm{SO}} + \hat{\mathscr{H}}_{\mathrm{rot}}, \tag{9}$$

where $\hat{\mathscr{H}}_{\mathrm{T}}$ is the kinetic energy of the nuclei, $\hat{\mathrm{V}}$ is the electrostatic potential involving the nuclei and electrons, $\hat{\mathscr{H}}_{\mathrm{SO}}$ is the spin–orbit coupling operator and $\hat{\mathscr{H}}_{\mathrm{rot}}$ is the Hamiltonian for the rotation of the molecule, which we shall return to in section 4.

The potential $\hat{\mathrm{V}}$ can be expressed as a Taylor series expansion about the symmetric point in increasing powers of the vibrational normal coordinates,

$$\hat{\mathrm{V}} = \sum_{k=0} \frac{1}{k!} \sum_{i=1}^{3N-6} \left(\frac{\partial^k \hat{\mathrm{V}}}{(\partial Q_i)^k}\right)_0 Q_i^k, \tag{10}$$

where the summation over k runs to infinity and the summation over i runs over the $3N - 6$ normal modes. The normal coordinates of the p Jahn–Teller active vibrational modes $Q_{i,\pm}$ are the complex combinations of the Cartesian coordinates $(Q_{i,1}, Q_{i,2})$ for each mode i:

$$Q_{i,\pm} = Q_{i,1} \pm \mathrm{i} Q_{i,2}. \tag{11}$$

where $\mathrm{i} = (-1)^{1/2}$. Expression of the normal coordinates can be made in terms of

Table 1. Terms in the vibronic potential of equation (13).

Term	Description	Form
$\hat{\mathscr{H}}_{\mathrm{e}}^{0}$	Electronic potential at the symmetric configuration	Coulomb, exchange,...
$\hat{\mathscr{H}}_{\mathrm{h,a}}$	Harmonic oscillator for the modes that are not Jahn–Teller active	$\sum_{i=1}^{3N-6-2p} \frac{1}{2}\lambda_i \lvert Q_i \rvert^2$
$\hat{\mathscr{H}}_{\mathrm{h,e}}$	Harmonic oscillator for the p Jahn–Teller active modes	$\sum_{i=1}^{p} \sum_{r=+,-} \frac{1}{2}\lambda_i \lvert Q_{i,r} \rvert^2$
$\hat{\mathscr{H}}_{1}$	Linear Jahn–Teller coupling	$\sum_{i=1}^{p} \sum_{r=+,-} k_i Q_{i,r}$
$\hat{\mathscr{H}}_{q_{ii}}$	Quadratic Jahn–Teller coupling within a single mode	$\sum_{i=1}^{p} \sum_{r=+,-} \frac{1}{2} g_{ii} \left(Q_{i,r}\right)^2$
$\hat{\mathscr{H}}_{q_{ij}}$	Quadratic Jahn–Teller coupling between two modes	$\sum_{i=1}^{p} \sum_{r=+,-} \sum_{j>i} \frac{1}{2} g_{ij} Q_{i,r} Q_{j,r}$

cylindrical coordinates,

$$Q_{i,\pm} = \rho_i \exp(\pm \mathrm{i}\phi_i), \tag{12}$$

which will be useful later in the visualization of the PESs.

The Taylor expansion of $\hat{\mathrm{V}}$ is normally truncated at the quadratic terms and can be rewritten as

$$\hat{\mathrm{V}} = \hat{\mathscr{H}}_{\mathrm{e}}^{0} + \hat{\mathscr{H}}_{\mathrm{h,a}} + \hat{\mathscr{H}}_{\mathrm{h,e}} + \hat{\mathscr{H}}_{1} + \hat{\mathscr{H}}_{q_{ii}} + \hat{\mathscr{H}}_{q_{ij}}, \tag{13}$$

where the explicit form for each term is given in table 1. The first term, $\hat{\mathscr{H}}_{\mathrm{e}}^{0}$, is the electronic potential at the symmetric configuration. The second term, $\hat{\mathscr{H}}_{\mathrm{h,a}}$, is the harmonic oscillator potential for the modes that are not Jahn–Teller active and need not be considered further. The last four terms describe the potential for the p Jahn–Teller active modes. The first of these four terms, $\hat{\mathscr{H}}_{\mathrm{h,e}}$, is the harmonic oscillator potential for each Jahn–Teller vibrational mode, the second, $\hat{\mathscr{H}}_{1}$, is the linear Jahn–Teller coupling potential, the third, $\hat{\mathscr{H}}_{q_{ii}}$, is the quadratic Jahn–Teller interaction within a single vibrational mode, and the last term, $\hat{\mathscr{H}}_{q_{ij}}$, is the quadratic Jahn–Teller effect between two different Jahn–Teller active modes. The last three terms of equation (13) are zero for a non-degenerate state but can be non-zero for an orbitally degenerate state. All of the terms in equation (13) except the second (noted above) and the last will be discussed in detail in this paper. To date, little work has been done involving $\hat{\mathscr{H}}_{q_{ij}}$. We shall also neglect it because, to the best of our knowledge, no spectroscopic analysis thus far has necessitated its inclusion in the Hamiltonian. That is not to say, however, that the vibrational modes of the molecule are not mixed via Jahn–Teller coupling, we shall return to this point in section 3.2.4. A 'bilinear coupling' term has also been described that mixes the totally symmetric modes with the Jahn–Teller active modes [42–44]. While such a term is certainly possible in $\hat{\mathrm{V}}$, we shall not consider it in detail as it has never been invoked in the analysis of experimental spectra and probably would be significant only with respect to combination levels involving both Jahn–Teller active and inactive modes.

The parameters λ_i, k_i, and g_{ij} of table 1 are defined as

$$\lambda_i = \langle \Lambda | \left(\frac{\partial^2 \hat{V}}{\partial Q_{i,+} \partial Q_{i,-}} \right)_0 | \Lambda \rangle, \tag{14}$$

$$k_i = \langle \Lambda | \left(\frac{\partial \hat{V}}{\partial Q_{i,\pm}} \right)_0 | -\Lambda \rangle, \tag{15}$$

$$g_{ij} = \langle \Lambda | \left(\frac{\partial^2 \hat{V}}{\partial Q_{i,\pm} \partial Q_{j,\pm}} \right)_0 | -\Lambda \rangle, \tag{16}$$

where the subscript 0 indicates that the evaluation is to be performed at the symmetric or 'equilibrium' configuration. The parameter λ_i is the curvature of the PES at the symmetric point with respect to the ith vibrational mode. The corresponding vibrational frequency is given by

$$\omega_{e,i} = \frac{1}{2\pi c} \left(\frac{\lambda_i}{M_i} \right)^{1/2}, \tag{17}$$

where M_i is the reduced mass of the vibrational mode.

The driving force behind Jahn–Teller coupling is the spontaneous distortion of the molecule to lower its energy, which arises through the last three terms of equation (13) and the parameters defined by equations (15) and (16). These parameters, k_i and g_{ii}, are non-zero only between the two different components of the degenerate electronic wavefunction $|\Lambda\rangle$. Because they involve the nuclear coordinates $Q_{i,\pm}$, the terms $\hat{\mathscr{H}}_1$ and $\hat{\mathscr{H}}_{q_{ii}}$ in the Hamiltonian are what give rise to the coupling of the electronic and vibrational degrees of freedom. In a non-degenerate electronic state, k_i and g_{ii} are zero by symmetry. In a degenerate state, the Jahn–Teller theorem shows that the gradient at the symmetric point is non-zero, the potential energy surface has a cusp at the symmetric point, and the PES has its minimum at an asymmetric configuration of the nuclei. We shall consider visualizations of the potential energy surface after we consider the symmetry properties of the basis set with which we shall approach the Hamiltonian.

The third term of the Hamiltonian (9) is the spin–orbit coupling operator, $\hat{\mathscr{H}}_{SO}$, which can be written as

$$\hat{\mathscr{H}}_{SO} = a \hat{\mathbf{L}} \cdot \hat{\mathbf{S}} = a \hat{L}_z \hat{S}_z. \tag{18}$$

As Hougen [35] pointed out, for molecules with an n-fold ($n > 3$) symmetry axis (z), first-order contributions from the term $a(\hat{L}_x \hat{S}_x + \hat{L}_y \hat{S}_y)$ will vanish because of symmetry [45], thereby yielding the second equality of equation (18), though second-order terms are potentially significant for the spin–rotation interactions of the state [35, 46, 47]. Furthermore, rather than use the exact form of the spin–orbit operator, we have chosen the traditional form for it of $a\hat{L} \cdot \hat{S}$, which suffices so long as spin–orbit coupling between states of different L and S is unimportant, as is the case with Russell–Saunders coupling in atoms [48–50].

2.3. *Symmetry properties of the Hamiltonian and the basis set*

2.3.1. *Symmetry of Jahn–Teller active modes*

Up to this point no restrictions have been placed on the symmetry of the vibrational modes that are Jahn–Teller active, other than the obvious restriction that they not be totally symmetric. The symmetries of the Jahn–Teller active modes

can be derived by examining the transformation properties under the $\hat{C}_n$ rotation of the terms in the Taylor series expansion of the potential, equation (10). Our approach is modelled after derivations by Brown [34] and Hougen [51], but is more general.

If the electronic coordinates are written in cylindrical coordinates, the angular portion of the kth derivative $\partial^k \hat{\mathrm{V}} / \left(\partial Q_\pm\right)^k$, transforms under rotations as

$$\exp\left(\mathrm{i}p\theta\right), \tag{19}$$

where θ is the electronic angular coordinate. The restrictions on p can be determined from the symmetry properties of the matrix element,

$$\hat{C}_n \left\langle \Lambda \right| \exp\left(\mathrm{i}p\theta\right) \left| \Lambda' \right\rangle = \exp\left(-\frac{2\pi\mathrm{i}}{n}(s_\mathrm{e}\,\Delta\Lambda + p)\right) \left\langle \Lambda \right| \exp\left(\mathrm{i}p\theta\right) \left| \Lambda' \right\rangle, \tag{20}$$

with

$$\Delta\Lambda = \Lambda' - \Lambda \tag{21}$$

where Λ and Λ' are components of the same degenerate electronic state. For the matrix element not to vanish, the only possible values for $\Delta\Lambda$ are 0 and ± 2, so p must be either 0 or $\mp 2s_\mathrm{e}$. Those operators that transform as $\exp\left(0\theta\right)$ are the harmonic oscillator and symmetric anharmonicity terms, while those that are of the form $\exp\left(\pm 2\mathrm{i}s_\mathrm{e}\theta\right)$ correspond to the Jahn–Teller operators. Higher-order values of $p = \pm 2s_\mathrm{e} + mn$ (m is an integer) are possible but still transform the same, and consideration of them is therefore redundant.

The vibrational coordinate operator $Q_\pm^k$ transforms as the kth symmetric direct product of Γ_Q. In cylindrical coordinates ρ and ϕ, we need only consider the function that transforms as

$$\rho^k \exp\left(\pm \mathrm{i}ks_\mathrm{v}\phi\right). \tag{22}$$

The kth-order symmetric product of Γ_Q also contains functions of the form $\exp\left(\pm \mathrm{i}x\phi\right)$ where $|x| < |ks_\mathrm{v}|$. However these functions can be viewed as just higher-order corrections to terms resulting from lower-order Jahn–Teller terms, $Q_\pm^x$, somewhat analogous to anharmonicity corrections to harmonic frequencies, and therefore do not merit special attention. The most general form of the kth-order Jahn–Teller coupling Hamiltonian therefore transforms as the sum of the possible combinations of these functions:

$$\begin{aligned}\hat{\mathscr{H}}_{\mathrm{JT}}^{(k)} = {} & \exp\left(+2\mathrm{i}s_\mathrm{e}\theta\right)\left[\rho^k \exp\left(+\mathrm{i}ks_\mathrm{v}\phi\right) + \rho^k \exp\left(-\mathrm{i}ks_\mathrm{v}\phi\right)\right] \\ & + \exp\left(-2\mathrm{i}s_\mathrm{e}\theta\right)\left[\rho^k \exp\left(+\mathrm{i}ks_\mathrm{v}\phi\right) + \rho^k \exp\left(-\mathrm{i}ks_\mathrm{v}\phi\right)\right].\end{aligned} \tag{23}$$

However, only the terms of equation (23) that are totally symmetric for the molecular symmetry point group will be non-zero.

Operating on the first terms of equation (23) with the $\hat{C}_n$ rotation yields

$$\begin{aligned}\hat{C}_n \exp\left(+2\mathrm{i}s_\mathrm{e}\theta\right)\rho^k \exp\left(+\mathrm{i}ks_\mathrm{v}\phi\right) = {} & \exp\left[-\frac{2\pi\mathrm{i}}{n}(2s_\mathrm{e} - ks_\mathrm{v})\right] \\ & \times \exp\left(+2\mathrm{i}s_\mathrm{e}\theta\right)\rho^k \exp\left(+\mathrm{i}ks_\mathrm{v}\phi\right)\end{aligned} \tag{24}$$

and

$$\begin{aligned}\hat{C}_n \exp\left(+2\mathrm{i}s_\mathrm{e}\theta\right)\rho^k \exp\left(-\mathrm{i}ks_\mathrm{v}\phi\right) = {} & \exp\left[-\frac{2\pi\mathrm{i}}{n}(2s_\mathrm{e} + ks_\mathrm{v})\right] \\ & \times \exp\left(+2\mathrm{i}s_\mathrm{e}\theta\right)\rho^k \exp\left(-\mathrm{i}ks_\mathrm{v}\phi\right)\end{aligned} \tag{25}$$

Table 2. Allowed values of s_e, s_v and s_k for $n \leqslant 6$ and $k = 1$ or 2: N/A, not applicable.

n	k	s_e	s_v	s_k	$j^{(k)}$
3	1	1	1	0	$l + \frac{1}{2}\Lambda$
	2	1	1	1	$\frac{1}{2}l - \frac{1}{2}\Lambda$
4	1	1	2	0 or 1	N/A
	2	1	1	0 or 1	N/A
5	1	1	2	1	$l - \frac{1}{2}\Lambda$
		2	1	0	$l + \frac{1}{2}\Lambda$
	2	1	1	1	$\frac{1}{2}l - \frac{1}{2}\Lambda$
		2	2	1	$\frac{1}{2}l - \frac{1}{2}\Lambda$
6	1	1	2	1	$l - \frac{1}{2}\Lambda$
		2	2	0	$l + \frac{1}{2}\Lambda$
	2	1	1	1	$\frac{1}{2}l - \frac{1}{2}\Lambda$
		1	2	0	$\frac{1}{2}l + \frac{1}{2}\Lambda$
		2	1	0	$\frac{1}{2}l + \frac{1}{2}\Lambda$
		2	2	1	$\frac{1}{2}l - \frac{1}{2}\Lambda$

(A similar pair of equations will be obtained for the last two terms of equation (23).) For one of these two terms of $\hat{\mathscr{H}}_{\mathrm{JT}}^{(k)}$ to be totally symmetric, the quantity $(2s_e \pm ks_v)$ must be an integer multiple of n:

$$[2s_e + (-1)^{s_k} k s_v] \bmod n = 0, \tag{26}$$

where s_k is either 0 or 1. For a given vibrational mode e_{s_v} and a given electronic state of symmetry E_{s_e}, a value for s_k of either 0 or 1 can be chosen to satisfy equation (26). For a given combination of s_e and s_v, only *one* of the first two terms of equation (23) and only *one* of the last two terms of equation (23) will survive, reducing it to

$$\hat{\mathscr{H}}_{\mathrm{JT}}^{(k)} = \exp(+2\mathrm{i}s_e\theta)\rho^k \exp[-(-1)^{s_k}\mathrm{i}ks_v\phi] + \exp(-2\mathrm{i}s_e\theta)\rho^k \exp[+(-1)^{s_k}\mathrm{i}ks_v\phi]. \tag{27}$$

For $k \geqslant 2$, there may be more than one symmetry s_v of vibrational mode for which equation (26) may be satisfied, they will not necessarily have the same form for the kth-order Jahn–Teller Hamiltonian. In table 2 we have listed the allowable values of s_k for all the combinations of s_e and s_v for the C_n point groups ($n \leqslant 6$) and hence determined which terms of the Jahn–Teller Hamiltonian need to be considered further. (The point groups with C_4 axes require special treatment. In these point groups, the symmetry species that transforms as $s_v = 2$ is not e_2, which does not exist for these point groups, but separates into b_1 and b_2.) Table 2 gives the only allowable combinations of s_e, s_v and s_k for non-vanishing terms in the Hamiltonian. For a state of a given electronic symmetry E_{s_e} only certain vibrational modes of symmetry e_{s_v} give rise to Jahn–Teller effects of order k. For example, in point groups with a C_5 axis, an E_2 electronic state can only have a linear Jahn–Teller effect for an e_1 vibrational mode, whereas only e_2 vibrational modes give rise to quadratic Jahn–Teller coupling.

In a recent paper [19] studying the Jahn–Teller (and pseudo-Jahn–Teller) effect in the excited $\tilde{B}\,^2E_{2g}$ state of benzene, it was suggested that the linear Jahn–Teller effect should be quite small. It was argued that, as the aromatic system is enlarged and approaches the circular limit, linear Jahn–Teller coupling should vanish altogether.

However, we note that table 2, and previous group-theoretical approaches, clearly predict a non-vanishing linear Jahn–Teller interaction for E_{2g} electronic states of D_{6h} symmetry. We agree with Goode *et al.* [19] that, as a molecular system approaches circular symmetry, the linear Jahn–Teller effect vanishes, as is well known for linear molecules. Our present approach shows that in D_{6h} symmetry the electronic part of the Jahn–Teller operator is of the form $\exp(\pm 2is_e\theta)$, which for the E_{2g} state corresponds to $\exp(\pm 4i\theta)$. This operator is formally of higher order than the operator responsible for linear Jahn–Teller coupling in the C_{3v} point group, which is $\exp(\pm 2i\theta)$. Whether the higher-order dependence on θ leads to a much smaller linear Jahn–Teller interaction is a question that only experiment or perhaps detailed numerical calculations can answer.

In addition to the restrictions based on the symmetry properties about a rotational axis of the molecule, restrictions can also be placed on the vibrational modes' symmetry with respect to a centre of inversion and mirror planes. In practice these additional operations determine whether the active modes are *g* or *u*, with respect to the centre of inversion, or symmetric ($'$) or antisymmetric ($''$), with respect to mirror planes. Since the linear Jahn–Teller term must be symmetric with respect to these operations, the linear Jahn–Teller active modes are restricted to *g* and symmetric ($'$) modes. These restrictions are lifted for the quadratic modes. Table 3, which includes the cubic point groups T_d and O_h and the linear point groups $C_{\infty v}$ and $D_{\infty h}$, is derived from these principles and is similar to a less comprehensive table produced by Herzberg [37]. It contains a list of the symmetries of vibrational modes that are active for linear and quadratic coupling for most of the common point groups. For a given electronic state of the non-cubic point groups, only one symmetry of vibrational mode will be active under linear Jahn–Teller coupling while more than one type may be active via quadratic Jahn–Teller coupling.

A seemingly peculiar result is contained within table 3. As the table shows, a vibrational mode may have a non-zero linear Jahn–Teller coupling constant, but *by symmetry* must have zero quadratic Jahn–Teller coupling. The reverse may also hold true. This point was demonstrated earlier by Hougen [38] for molecules of D_{4h} symmetry and by Scharf and co-workers [52, 53] for molecules of D_{6h} symmetry. Another good example of this situation is the $X\ ^2E_1''$ state of the cyclopentadienyl radical, C_5H_5 (D_{5h}), in which the e_2' vibrational modes are active under linear Jahn–Teller coupling but are not active under quadratic coupling [11, 15]. Conversely, the e_1' and e_1'' modes may show quadratic Jahn–Teller activity, but no linear Jahn–Teller coupling. While it might seem odd that a molecule would exhibit linear Jahn–Teller coupling only in one vibrational mode and quadratic Jahn–Teller coupling only in a different vibrational mode, there is no *a priori* reason that this should not be the case.

Table 3 also contains entries for the linear point groups. For all degenerate states of the linear point groups $C_{\infty v}$ and $D_{\infty h}$, no linear Jahn–Teller coupling is possible. However, 'quadratic Jahn–Teller' coupling is possible for Π states, but not for any others. Quadratic Jahn–Teller coupling in Π states of linear molecules is normally referred to as Renner–Teller coupling [54–56]. Renner–Teller coupling for linear molecules and quadratic Jahn–Teller coupling for nonlinear molecules are identical, except that the higher symmetry of the linear molecules preserves more good quantum numbers and hence creates more symmetry blocking in the Hamiltonian matrix. In Δ states of linear molecules, a distortion occurs only upon going to quartic Jahn–Teller coupling, hence, the Renner–Teller effect in Δ states is not directly analogous to quadratic coupling in nonlinear molecules [56, 57].

Table 3. Symmetry species of normal modes that may produce linear and quadratic Jahn–Teller distortions for a degenerate electronic state.

Point group	Electronic state	Symmetry of linear Jahn–Teller modes	Symmetry of quadratic Jahn–Teller modes
$D_{3h}, (C_{3v}, D_3, C_{3h}, C_3)^a$	E'	e'	e', e''
	E''	e'	e', e''
$D_{4h}, (C_{4v}, D_4, D_{2d}, C_{4h}, C_4, S_4)^b$	E_g	b_{1g}, b_{2g}	e_g, e_u
	E_u	b_{1g}, b_{2g}	e_g, e_u
D_{4d}	E_1	e_2	e_1, e_3
	E_2	b_1, b_2	e_2
	E_3	e_2	e_1, e_3
$D_{5h}, (C_{5v}, D_5, C_{5h}, C_5)^c$	E_1'	e_2'	e_1', e_1''
	E_1''	e_2'	e_1', e_1''
	E_2''	e_1'	e_2', e_2''
	E_2'	e_1'	e_2', e_2''
	E_2	e_1	e_2, e_2
C_{6v}, C_6	E_1	e_2	e_1, e_2
	E_2	e_2	e_1, e_2
$D_{6h}, C_{6h}, (D_6, D_{3d}, S_6)^d$	E_{1g}	e_{2g}	$e_{1g}, e_{2g}, e_{1u}, e_{2u}$
	E_{1u}	e_{2g}	$e_{1g}, e_{2g}, e_{1u}, e_{2u}$
	E_{2g}	e_{2g}	$e_{1g}, e_{2g}, e_{1u}, e_{2u}$
	E_{2u}	e_{2g}	$e_{1g}, e_{2g}, e_{1u}, e_{2u}$
T_d	E	e	e, t_1, t_2
	T_1,T_2	e, t_2	e, t_1, t_2
O_h	E_g	e_g	$e_{1g}, e_{2g}, e_{1u}, e_{2u}$
	E_u	e_g	$e_{1g}, e_{2g}, e_{1u}, e_{2u}$
	T_{1g}	e_g, t_{2g}	$e_{1g}, e_{2g}, e_{1u}, e_{2u}$
	T_{1u}	e_g, t_{2g}	$e_{1g}, e_{2g}, e_{1u}, e_{2u}$
	T_{2g}	e_g, t_{2g}	$e_{1g}, e_{2g}, e_{1u}, e_{2u}$
	T_{2u}	e_g, t_{2g}	$e_{1g}, e_{2g}, e_{1u}, e_{2u}$
$D_{\infty h}(C_{\infty v})^e$	Π_g	none	π_g, π_u
	Π_u	none	π_g, π_u
	$\Delta_g, \Phi_g, \ldots$	none	none
	$\Delta_u, \Phi_u, \ldots$	none	none

[a] For C_{3v}, D_3 and C_3, $'$ and $''$ should be omitted.
[b] For C_{4v}, D_4, D_{2d}, the subscripts g and u should be omitted, for C_{4h} the subscripts 1 and 2 should be omitted, and for C_4 and S_4 all subscripts should be omitted.
[c] For C_{5v}, D_5, and C_5, $'$ and $''$ should be omitted.
[d] For D_6 the subscripts g and u should be omitted. For D_{3d} the subscripts 1 and 2 should be omitted.
[e] For $C_{\infty v}$, the subscripts g and u should be omitted.

Before concluding this section it is useful to mention 'pseudo-Jahn–Teller' coupling which is, as the name implies, closely related to Jahn–Teller coupling. Unfortunately, 'pseudo-Jahn–Teller coupling' has often been referred to as 'second-order Jahn–Teller coupling'. In our usage, 'second-order Jahn–Teller coupling' and 'quadratic Jahn–Teller coupling' are synonymous and refer to Jahn–Teller coupling in a degenerate electronic state with an interaction term involving the square of the vibrational normal mode, whereas 'pseudo-Jahn–Teller coupling' is the coupling of two different electronic states via a vibrational coordinate to the first power. However, it is important to remember these two mechanisms result in the same *effective* Hamiltonian within a degenerate electronic state and hence are not usually experi-

mentally distinguishable. The pseudo-Jahn–Teller effect occurs when one electronic state is mixed with another electronic state not degenerate with the first via vibronic coupling. However, the Hamiltonian operator responsible for this 'non-adiabatic' interaction is identical with that for linear Jahn–Teller coupling, equation (27) with $k = 1$. Pseudo-Jahn–Teller coupling is obviously strongest between states close in energy. We shall not discuss pseudo-Jahn–Teller coupling any further in this review.

2.3.2. *Jahn–Teller quantum numbers*

The kth-order Jahn–Teller Hamiltonian, equation (27), is not diagonal in either Λ or l_i, but will be diagonal in some linear combination of them. We shall restrict our analysis to only the first term of equation (27), equivalent results can be obtained with the second term. The kth-order Jahn–Teller Hamiltonian operator will have matrix elements in the basis set of equation (8), excluding spin, that will transform under the $\hat{C}_n$ rotation as

$$\hat{C}_n \prod_{i=1}^{p} \langle v_i, l_i| \langle \Lambda| \exp(+2\mathrm{i}s_\mathrm{e}\theta)\rho^k \exp[-(-1)^{s_k}\mathrm{i}ks_\mathrm{v}\phi]\,|\Lambda'\rangle \prod_{i=1}^{p} |v_i', l_i'\rangle$$
$$= \hat{C}_n \langle \Lambda| \exp(+2\mathrm{i}s_e\theta)\,|\Lambda'\rangle \left(\prod_{i=1}^{p} \langle v_i, l_i|\rho^k \exp[-(-1)^{s_k}\mathrm{i}ks_v\phi] \prod_{i=1}^{p} |v_i', l_i'\rangle \right). \quad (28)$$

We have already shown in equation (20) that the matrix element $\langle \Lambda| \exp(+2\mathrm{i}s_\mathrm{e}\theta)\,|\Lambda'\rangle$ will have a selection rule on Λ of $\Delta\Lambda = -2$. The selection rule on l_t can be obtained by continuing with the second half of equation (28):

$$\hat{C}_n \prod_{i=1}^{p} \langle v_i, l_i|\rho^k \exp[-(-1)^{s_k}\mathrm{i}ks_\mathrm{v}\phi] \prod_{i=1}^{p} |v_i', l_i'\rangle = \exp\left(-\frac{2\pi\mathrm{i}}{n}[(-1)^{s_k}s_\mathrm{v}k - s_\mathrm{v}\Delta l_t]\right)$$
$$= \exp\left(-\frac{2\pi\mathrm{i}}{n}s_\mathrm{v}[(-1)^{s_k}k - \Delta l_\mathrm{t}]\right), \quad (29)$$

where $\Delta l_\mathrm{t} = \sum_i (l_i' - l_i)$. From equations (20) and (29) we have the following selection rules on Λ and l_t for the first term of $\hat{\mathscr{H}}_\mathrm{JT}^{(k)}$,

$$\Delta\Lambda = -2 \quad (30)$$
$$\Delta l_\mathrm{t} = (-1)^{s_k}k. \quad (31)$$

This pair of selection rules can be combined to give

$$\frac{1}{k}\Delta l_t + \tfrac{1}{2}(-1)^{s_k}\Delta\Lambda = 0. \quad (32)$$

A new quantum number can therefore be defined as

$$j^{(k)} = \frac{1}{k}l_\mathrm{t} + \tfrac{1}{2}(-1)^{s_k}\Lambda. \quad (33)$$

for which $\hat{\mathscr{H}}_\mathrm{JT}^{(k)}$ is diagonal. The specific relationships between $j^{(k)}$, l_t, and Λ are given in table 2 for the common point groups.

The definition of $j^{(k)}$ is one instance where the phase convention of equations (3) and (5) has an impact. If the alternative phase convention is chosen, the sign in front of s_v in equation (29) will be positive, rather than negative, which will lead to $j^{(k)}$ being defined as $j^{(k)} = (1/k)l_\mathrm{t} - \frac{1}{2}(-1)^{s_k}\Lambda$. Using the current phase convention,

one can see from table 2 that for point groups with a C_3 axis, $j^{(1)} = l_t + \frac{1}{2}\Lambda$, in agreement with the traditional definition.

It is often very useful to have an expression for $\Delta j^{(k)}$ in terms of $j^{(k-1)}$, for example to simplify the matrix elements of the quadratic Jahn–Teller operator in terms of the linear Jahn–Teller quantum number. From equation (33) we have the following two relationships:

$$\Delta j^{(k)} = \frac{1}{k}\Delta l_t + \tfrac{1}{2}(-1)^{s_k}\Delta\Lambda, \tag{34}$$

$$\Delta j^{(k-1)} = \frac{1}{k-1}\Delta l_t + \tfrac{1}{2}(-1)^{s_{k-1}}\Delta\Lambda, \tag{35}$$

whose difference is

$$\Delta j^{(k)} - \Delta j^{(k-1)} = \left(\frac{1}{k} - \frac{1}{k-1}\right)\Delta l_t + \tfrac{1}{2}\Delta\Lambda[(-1)^{s_k} - (-1)^{s_{k-1}}]. \tag{36}$$

From equations (30) and (31), equation (36) becomes

$$\Delta j^{(k)} - \Delta j^{(k-1)} = -\left(\frac{1}{k} - \frac{1}{k-1}\right)(-1)^{s_k}k + [(-1)^{s_k} - (-1)^{s_{k-1}}]. \tag{37}$$

Rearranging this equation leads to a selection rule on $j^{(k)}$ in terms of $j^{(k-1)}$ for the first term of $\hat{\mathscr{H}}_{JT}^{(k)}$:

$$\Delta j^{(k)} = \Delta j^{(k-1)} + \left((-1)^{s_k}\frac{k}{k-1} - (-1)^{s_{k-1}}\right). \tag{38}$$

The second term of $\hat{\mathscr{H}}_{JT}^{(k)}$ will lead to a selection rule identical with this, but with a minus sign in front of the quantity on the right. For $j^{(k)}$ to be a good quantum number, it must be conserved with $\Delta j^{(k)} = 0$. Therefore, the generalized selection rule on $j^{(k)}$ in terms of $j^{(k-1)}$ is

$$\Delta j^{(k)} = \Delta j^{(k-1)} \pm \left((-1)^{s_k}\frac{k}{k-1} - (-1)^{s_{k-1}}\right) = 0. \tag{39}$$

All the values of k, s_k and s_{k-1} are determined by the symmetry of the electronic state and the symmetry of the Jahn–Teller active vibrational mode and are contained in table 2 for $k \leqslant 2$. Consulting table 2, we note that for a given value of s_e, if a mode (with a given value of s_v) is active in the linear and quadratic Jahn–Teller effect, $s_{k=1}$ and $s_{k=2}$ are never both odd or both even, leading to the general relationship

$$\Delta j^{(2)} = \Delta j^{(1)} \pm 3 = 0, \tag{40}$$

which is the familiar identity quoted for C_{3v} molecules.

2.3.3. *Symmetry of the vibronic basis functions*

In the next section, we deal with the symmetry of the spin–vibronic basis functions, but under more restrictive conditions. In this section, we consider the symmetry of the vibronic basis function $|\Lambda\rangle\prod_{i=1}^{p}|v_i, l_i\rangle$ and its relationship to $j^{(1)}$. Because in all our examples the linear ($k = 1$) Jahn–Teller term is by far the most important, the behaviour of the basis functions with respect to $j^{(1)}$ is of unique importance.

The $\hat{C}_n$ rotation operating on the basis function gives

$$\hat{C}_n |\Lambda\rangle \prod_{i=1}^{p} |v_i, l_i\rangle = \exp\left(-\frac{2\pi i}{n}(s_e\Lambda - s_v l_t)\right) |\Lambda\rangle \prod_{i=1}^{p} |v_i, l_i\rangle. \tag{41}$$

Because $l_t = j^{(1)} - \frac{1}{2}(-1)^{s_1}\Lambda$ (equation (33)), equation (41) is equivalent to

$$\begin{aligned}
\hat{C}_n |\Lambda\rangle \prod_{i=1}^{p} |v_i, l_i\rangle &= \exp\left(-\frac{2\pi i}{n}\left[s_e\Lambda - s_v\left[j^{(1)} - \tfrac{1}{2}(-1)^{s_1}\Lambda\right]\right]\right) |\Lambda\rangle \prod_{i=1}^{p} |v_i, l_i\rangle \\
&= \exp\left(-\frac{2\pi i}{n}\left[\tfrac{1}{2}\Lambda[2s_e + s_v(-1)^{s_1}] - s_v j^{(1)}\right]\right) |\Lambda\rangle \prod_{i=1}^{p} |v_i, l_i\rangle \\
&= \exp\left(-\frac{\pi i}{n}\Lambda mn\right) \exp\left(+\frac{2\pi i}{n} s_v j^{(1)}\right) |\Lambda\rangle \prod_{i=1}^{p} |v_i, l_i\rangle \\
&= -\exp\left(+\frac{2\pi i}{n} s_v j^{(1)}\right) |\Lambda\rangle \prod_{i=1}^{p} |v_i, l_i\rangle.
\end{aligned} \tag{42}$$

Therefore, those levels with $j^{(1)} = n/2 + mn$ (m is an integer) will transform into themselves under the $\hat{C}_n$ rotation and will therefore transform as a non-degenerate representation. Those basis functions with $j^{(1)} \neq n/2 + mn$ transform as a degenerate representation.

One might think that, because $j^{(1)}$ is a half-integer quantum number, a double group should be required to describe the symmetry properties of the basis functions. To see why this is not the case, the $\hat{C}_n^n$ rotation on the basis function gives

$$\hat{C}_n^n |\Lambda\rangle \prod_{i=1}^{p} |v_i, l_i\rangle = \exp[-2\pi i(s_e\Lambda - s_v l_t)] |\Lambda\rangle \prod_{i=1}^{p} |v_i, l_i\rangle. \tag{43}$$

Because s_e, Λ, s_v, and l_t are all integers, $\exp[-2\pi i(s_e\Lambda - s_v l_t)]$ will be unity. Therefore, the basis functions that are labelled by $j^{(1)}$ belong to a normal single-valued point group. This may seem a little strange considering the extensive commentary in the literature concerning the double-valuedness of the wavefunction in Jahn–Teller problems. However, as was pointed out by Longuet-Higgins [33], it is the eigenfunctions of the Jahn–Teller potential, for fixed ρ, that are double valued. See section 2.4.1 for details.

2.3.4. *Example: the C_{3v} point group*

The equations of the previous section are general for any point group with a C_n axis but are somewhat abstract. In this section we work through these equations for the specific case of the C_{3v} point group and then extend it to the spin–vibronic basis functions and the C_{3v} double group.

In the C_{3v} point group there is only one degenerate representation and $s_e = s_v = 1$. From equation (26) and table 2, $s_{k=1} = 0$ and $s_{k=2} = 1$. The Jahn–Teller operators are (equation (27)),

$$\hat{\mathscr{H}}_{JT}^{(1)}(C_{3v}) = \exp(+2i\theta)\rho \exp(-i\phi) + \exp(-2i\theta)\rho \exp(+i\phi), \tag{44}$$

$$\hat{\mathscr{H}}_{JT}^{(2)}(C_{3v}) = \exp(+2i\theta)\rho^2 \exp(+2i\phi) + \exp(-2i\theta)\rho^2 \exp(-2i\phi), \tag{45}$$

which are the familiar forms of the Jahn–Teller operators [35, 51].

For the C_{3v} point group, the Jahn–Teller quantum numbers $j^{(k)}$ become

$$j^{(1)} = l_t + \tfrac{1}{2}\Lambda \tag{46}$$

$$j^{(2)} = \tfrac{1}{2}l_t - \tfrac{1}{2}\Lambda \tag{47}$$

The Jahn–Teller quantum number $j^{(k)}$ is conserved for kth-order Jahn–Teller coupling in that the selection rule on $j^{(k)}$ is $\Delta j^{(k)} = 0$, as noted earlier. In terms of $j^{(1)}$, the selection rule on $j^{(2)}$ is

$$\Delta j^{(2)} = \Delta j^{(1)} \pm 3 = 0.$$

Therefore

$$\Delta j^{(1)} = \mp 3. \tag{48}$$

The symmetry of the basis functions and therefore the vibronic energy levels is dictated by $j^{(1)}$, equation (42). Those functions with $j^{(1)} = \pm\frac{3}{2}, \pm\frac{9}{2}, \ldots$ will transform as a_1 or a_2, while all others, $j^{(1)} = \pm\frac{1}{2}, \pm\frac{5}{2}, \pm\frac{7}{2}, \pm\frac{11}{2}, \ldots$, will transform as e.

When spin is included in the basis set, the $\hat{C}_3$ rotation on the basis function gives

$$\hat{C}_3 |\Lambda\rangle \prod_{i=1}^{p} |v_i, l_i\rangle |\Sigma\rangle = -\exp\left(+\frac{2\pi i}{3}(j^{(1)} - \Sigma)\right) |\Lambda\rangle \prod_{i=1}^{p} |v_i, l_i\rangle |\Sigma\rangle. \tag{49}$$

From equation (49), it is clear that a rotation by 2π ($\hat{C}_3^3$) now changes the basis function into minus itself if the spin is half-integer, and hence the double group must be used. From the character table of the double group of C_{3v}, if $(j^{(1)} - \Sigma)$ is a multiple of 3, the function transforms as $e_{3/2}$. If $(j^{(1)} - \Sigma)$ is not a multiple of 3, the function transforms as $e_{1/2}$. Therefore, all levels from $j^{(1)} = \pm\frac{3}{2} \pm 3m$ will belong to the $e_{1/2}$ irreducible representation, while the $j^{(1)} = \pm\frac{1}{2} \pm 3m$ and $j^{(1)} = \pm\frac{5}{2} \pm 3m$ levels will have one spin component of $e_{1/2}$ symmetry and one component of $e_{3/2}$ symmetry.

An alternative approach to the symmetry of the spin–vibronic basis functions is to define a new quantum number Ω:

$$\Omega = \Lambda - l_t + \Sigma. \tag{50}$$

The negative sign on l_t is less than intuitive but follows as a result of the phase convention chosen in equations (3) and (5). This reversal of the sign on l_t bears some analogy to the reversed internal angular momentum convention espoused by Van Vleck [48] to deal with the well known change of sign of i in the commutation relations for the rotational angular momentum quantized in the molecular frame. The analogy is less than complete, nature dictates the change in sign for i, while history is responsible for the sign of l_t. However, since we are able to change neither nature nor history, we have accepted this convention for the vibrational angular momentum.

The above definition of Ω is analogous to the definition of Ω for a diatomic molecule, with the addition of the vibrational angular momentum. The symmetry properties of the basis functions are easily determined by their value of Ω:

$$\begin{aligned}\hat{C}_3 |\Lambda\rangle \prod_{i=1}^{p} |v_i, l_i\rangle |\Sigma\rangle &= \exp\left(-\frac{2\pi i}{3}(\Lambda - l_t + \Sigma)\right) |\Lambda\rangle \prod_{i=1}^{p} |v_i, l_i\rangle |\Sigma\rangle \\ &= \exp\left(-\frac{2\pi i}{3}\Omega\right).\end{aligned} \tag{51}$$

If $\Omega \bmod 3 = \pm\frac{1}{2}$, the basis function transforms as $e_{1/2}$, otherwise it transforms as $e_{3/2}$.

2.4. *Potential energy surfaces*

The concept of a PES is one attributable to human intellect and not to nature. It has its origins in the Born–Oppenheimer approximation, in which the electronic PES is reasonably well defined, particularly if spin–orbit coupling is not considered. On the other hand, the Jahn–Teller effect is perhaps the quintessential example of a breakdown of the Born–Oppenheimer approximation. Because we want to consider the PESs for Jahn–Teller active molecules for which spin–orbit coupling is significant, it may be reasonable to ask whether the concept of a PES remains appropriate. The PES concept is still useful for these molecules, but it must be treated with a great deal more care than in the usual cases. At least two types of PES are useful. The first corresponds to the eigenvalues within the degenerate electronic space of $\hat{\mathscr{H}}_e$. The second corresponds to the eigenvalues of $\hat{\mathscr{H}}_e + \hat{\mathscr{H}}_{SO}$ within the space of the electronic and spin functions. We now treat each of these cases in turn.

2.4.1. *Potential energy surface without spin–orbit coupling*

For simplicity, we shall only consider the PES for an ^{2}E state of a nominally C_{3v} molecule. Liehr [3] has considered the PES corresponding to other symmetries. We can obtain a useful definition of a PES in the following way. The first and last terms of the Hamiltonian (9) represent the kinetic energy of the nuclei and have no role in defining their PES, leaving $\hat{V} + \hat{\mathscr{H}}_{SO}$. In traditional treatments, $\hat{\mathscr{H}}_{SO}$ has been neglected under the assumption that it is small compared with $\hat{V}$. If we use the basis set $|\Lambda\rangle|\Sigma\rangle$, we obtain the following matrix for $\hat{V}$:

$$\begin{bmatrix} \frac{\lambda_i}{2}\rho_i^2 & \rho_i k_i \exp(-i\phi_i) + \rho_i^2 g_{ii} \exp(-2i\phi_i) \\ \rho_i k_i \exp(-i\phi_i) + \rho_i^2 g_{ii} \exp(2i\phi_i) & \frac{\lambda_i}{2}\rho_i^2 \end{bmatrix} \begin{bmatrix} |\Lambda = -1\rangle|\Sigma\rangle \\ |\Lambda = +1\rangle|\Sigma\rangle \end{bmatrix}. \tag{52}$$

Equation (52) is independent of spin, and so $2S + 1$ equivalent versions of it exist, one for each possible value of Σ. The eigenvalues of equation (52), denoted $U_{i,\pm}$, that can be identified with the PES, are

$$U_{i,\pm} = \tfrac{1}{2}\lambda_i\rho_i^2 \pm \rho_i k_i \left(1 + \frac{2g_{ii}\rho_i}{k_i}\cos(3\phi_i) + \frac{g_{ii}^2\rho_i^2}{k_i^2}\right)^{1/2} \tag{53}$$

$$\approx \tfrac{1}{2}\lambda_i\rho_i^2 \pm \left[k_i\rho_i + g_{ii}\rho_i^2\cos(3\phi_i)\right], \tag{54}$$

where in the last equality the expansion of the radical has been truncated at terms quadratic in ρ_i. Figure 1(*a*) shows this surface in the absence of Jahn–Teller coupling, that is $k_i = g_{ii} = 0$. Figure 1(*b*) is a three-dimensional representation of the PES when there is only linear Jahn–Teller coupling ($k_i \neq 0, g_{ii} = 0$). Figures 2(*a*),(*b*),(*c*) and (*d*) show representative slices for $\phi_i = 0$ through the three-dimensional PES for a single Jahn–Teller active mode for the following conditions respectively: $k_i = g_{ii} = 0$, $k_i \neq 0$, $g_{ii} = 0$, $k_i \neq 0$, $g_{ii} \neq 0$, $k_i = 0$, $g_{ii} \neq 0$. Note that these surfaces are $(2S + 1)$-fold degenerate, corresponding to the possible values of Σ.

As shown in the figures, the PES has a global minimum at the bottom of the moat, owing to the linear Jahn–Teller coupling term. Quadratic Jahn–Teller coupling creates around this moat local minima and maxima. The minima and local maxima

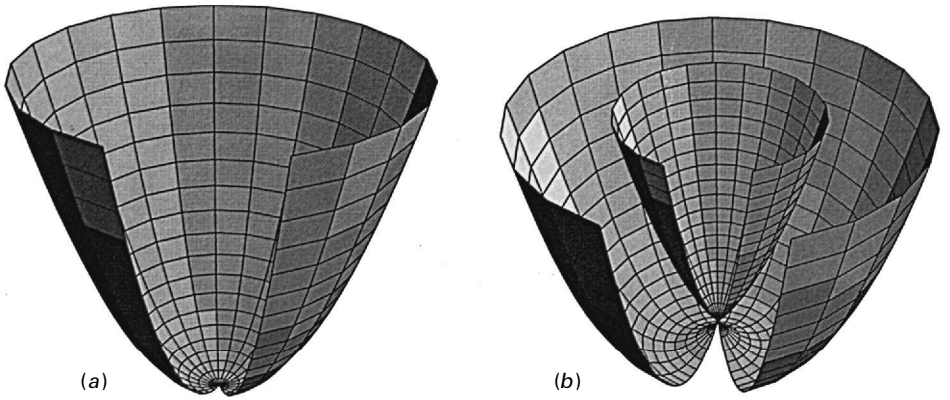

Figure 1. PES for (*a*) zero Jahn–Teller and zero spin–orbit coupling and (*b*) linear Jahn–Teller coupling for a single active mode.

of the moat of the lower potential surface of equation (54) are given by

$$\rho_{\min,i} = \frac{k_i}{\lambda_i(1 - K_i)}, \quad \phi_{\min,i} = 0, \frac{2\pi}{3}, \frac{4\pi}{3} \tag{55}$$

$$E_{\min,i} = -\frac{k_i^2}{2\lambda_i(1 - K_i)} = -\frac{D_i\omega_{e,i}}{(1 - K_i)} \approx -D_i\omega_{e,i}(1 + K_i), \tag{56}$$

$$\rho_{\max,i} = \frac{k_i}{\lambda_i(1 + K_i)}, \quad \phi_{\max,i} = \frac{\pi}{3}, \pi, \frac{5\pi}{3}, \tag{57}$$

$$E_{\max,i} = -\frac{k_i^2}{2\lambda_i(1 + K_i)} = -\frac{D_i\omega_{e,i}}{(1 + K_i)} \approx -D_i\omega_{e,i}(1 - K_i). \tag{58}$$

These formulae introduce two commonly used Jahn–Teller parameters: D_i is the linear Jahn–Teller coupling constant for the ith mode and K_i is its quadratic Jahn–Teller coupling constant. Both are dimensionless and are defined in terms of the reduced mass M_i of the mode and the parameters of table 1:

$$D_i = \frac{k_i^2}{2\hbar}\left(\frac{M_i}{\lambda_i^3}\right)^{1/2} \tag{59}$$

and

$$K_i = \frac{g_{ii}}{\lambda_i}. \tag{60}$$

These parameters will be used henceforth to describe the Jahn–Teller coupling. The energies of equations (56) and (58) are relative to the symmetric configuration, which is defined as the zero of energy. The depth ε of the moat is the Jahn–Teller stabilization energy and is a direct measure of the net effect the Jahn–Teller coupling has on the energy of the molecule. From equations (56) and (58), for vanishing K_i, $E_{\min,i} = E_{\max,i} \equiv -\varepsilon_i$, and we have

$$\varepsilon_i = D_i\omega_{e,i}. \tag{61}$$

The total Jahn–Teller stabilization energy can conveniently be defined as the sum

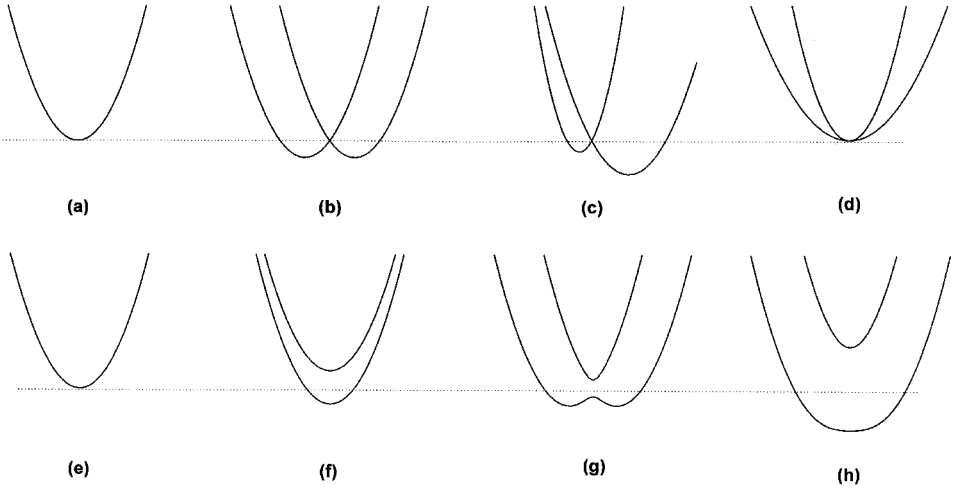

Figure 2. PES for the various possible spin–orbit and Jahn–Teller coupling schemes. All the curves with non-zero Jahn–Teller coupling (*b*)–(*d*), (*g*) and (*h*) are constructed for the same strength of linear Jahn–Teller coupling. The top curves are all for cases with zero spin–orbit coupling: (*a*) zero Jahn–Teller and zero spin–orbit coupling (i.e. the harmonic oscillator only, $D_i = 0.0$, $K_i = 0$, $a\zeta_e = 0$), (*b*) linear Jahn–Teller coupling ($D_i = 0.25$, $K_i = 0$, $a\zeta_e = 0$), (*c*) linear plus quadratic Jahn–Teller coupling ($D_i = 0.25$, $K_i = 0.1$, $a\zeta_e = 0$), (*d*) quadratic Jahn–Teller coupling with exactly zero linear coupling $D_i = 0$, $K_i = 0.25$, $a\zeta_e = 0$). The bottom curves, except for (*e*), illustrate the cases with non-zero spin–orbit coupling: (*e*) zero Jahn–Teller and zero spin–orbit coupling ($D_i = 0$, $K_i = 0$, $a\zeta_e = 0$), (*f*) zero Jahn–Teller and non-zero spin–orbit coupling ($D_i = 0$, $K_i = 0$, $a\zeta_e/\omega_{e,i} = 0.5$), (*g*) linear Jahn–Teller plus spin–orbit coupling, when $a\zeta_e < 4D_i\omega_{e,i}$ ($D_i = 0.25$, $K_i = 0$, $a\zeta_e/\omega_{e,i} = 0.25$), (*h*) linear Jahn–Teller plus spin–orbit coupling when $a\zeta_e > 4D_i\omega_{e,i}$ ($D_i = 0.25$, $K_i = 0$, $a\zeta_e/\omega_{e,i} = 2.0$). The curves are slices through the potential surface of a Jahn–Teller active normal mode with $\phi_i = 0$. (Only cases (*c*) and (*d*) will have a dependence on ϕ_i.) For simplicity, the slice through only a single Jahn–Teller active mode is depicted. The dotted lines are the zero of energy, defined as the bottom of the well of the harmonic oscillator potential.

over each individual mode's contribution:

$$\varepsilon_{\text{total}} = \sum_{i=1}^{p} \varepsilon_i = \sum_{i=1}^{p} D_i \omega_{e,i}. \tag{62}$$

Because the Jahn–Teller stabilization energy ε is assumed to be a positive number, the linear coupling constants D_i are also positive. However, no such constraint exists for the quadratic coupling constants K_i, which can be positive or negative. From equations (55)–(58), it can be seen that the effect of the sign of K_i on the PES is to exchange the positions of the minima and the maxima around the moat with respect to the angular vibrational coordinate.

Figure 2(*d*) illustrates the point made in the previous section that quadratic Jahn–Teller coupling for nonlinear molecules is analogous to Renner–Teller coupling for linear molecules. The potential drawn in figure 2(*d*) is for the case of non-zero quadratic coupling, but zero linear coupling. The potential is identical with that for Renner–Teller coupling in Π states of linear molecules (for example, see figure 4(*b*) of [37]).

Finally, a word about the eigenfunctions of equation (52) is in order. As pointed out by Longuet–Higgins [33], for fixed ρ, as ϕ goes from 0 to 2π the eigenfunctions change sign. This is the origin of the extensive discussion in the literature about the double-valuedness of the wavefunction in problems involving the Jahn–Teller effect and related problems involving Berry's [58] phase. Some workers have, at least conceptually, used basis functions of the form of the eigenfunctions of equation (52) and hence had to consider the double-valuedness of both their 'electronic' and their 'vibrational' basis functions. We, on the other hand, use as our basis the vibronic functions of equation (43) and never explicitly deal with double-valuedness (except for the spin functions) as in either approach the overall wavefunction (excluding spin) must be single valued.

2.4.2. *Potential energy surface with spin–orbit coupling*

All the equations and figures of the previous section assume that spin–orbit coupling is negligible. Because the introduction of spin–orbit coupling partially quenches the Jahn–Teller coupling (and vice versa), these equations must be modified for molecules that have significant spin–orbit coupling, for which $\hat{\mathscr{H}}_{SO}$ cannot be neglected. The addition of spin–orbit coupling means that the form of the potential must be modified to account for it. Now the matrix of $\hat{V} + \hat{\mathscr{H}}_{SO}$ is formed in the same basis as before:

$$\begin{bmatrix} \frac{\lambda_i}{2}\rho_i^2 - \frac{a\zeta_e}{2} & \rho_i k_i \exp(+i\phi_i) & 0 & 0 \\ \rho_i k_i \exp(-i\phi_i) & \frac{\lambda_i}{2}\rho_i^2 + \frac{a\zeta_e}{2} & 0 & 0 \\ 0 & 0 & \frac{\lambda_i}{2}\rho_i^2 + \frac{a\zeta_e}{2} & \rho_i k_i \exp(+i\phi_i) \\ 0 & 0 & \rho_i k_i \exp(-i\phi_i) & \frac{\lambda_i}{2}\rho_i^2 - \frac{a\zeta_e}{2} \end{bmatrix} \times \begin{bmatrix} |\Lambda = -1\rangle |\Sigma = +\tfrac{1}{2}\rangle \\ |\Lambda = +1\rangle |\Sigma = +\tfrac{1}{2}\rangle \\ |\Lambda = -1\rangle |\Sigma = -\tfrac{1}{2}\rangle \\ |\Lambda = +1\rangle |\Sigma = -\tfrac{1}{2}\rangle \end{bmatrix}, \tag{63}$$

where for simplicity it is assumed that quadratic Jahn–Teller coupling is negligible and that $S = \frac{1}{2}$. Generalization to higher spin multiplicities is straightforward. Because Σ is still preserved, the eigenvalues $U_{\pm}$ associated with the PES are each degenerate, where

$$U_{i,\pm} = \tfrac{1}{2}\lambda_i\rho_i^2 \pm \tfrac{1}{2}[4k_i^2\rho_i^2 + (a\zeta_e)^2]^{1/2}. \tag{64}$$

Spin–orbit interactions can have a tremendous impact on the shape of the PES, as is evident by the changes in the location of the radial minimum, energies at the minima, and Jahn–Teller stabilization energies:

$$\rho_{\min,i} = \begin{cases} \dfrac{1}{2k_i\lambda_i}(4k_i^4 - a^2\zeta_e^2\lambda_i^2)^{1/2}, & a\zeta_e < 4D_i\omega_{e,i}, \\ 0, & a\zeta_e \geqslant 4D_i\omega_{e,i}, \end{cases} \tag{65}$$

$$-\varepsilon_i^{so} = E_{\min,i} = \begin{cases} -D_i\omega_{e,i} + \dfrac{(a\zeta_e)^2}{16D_i\omega_{e,i}}, & a\zeta_e < 4D_i\omega_{e,i}, \\ 0, & a\zeta_e \geqslant 4D_i\omega_{e,i}, \end{cases} \tag{66}$$

where ε_i^{SO} is the Jahn–Teller stabilization energy for mode i calculated including spin–orbit coupling. As we mentioned in the introduction, spin–orbit coupling and Jahn–Teller coupling involve the coupling of the electronic orbital angular momentum of the molecule with spin angular momentum and vibrational angular momentum respectively. Thus, both effects are competing for the electronic orbital angular momentum. It is not surprising, therefore, that in equations (65) and (66) the spin–orbit contribution has the opposite sign to the Jahn–Teller term, spin–orbit coupling quenches Jahn–Teller coupling and Jahn–Teller coupling quenches spin–orbit coupling. Indeed, two separate regimes can be usefully defined: one where spin–orbit coupling largely eliminates the Jahn–Teller distortion (the case when $a\zeta_e > 4D_i\omega_{e,i}$) and one where the molecule is distorted, but with a much quenched spin–orbit splitting ($a\zeta_e < 4D_i\omega_{e,i}$).

Figures 2(*f*) and (*g*) show the effects of moderate and large spin–orbit couplings, respectively on the linear Jahn–Teller PESs. As can be seen, when the spin–orbit coupling is not zero, the two surfaces no longer intersect at $\rho_i = 0$, they are separated by an energy difference of $a\zeta_e$. Second, the minimum of the moat has contracted and risen in energy. In fact, if $a\zeta_e > 4D_i\omega_{e,i}$ the minimum occurs at the symmetric point and there is no longer any stabilization at asymmetric geometries (figure 2(*g*)). This statement does not, however, mean that, if $a\zeta_e > 4D_i\omega_{e,i}$ the Jahn–Teller terms in the Hamiltonian can be neglected. As we shall see in the rest of this paper, when Jahn–Teller coupling and spin–orbit coupling are both non-negligible, the exact eigenvalues and eigenfunctions of the entire Hamiltonian must be numerically computed if spectroscopic accuracy is to be attained.

There is one other significant change in the PES upon the addition of spin–orbit coupling. In the absence of spin–orbit coupling, the two potentials cross as a conical intersection at the symmetric configuration, $\rho_i = 0$, forming a cusp. However, when spin–orbit coupling is present, the two curves do not intersect and the two curves look more like an avoided crossing. Rather than forming a cusp at $\rho_i = 0$, the two curves each smoothly change slope, with the upper surface having a minimum at the symmetric configuration and the lower surface having a maximum, for small spin–orbit coupling. When spin–orbit coupling is much larger, each of the two surfaces has a minimum at the symmetric configuration and no other minima or maxima. However, the curvature of the surfaces is such that it is not the same as the curvature of the surface in the absence of Jahn–Teller coupling, note how much broader and flatter the potential of figure 2(*h*) is in comparison with figure 2(*f*). In a sense, then, the two potential surfaces never cross and never form a cusp, as spin–orbit coupling will always be present to some extent, although it may be sufficiently small for the intersection to be practically a cusp.

Equations (52)–(66) have all been given for a single Jahn–Teller active vibrational mode. For the case when there is more than one Jahn–Teller active mode, radial minima and maxima exist for each mode, and each mode has its own Jahn–Teller stabilization energy (equation (61) or (66)). The total Jahn–Teller stabilization energy may therefore be considered as a summation of equation (56) or equation (66) over all the active modes. However, there is no guarantee that a point exists on the true PES having a stabilization energy this great. An intriguing possibility in the multimode case is that the spin–orbit coupling may be large enough to quench completely the Jahn–Teller distortion in one of the modes, but not large enough to quench it in another mode.

2.5. *Hamiltonian matrix*

In the previous section we obtained the PESs for the molecule, first without and then with spin–orbit coupling. To determine the vibronic (or spin–vibronic) energy levels on these PESs, we now need to quantize the nuclear motion. We do this by including the nuclear kinetic energy $\hat{\mathscr{H}}_{\mathrm{T}}$ of equation (9) and computing the matrix elements of the nuclear coordinate operators in equations (52) and (63). Conceptually it might be simplest to calculate the appropriate 'vibrational matrix elements' in the eigenfunction basis corresponding to the electronic or spin–electronic PES. However, it is more efficient, and ultimately more accurate, to use the 'primitive' basis set that spans all three spaces (electronic, vibrational and spin) rather than a product of a vibrational basis and an eigenfunction of the electronic or spin–electronic PES. In the truest sense then, our calculations, like nature itself, avoids the concept of a PES. Rather, it proceeds directly to the observable quantized energy levels. Nonetheless the nature of the surface that could support the calculated levels is of considerable conceptual interest, and for this reason we shall often refer back to the PES created by the molecular parameters consistent with the experimental eigenenergies and eigenfunctions.

The matrix elements of the spin–orbit Jahn–Teller Hamiltonian, (9) are as follows:

$$\langle \Sigma | \prod_{i=1}^{p} \langle v_i, l_i | \langle \Lambda | \, \hat{\mathscr{H}}_{\mathrm{e}} \, | \Lambda \rangle \prod_{i=1}^{p} | v_i, l_i \rangle \, | \Sigma \rangle = E_0 \equiv 0, \tag{67}$$

$$\langle \Sigma | \prod_{i=1}^{p} \langle v_i, l_i | \langle \Lambda | \, \hat{\mathscr{H}}_{\mathrm{T}} + \hat{\mathscr{H}}_{\mathrm{h,e}} + \hat{\mathscr{H}}_{\mathrm{anh,e}} \, | \Lambda \rangle \prod_{i=1}^{p} | v_i, l_i \rangle \, | \Sigma \rangle = \sum_{i=1}^{p} \omega_{\mathrm{e},i}(v_i + 1) - \omega_{\mathrm{e},i} x_{\mathrm{e},i}(v_i + 1)^2, \tag{68}$$

$$\langle \Sigma | \prod_{i=1}^{p} \langle v_i, l_i | \langle \Lambda | \, \hat{\mathscr{H}}_{\mathrm{SO}} \, | \Lambda \rangle \prod_{i=1}^{p} | v_i, l_i \rangle \, | \Sigma \rangle = a \zeta_{\mathrm{e}} \Lambda \Sigma, \tag{69}$$

$$\begin{aligned}
&\langle \Sigma | \prod_{i=1}^{p} \langle v_i, l_i | \langle \pm | \, \hat{\mathscr{H}}_1 \, | \mp \rangle \prod_{i=1}^{p} \left| v_i', l_i' \right\rangle \, | \Sigma \rangle \\
&\quad = \sum_i \omega_{\mathrm{e},i} \left\{ [D_i (v_i \mp (-1)^{s_1} l_i + 2)]^{1/2} \right. \\
&\qquad \left. \times \left[\delta_{v_i + 1, v_i'} \delta_{l_i \mp (-1)^{s_1}, l_i'} \left(\prod_{j \neq i} \delta_{v_j, v_j'} \delta_{l_j, l_j'} \right) \right] \right\} \\
&\qquad + \sum_i \omega_{\mathrm{e},i} \left\{ [D_i (v_i \pm (-1)^{s_1} l_i)]^{1/2} \right. \\
&\qquad \left. \times \left[\delta_{v_i - 1, v_i'} \delta_{l_i \mp (-1)^{s_1}, l_i'} \left(\prod_{j \neq i} \delta_{v_j, v_j'} \delta_{l_j, l_j'} \right) \right] \right\},
\end{aligned} \tag{70}$$

$$\begin{aligned}
&\langle\Sigma|\prod_{i=1}^{p}\langle v_i, l_i|\langle\pm|\,\hat{\mathscr{H}}_{q_{ii}}\,|\mp\rangle\prod_{i=1}^{p}\left|v_i', l_i'\right\rangle|\Sigma\rangle \\
&\quad=\sum_i \omega_{e,i}\left\{\frac{K_i}{4}\left[(v_i\mp(-1)^{s_2}l_i)(v_i\mp(-1)^{s_2}l_i-2\right]^{1/2}\right. \\
&\qquad\left.\times\left[\delta_{v_i-2,v_i'}\delta_{l_i\pm 2(-1)^{s_2},l_i'}\left(\prod_{j\neq i}\delta_{v_j,v_j'}\delta_{l_j,l_j'}\right)\right]\right\} \\
&\qquad+\sum_i \omega_{e,i}\left\{\frac{K_i}{2}\left[(v_i\pm(-1)^{s_2}l_i+2)(v_i\mp(-1)^{s_2}l_i)\right]^{1/2}\right. \\
&\qquad\left.\times\left[\delta_{v_i,v_i'}\delta_{l_i\pm 2(-1)^{s_2},l_i'}\left(\prod_{j\neq i}\delta_{v_j,v_j'}\delta_{l_j,l_j'}\right)\right]\right\} \\
&\qquad+\sum_i \omega_{e,i}\left\{\frac{K_i}{4}\left[(v_i\pm(-1)^{s_2}l_i+4)(v_i\pm(-1)^{s_2}l_i+2\right]^{1/2}\right. \\
&\qquad\left.\times\left[\delta_{v_i+2,v_i'}\delta_{l_i\pm 2(-1)^{s_2},l_i'}\left(\prod_{j\neq i}\delta_{v_j,v_j'}\delta_{l_j,l_j'}\right)\right]\right\}. \qquad (71)
\end{aligned}$$

The first term in the potential (13), $\hat{\mathscr{H}}_e$, is the electronic operator that will give the total energy E_0 of the molecule at the symmetric point. Because it plays no role in determining the vibronic structure within the state, we define it as the zero of energy for the state.

The harmonic oscillator operator $\hat{\mathscr{H}}_{h,e}$ is diagonal in the basis set of equation (8) with matrix elements of $\omega_{e,i}(v_i + 1)$ for each of the Jahn–Teller active modes. We have also included the symmetric anharmonicity of the mode, although we shall not discuss this term in any detail. The spin–orbit coupling operator $\hat{\mathscr{H}}_{SO}$ also has diagonal matrix elements in the basis and are given in equation (69). Note that $\omega_{e,i}$ and a have units of energy, typically given in reciprocal centimetres, while ζ_e is dimensionless (see below and also appendix A).

A few words of explanation are in order with respect to our writing the matrix elements of $\hat{\mathscr{H}}_{SO}$ as $a\zeta_e\Lambda\Sigma$. As our basis corresponds to eigenfunctions of S_z with eigenvalues Σ, the last factor is obvious. The remainder of the expression requires

$$\langle\Lambda|\,a\hat{L}_z\,|\Lambda\rangle = a\zeta_e\Lambda \qquad (72)$$

where it must be remembered that, in our usage, Λ distinguishes between the two components of the degenerate electronic wavefunction and can therefore only take upon the values $\Lambda = \pm 1$. The parameter ζ_e is defined as the projection of the electronic orbital angular momentum on the symmetry axis:

$$\langle E_+|\,\hat{L}_z\,|E_+\rangle = -\langle E_-|\,\hat{L}_z\,|E_-\rangle = \zeta_e. \qquad (73)$$

In the cylindrically symmetric limit, $\zeta_e\Lambda \to \Lambda'$, where Λ' takes on the conserved integer projections of the electronic angular momentum. For linear molecules, $|\Lambda'|$ can have the values 0, 1, 2,..., corresponding to states of Σ, Π, Δ,... symmetry. In the nonlinear point groups, the symmetry label $\pm s_e$ corresponds to Λ' of the

cylindrical limit. When one moves away from the cylindrical limit, the spin–orbit coupling is modified by two physically distinct mechanisms. First, the electronic angular momentum is reduced by the electrostatic impediments to electronic motion created by the presence of off-axis atoms, to a value of $\zeta_e \Lambda$, where ζ_e is in general non-integer and hence $\zeta_e \Lambda$ is smaller in magnitude than Λ'. The second effect involves the delocalization of the 'unpaired' electron(s) from atoms on the axis to those off the axis, which can cause a to increase or decrease, depending on which atoms are off the axis and what the strengths of their respective contributions to the spin–orbit coupling are. The value of a is an approximate measure of the strength of the interaction of the electron(s) with the individual nuclei, which depends upon the nature of the nucleus and the spatial extent of the electronic wavefunction. In section 3.2.2 we shall see that a third factor can also reduce the observed spin splitting. This is the Ham [29, 59] reduction factor, which physically corresponds to the lowering of the molecule's symmetry and concomitant quenching of the orbital angular momentum by the Jahn–Teller distortion.

The linear Jahn–Teller operator is clearly not diagonal in the basis set (8) and is responsible for the mode mixing, geometric distortions and changes in vibronic transition intensities. Its matrix elements [60] follow the selection rules $\Delta\Sigma = 0$, $\Delta v_i = \pm 1$, and a simultaneous change in Λ and l_i, $\Delta\Lambda = -2(-1)^{s_1}$ $\Delta l_i = \pm 2$, so that $\Delta j^{(1)} = 0$. This selection rule depends upon the value of s_1, which depends upon s_e and s_v. This dependence has been implemented in equations (67)–(71) and our computer program that diagonalizes this matrix. For a given non-zero off-diagonal matrix element, only one vibrational mode changes quantum numbers, if a matrix element is non-diagonal in more than one mode, its value is exactly zero. Each Jahn–Teller active mode has associated with it a dimensionless linear Jahn–Teller coupling constant D_i (equation (59)). Of the original quantum numbers in the basis set (8), only Σ remains a good quantum number under spin–orbit coupling and linear Jahn–Teller coupling. However, as we saw from symmetry arguments in section 2.3 and explicitly in equations (67)–(71), j can be defined as a good quantum number under linear Jahn–Teller coupling. (From here on we drop the superscript (1) from $j^{(1)}$.) In the absence of quadratic Jahn–Teller interactions the energy levels of $+j$ are degenerate with those of $-j$ [31].

The matrix elements for the quadratic Jahn–Teller portion of the Hamiltonian are slightly more complicated than those for the linear case. The selection rules for the quadratic matrix elements are $\Delta\Sigma = 0$, $\Delta v_i = 0, \pm 2$, and a simultaneous change in Λ and l_i, $\Delta\Lambda = -(-1)^{s_2}\Delta l_i = \pm 2$. Each Jahn–Teller active mode has a quadratic coupling constant K_i which is dimensionless (equation (60)). The spin angular momentum quantum number Σ is still a good quantum number, but the quadratic Jahn–Teller effect destroys the j quantum number. However, the matrix will still be block diagonal in $j^{(2)}$.

The diagonalization of the Hamiltonian is now a straightforward process. The general form for the eigenfunctions $|j, n_j, \alpha, \Sigma\rangle$ is

$$|j, n_j, \alpha, \Sigma\rangle = \sum_i \left(c_{i,n_j,\Sigma} \, |\Lambda_i\rangle \prod_{m=1}^{p} |v_{m,i}, l_{m,i}\rangle \, |\Sigma_i\rangle \right), \tag{74}$$

where the summation runs over all the basis functions used in the calculation. For a coefficient $c_{i,n_j,\Sigma}$ to be non-zero, the selection rule on j must be satisfied by the basis function. Each eigenvector $|j, n_j, \alpha, \Sigma\rangle$ has an associated eigenvalue $E_{j,n_j,\Sigma}$. The

notation $|j, n_j, \alpha, \Sigma\rangle$ indicates to which j block the level corresponds and which eigenvector n_j it is from that symmetry block corresponding to a given j (j mod 3 when quadratic coupling is included) and Σ combination, with the lowest-energy solution of each symmetry block being $n_j = 1$. If quadratic coupling is small relative to linear coupling, states of different j will be mixed only slightly, and j remains a useful descriptor of the states even though it is rigorously not a good quantum number under quadratic Jahn–Teller coupling. This is the case for all the examples that we show later, and probably many others. Because j is not always a good quantum number, we have included into the ket the label α, which is the symmetry species of the state. If non-integer spin is included in the basis set, the spin double group must be used. For the example case of a doublet state of C_{3v} symmetry, the species of the basis function may be either $e_{1/2}$ or $e_{3/2}$, see the discussion of section 2.3.4. Note also that there are now two subscripts on the quantum numbers v and l in the basis functions of equation (74). The first, m, corresponds to which vibrational mode the quantum number refers while the second, i, represents the basis function to which the quantum number belongs.

The quantum number Σ is included in the summation only when spin–orbit coupling is included in the Hamiltonian, in its absence, equation (74) becomes

$$|j, n_j, \alpha\rangle |\Sigma\rangle = \sum_i \left(c_{i,n_j} |\Lambda_i\rangle \prod_{m=1}^{p} |v_{m,i}, l_{m,i}\rangle \right) |\Sigma\rangle . \tag{75}$$

In the two limits of small spin–orbit coupling or large Jahn–Teller coupling the spin–vibronic wavefunction is approximately identical with the vibronic wavefunction, that is $|j, n_j, \alpha\rangle |\Sigma\rangle \approx |j, n_j, \alpha, \Sigma\rangle$. At these limits, the two components of the spin–orbit doublet have essentially identical vibronic wavefunctions and PESs. In this case, α denotes the vibronic symmetry of the level, a_1, a_2 or e, for the C_{3v} group.

Our choice of basis set is not the only choice. For all the vibronic energy levels of e symmetry, there will be two eigenvectors that differ by their signs of j, Λ_i, $l_{m,i}$ and Σ. The $-j$ analogue of equation (74) is

$$|-j, n_j, \alpha, \Sigma\rangle = \sum_i \left(c_{i,n_j,\Sigma} |-\Lambda_i\rangle \prod_{m=1}^{p} |v_{m,i}, -l_{m,i}\rangle |-\Sigma_i\rangle \right) . \tag{76}$$

For the levels of e symmetry, any linear combination of the two $\pm j$ components will be a valid solution. In solving the rotational problem for a ^{2}E state, a common choice for the vibronic portion of the basis set is [34]

$$|(\Lambda, v, l, j), \Sigma, \pm\rangle = 2^{-1/2} \left[|j, n_j, \alpha, \Sigma\rangle \pm |-j, n_j, \alpha, -\Sigma\rangle \right] . \tag{77}$$

(The left-hand side of equation (77) is the normal vibronic notation, written for a single active mode. If more than one mode is Jahn–Teller active, v should be replaced by a product over all v_i and l should be replaced by l_t.) This choice of basis set is often made for solving the rotational problem because, once the rotational quantum numbers have been added, the size of the effective Hamiltonian matrix is decreased by a factor of two over the matrix that would be created using only equation (74) [61].

There are several limitations of this approach that need to be addressed. First, higher-order terms ($k > 2$) in the Hamiltonian have been neglected to make the problem manageable. Quadratic Jahn–Teller terms that involve only a single mode have been included in these calculations, while the term $\hat{\mathcal{H}}_{q_{ij}}$ involves coupling

between two different Jahn–Teller active modes has not. Likewise quadratic or bilinear coupling between Jahn–Teller and symmetric modes has not been included. However, these inter-mode quadratic off-diagonal elements are expected to be small, provided that the intra-mode quadratic coupling of equation (71) is reasonably small. In all the molecules investigated to date, there has been no spectral evidence to support the inclusion of inter-mode quadratic coupling, or other higher order Jahn–Teller terms.

We have also included in the computer program that we have written for the diagonalization a diagonal matrix element that accounts for the anharmonicity of the modes. As is the case for the inter-mode quadratic Jahn–Teller terms, the spectra for most molecules studied so far have not been complete enough to necessitate the inclusion of vibrational anharmonicity. Anharmonic terms become more important at higher internal energies, which are typically not observed or assigned in the spectra of Jahn–Teller molecules. The last deficiency in our approach is the truncation of the basis set to a finite size for the numerical computation. As mentioned earlier, this problem can be overcome by iterating the calculations with an increasing basis set, converging the calculated energies to a specified precision.

2.6. *Isotopic substitutions*

An intriguing area of inquiry, which we shall not discuss in detail, is the effect of isotopic substitution on the vibronic energy levels of a Jahn–Teller state. In sections 6.2.2 and 6.2.4 we present the analyses of the spectra of CH_3S–CD_3S and CH_3O–CD_3O respectively, for which relatively straightforward connections between the Jahn–Teller coupling constants exist. What happens in the case of partial isotopic substitution? This is an extremely interesting question and one for which a complete answer has not yet been provided.

Partial isotopic substitution of a symmetric top molecule will lower the point group symmetry of the molecule. The result on the Jahn–Teller energy levels will be to shift and split them in a complicated way. Although the nominal point group of the molecule will be lower than the unsubstituted molecule, the entire electronic PES in which the vibronic energy levels are eigenfunctions will still be one of those in figure 2, assuming that the change in the nuclear isotopes has a negligible effect on the electronic surface. The PES will still *not* be a harmonic surface and corrections to the harmonic oscillator energy levels and their properties will still need to be made. Only a few initial attempts have been made in this area [14, 62–64]. This effect has been observed in the esr spectra of the benzene-1-*d* anion [65] and the cyclooctatetraene-1-*d* anion [66], the absorption spectra of several asymmetrically deuterated benzene cations [63, 64] and the fluorescence spectra of the asymmetric isotopomers of the cyclopentadienyl radical [14].

It might be expected that one would have to be a terrific chemist to carry out successfully an experiment on a partially isotopically substituted Jahn–Teller molecule. However, we point out that, in an electronic transition, the isotope shift of the transition will be significant and will serve to separate the vibronic levels. In particular, if rotationally resolved spectra can be obtained, the rotational energy levels will clearly distinguish between the isotopomers [14]. In this way the istopomers can be separated spectroscopically, rather than chemically. An alternative is to use a mass-selective technique, such as resonance-enhanced multiphoton ionization or an ion beam technique, to separate the different isotopomers. We hope that in the

future more experiments will be done and more theoretical developments carried out on this fascinating possibility. Although the theory will be fairly complicated (on top of the already complicated Jahn–Teller theory of an unsubstituted molecule), isotopic substitution offers a way to derive a great amount of information about the state and its Jahn–Teller and spin–orbit coupling.

2.7. *General considerations*

A completely legitimate question to ask at this point is the following: if the Jahn–Teller effect distorts the molecule away from its symmetric configuration, how can a satisfactory analysis ever be obtained from a symmetric starting point, using the parameters of equations (14)–(16)? While linear and quadratic Jahn–Teller coupling both distort the molecule away from its symmetric configuration, it is imperative to remember that *the entire PES maintains the symmetry of the point group*. Therefore, *only* a Hamiltonian of the point group of the entire PES can adequately describe the molecule. A Hamiltonian appropriate for the point group of the distorted molecule is wholly inadequate to describe an experiment wherein the molecule exhibits behaviour consistent with it not being confined to a local minimum of the distorted surface. In fact, if a rotationally resolved spectrum of a Jahn–Teller molecule can be successfully analysed using a symmetric top Hamiltonian, then it has been experimentally proven that the Jahn–Teller coupling, if any, is not large enough to distort the molecule 'permanently', that is to localize it to a distorted minimum on the time scale of molecular rotation. A generally easier test to accomplish experimentally is that, if a spin–orbit splitting can be resolved, then the molecule must be analysed using a symmetric top Hamiltonian, for the existence of 'unquenched' orbital angular momentum implies the molecule is not localized at a geometry away from the symmetric position. If a spin–orbit splitting is not observed, the molecule may or may not still be symmetric, see, for example, the high resolution study of C_5H_5, where the spin–orbit splitting was too small to measure, but a Jahn–Teller effect on the rotational and vibrational energy levels was clearly resolvable, implying a dynamic Jahn–Teller effect [14].

When the Jahn–Teller effect becomes so large that the molecule is statically (permanently) distorted, a different approach may become useful in the spectroscopic analysis. In this case, the molecule is distorted to lower symmetry, typically C_s symmetry, and the normal, approximately harmonic oscillator energy levels are recovered, although using vibrational constants for a distorted rather than a symmetric molecule. If the molecule is not permanently distorted but close to that limit, it may still be more suitable to use a vibronic Hamiltonian for a distorted molecule, and add correction terms to it rather than starting with the symmetric Hamiltonian and correcting for Jahn–Teller coupling.

When does this cross-over point occur? It has often been stated that a static Jahn–Teller effect, that is the molecule is permanently distorted on the time scale of the experiment, occurs when the zero-point energy levels falls below the energy of the symmetric point, which occurs when $D_i \gtrsim 1$. The opposite case, when D_i is less than unity, has been referred to as the dynamic Jahn–Teller effect. (Recall that the cusp of the PES is defined as the zero of energy and that for a two-dimensional harmonic oscillator potential, the zero point level for a degenerate mode is at an energy of $\omega_{e,i}$.) This nomenclature is deceiving in that, while the zero point level of the molecule might fall below the symmetric cusp, there may still be little or no

barrier to pseudo-rotation about the moat (see figures 1(*b*) and 2(*b*)). If the quadratic Jahn–Teller coupling constants are large, a barrier to pseudo-rotation is created, and the molecule can become trapped in a distorted well. It is likely, however, that a large linear Jahn–Teller effect will be accompanied by a large quadratic Jahn–Teller effect that will produce a static distortion of the molecule. It is therefore convenient to retain the nomenclature of a static Jahn–Teller effect for $D_i \gtrsim 1$, while for $D_i < 1$ it implies a dynamic case. It should be remembered, however, that no such relationship is quantitatively implied for the corresponding 'geometric structure'.

2.8. *Computational details*

A Fortran90 computer program has been written to calculate the energies and wavefunctions of a molecule described by the Hamiltonian of equation (9), excluding $\hat{\mathscr{H}}_{\text{rot}}$. The program can handle an arbitrary number of active modes and the truncation of the basis set is limited only by available memory and computer time. Currently, the program runs on a Cray T90, however, transfer of the code to smaller workstations and personal computers is in progress. A complete description of the computer program will be given elsewhere [67]. It is this program that has provided the numerical results presented in the remainder of the paper.

3. Vibronic energy levels for C_{3v} molecules with spin–orbit and Jahn–Teller coupling

In section 2 we developed a fairly general theory for the Jahn–Teller effect, including those molecules that also exhibit significant spin–orbit coupling. The main purpose of this section is to demonstrate, via the results of numerical calculations for a model C_{3v} system, how the various interaction terms in the Hamiltonian give rise to particular energy level patterns and ultimately the corresponding spectra.

While there exists an extensive body of work on Jahn–Teller coupling, and calculations of vibronic energy levels for linear and quadratic Jahn–Teller effects are not new, numerically accurate calculations including spin–orbit coupling have been much rarer. Before presenting a detailed discussion of the effect of spin–orbit coupling on the Jahn–Teller problem, it is instructive to review the results of Jahn–Teller calculations in the absence of spin–orbit coupling. Many other workers have investigated this problem, and the presentation here is a distillation of the most important properties from those investigations.

3.1. *Qualitative considerations*

3.1.1. *Linear Jahn–Teller coupling*

Figure 3 illustrates several properties of the vibronic energy levels of a ^{2}E state of C_{3v} symmetry. The first item to be taken from figure 3 is the symmetries of the various levels, as symmetry has a tremendous impact on the spectroscopy. Under linear Jahn–Teller coupling, the levels that had been degenerate in the harmonic oscillator are split and can be differentiated by their vibronic symmetry (figure 3(*b*)). Those levels with $j = \pm\frac{3}{2}$ are of a_1 and a_2 symmetry while those with $j = \pm\frac{1}{2}$ or $\pm\frac{5}{2}$ are of e symmetry.† Note that the $\pm\frac{3}{2}$ levels are *not* degenerate by the symmetry of

† From here on we shall drop the somewhat burdensome notation of $\pm\left(\frac{1}{2} + 3n\right)$, $\pm\left(\frac{3}{2} + 3n\right)$, etc., and refer to these groups of states by the lead fraction, $\frac{1}{2}$, $\frac{3}{2}$, or $\frac{5}{2}$.

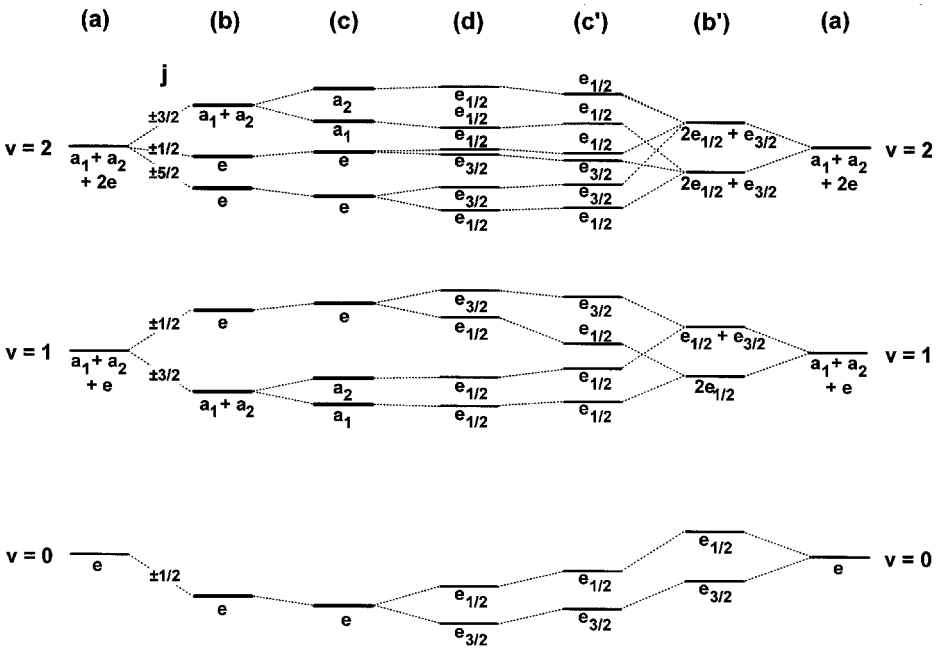

Figure 3. Qualitative energy level scheme of the vibronic energy levels of a ^{2}E state under C_{3v} symmetry, with a single Jahn–Teller active mode, for the following Hamiltonians: (*a*) $\hat{\mathscr{H}}_{h,e}$, (*b*) $\hat{\mathscr{H}}_{h,e} + \hat{\mathscr{H}}_{1}$, (*c*) $\hat{\mathscr{H}}_{h,e} + \hat{\mathscr{H}}_{1} + \hat{\mathscr{H}}_{q_{ii}}$, (*d*) $\hat{\mathscr{H}}_{h,e} + \hat{\mathscr{H}}_{1} + \hat{\mathscr{H}}_{q_{ii}} + \hat{\mathscr{H}}_{SO}$, (*c*′) $\hat{\mathscr{H}}_{h,e} + \hat{\mathscr{H}}_{SO} + \hat{\mathscr{H}}_{1}$, (*b*′) $\hat{\mathscr{H}}_{h,e} + \hat{\mathscr{H}}_{SO}$, (*a*) $\hat{\mathscr{H}}_{h,e}$. The far left and far right columns are identical. Column (*d*) is a representative ordering of the energy levels when linear and quadratic Jahn–Teller coupling and spin–orbit coupling is included in the calculation. The left-hand side of the diagram derives the energy levels of (*d*) via addition of the Jahn–Teller terms and then spin–orbit coupling, while the right-hand side takes the opposite approach. They do, however, have a common result in (*d*). The symmetry labels for (*a*)–(*c*) correspond to the irreducible representations of the C_{3v} group while those for (*b*′), (*c*′) and (*d*) are for the double group of C_{3v}.

the C_{3v} point group, they are degenerate because no term in the linear Jahn–Teller Hamiltonian raises the degeneracy.

3.1.2. *Quadratic Jahn–Teller coupling*

Quadratic Jahn–Teller coupling has two effects on the linear Jahn–Teller coupling energy levels (figure 3(*c*)). First, quadratic coupling, which causes the $j = \pm\frac{1}{2}, \pm\frac{5}{2}, \ldots$ levels to mix with the $j = \mp\frac{5}{2}, \mp\frac{1}{2}, \ldots$ levels, reduces the symmetry blocking of the Hamiltonian matrix to only three subblocks. However, by symmetry, the degeneracies of neither the $j = \pm\frac{1}{2}$ nor the $j = \pm\frac{5}{2}$ levels are lifted by $\hat{\mathscr{H}}_{q_{ii}}$. The second, and larger, effect of quadratic coupling is to break the degeneracy of the $j = \pm\frac{3}{2}, \pm\frac{9}{2}, \ldots$ levels into their a_1 and a_2 components. To gauge the magnitude of these two effects, a quadratic Jahn–Teller coupling constant K_i of 0.05 shifts the lowest several $j = \pm\frac{1}{2}$ and $\mp\frac{5}{2}$ levels by less than 5 cm^{-1} each, while it splits the lowest $\pm\frac{3}{2}$ level by 25 cm^{-1}.† While quadratic Jahn–Teller coupling makes a small contribution to the

† This calculation was done with $\omega_{e,i} = 250$ cm^{-1} and $D_i = 0.5$.

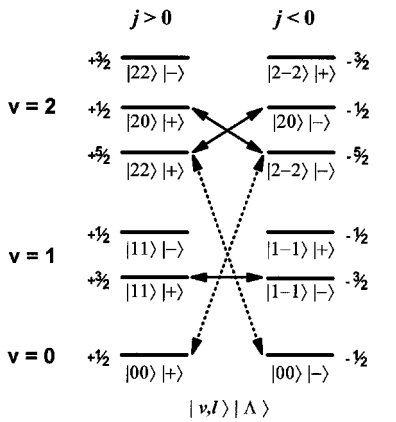

Figure 4. Schematic representation of the matrix elements of $\hat{\mathscr{H}}_{q_{ii}}$, equation (71), $\Delta v_i = \pm 2$ (dotted arrows) and $\Delta v_i = 0$ (solid arrows). The energy levels are shown for the case of linear Jahn–Teller coupling for a single vibrational mode. Arrows are drawn between energy levels that are connected via an off-diagonal matrix element of $\hat{\mathscr{H}}_{q_{ii}}$. Additional matrix elements of $\hat{\mathscr{H}}_{q_{ii}}$ exist between the $v = 1$ and $v = 3$ levels, and between the $v = 2$ and $v = 4$ levels, they are not shown for clarity.

stabilization of the molecule (equation (56)), it can have a huge impact upon the vibronic energy levels, as Hougen [68] first pointed out.

The reason for the disparity in the size of the effect of quadratic coupling on the levels is easily understood by examining the three off-diagonal matrix elements of $\hat{\mathscr{H}}_{q_{ii}}$ (equation (71)) using perturbation theory (figure 4). The matrix elements of equation (71) with $\Delta v_i = \pm 2$ ensures that the energy separation connecting these levels is comparable with twice the harmonic oscillator vibrational frequency of the mode. These two terms are responsible for mixing the $j = \pm\frac{1}{2}$ and $\mp\frac{5}{2}$ levels with each other and for a minor portion of the splitting of the $\pm\frac{3}{2}$ levels. The matrix element of $\hat{\mathscr{H}}_{q_{ii}}$, with a selection rule on v_i of $\Delta v_i = 0$, will have non-zero values between two $j = \pm\frac{3}{2}$ levels that are degenerate under linear Jahn–Teller coupling. Because the energy difference between the two levels connecting these off-diagonal elements is zero, a very small coupling constant K_i can produce a large splitting. $\hat{\mathscr{H}}_{q_{ii}}$ will also have matrix elements between the $j = \pm\frac{1}{2}$ and $\mp\frac{5}{2}$ levels that arise from the same harmonic oscillator level and are therefore close in energy, but not degenerate like the $j = \pm\frac{3}{2}$ levels. The effect of the matrix element on these levels will therefore be smaller than the effect it has on the $j = \pm\frac{3}{2}$ levels, but larger than the effects of the matrix elements with $\Delta v_i = \pm 2$.

We mentioned before that the sign of K_i has an effect on the positions of the local minima and maxima around the moat. The sign of K_i also has an effect on the a_1 and a_2 levels. If the sign of K_i is reversed, the energies of the a_1 and a_2 levels will be reversed. If the symmetries of these $j = \frac{3}{2}$ levels can be determined experimentally, then the phase of the minima and maxima of the PES has also been determined.

3.1.3. *Spin–orbit coupling*

The addition of spin–orbit coupling at first glance appears to double the number of levels, splitting each of them into two spin–orbit components (figure 3(*d*)). While

this is true for all the $j = \pm\frac{1}{2}$ and $\pm\frac{5}{2}$ levels, it is not true for the $\pm\frac{3}{2}$ levels. The $\pm\frac{1}{2}$ and $\pm\frac{5}{2}$ levels are of e symmetry under the C_{3v} point group. For an $S = \frac{1}{2}$ system, the spin function belongs to the $e_{1/2}$ irreducible representation of the C_{3v} spin double group [37, 35]. For the C_{3v} point group, the direct product of the spin function and an e vibronic function is $e_{1/2} \otimes e = e_{1/2} + e_{3/2}$, which shows that each of the $\pm\frac{1}{2}$ and $\pm\frac{5}{2}$ levels is split into two levels. In figure 3, the a_1 and a_2 levels derived from $j = \pm\frac{3}{2}$ levels are not shown to be split by spin–orbit coupling. This apparent lack of spin–orbit coupling in these levels is because in the absence of spin–orbit coupling the levels are of a_1 and a_2 symmetry, which when multiplied by the spin function give only $e_{1/2}$ symmetry. Neither of them can therefore, by symmetry, be split by spin–orbit coupling. However, since the two levels are of the same symmetry under the spin double group, they may be mixed with each other by spin–orbit coupling, causing some levels to shift upon the addition of spin–orbit coupling to the Hamiltonian. If, on the other hand, the quadratic Jahn–Teller effect is sufficiently small to render the a_1 and a_2 levels degenerate, then the effect of significant spin–orbit coupling will be to split the quasidegenerate a_1–a_2 pair in much the same way as it splits the e levels. The exact effects caused by spin–orbit coupling on these levels are determined by the relative sizes of the linear, quadratic and spin–orbit coupling constants, and will be discussed in the next section.

Two other features of the spin–orbit levels need to be pointed out. First, the relative ordering of the two spin–vibronic components $e_{\Omega'}$ ($\Omega' = |\Omega \bmod 3|$), of each $j = \pm\frac{1}{2}$ and $\pm\frac{5}{2}$ pair will be reversed if the sign of a is changed (see equations (18) and (69)). The symmetry labels of the spin–orbit levels of figure 3 are for the case when $a < 0$, which is appropriate for all the methoxy radicals. Second, the relative ordering of the two Ω' components alternates within a given manifold of j as the energies increase. (This is only strictly true for the case of a single active mode without quadratic coupling.) For example, the lowest $j = \frac{1}{2}$ spin–orbit doublet (nominally corresponding to $v_i = 0$) has the $e_{3/2}$ spin–vibronic level lower in energy than the $e_{1/2}$ level, while for the next higher energy doublet, arising from the $v_i = 1$ harmonic oscillator level, $e_{1/2}$ is lower in energy than $e_{3/2}$.† This alternation of symmetry will cause the two components of a spin–orbit doublet to have different spin–vibronic wavefunctions, whereas they are normally assumed to have effectively identical vibronic wavefunctions, with opposite values for Σ. As we shall see in later sections, the differences in the wavefunctions means that the two spin–orbit components will have different Coriolis coupling constants as well as different intensities in the electronic spectra. Understanding the spin–vibronic wavefunctions is very important in the interpretation of the experimentally observed spectra.

The discussion above has progressed across figure 3 from left to right, first linear Jahn–Teller coupling is introduced, then quadratic Jahn–Teller coupling is added, with the final addition being spin–orbit coupling. This is a useful way to derive the energy levels when spin–orbit coupling is small. If, however, spin–orbit coupling is large and dominates the Jahn–Teller coupling, it may be more useful first to

† Here, we refer to the spin–vibronic symmetry $e_{1/2}$ or $e_{3/2}$, which can often be experimentally determined from the rotational spectrum. This is not to be confused with the symmetry of the spin–electronic states $^2E_{1/2}$ and $^2E_{3/2}$, which correspond to when $\langle \hat{L}_z \rangle$ and $\langle \hat{S}_z \rangle$ are antiparallel and parallel to each other respectively.

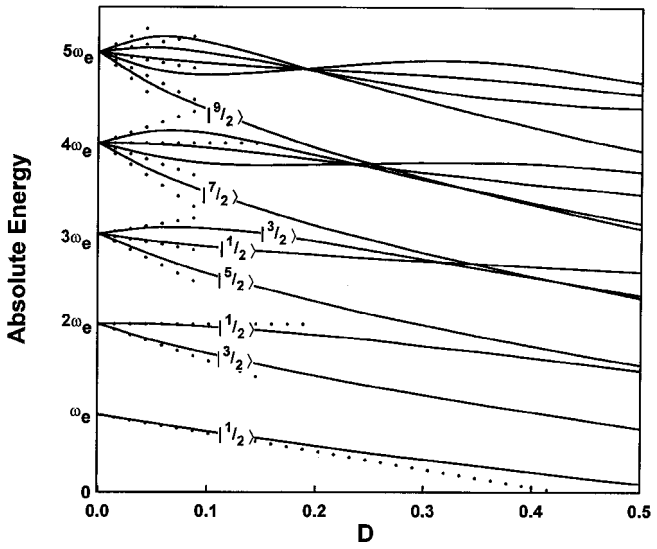

Figure 5. Absolute energies of the vibronic levels for linear Jahn–Teller coupling in a single active mode over the range from $D_i = 0$ to $D_i = 0.5$. The ordinate scale is in units of $\omega_{e,i}$ while the abscissa is the dimensionless linear Jahn–Teller coupling constant D_i. The dotted lines are the energies calculated via the approximation of equation (78). The labels on the lines refer to j. Levels with different j may cross, since with only linear Jahn–Teller coupling there are no terms in $\hat{\mathscr{H}}$ that connect different j states.

add spin–orbit coupling to the harmonic oscillator, followed by linear Jahn–Teller coupling and quadratic Jahn–Teller coupling, as the right-hand side of figure 3 shows. Either way, the vibronic energy levels of the central column of figure 3 are the same but, depending upon the situation, one or the other thought process used to derive them may be more pedagogical.

3.2. *Quantitative calculations of the vibronic energy levels*

3.2.1. *Linear Jahn–Teller coupling*

As usual in quantum mechanics, the quantification of the energies for a Jahn–Teller system must come from the diagonalization of the entire matrix. The ordering of the energy levels is a complex function of the various coupling constants. For linear and quadratic coupling, the results have been presented previously in many places. Approximate formulae have also been presented previously to estimate the spin–orbit splitting of each level, without explicitly including a spin–orbit term in the Hamiltonian. We shall first review this work and then evaluate it from the perspective of the inclusion of spin–orbit coupling directly in the Hamiltonian.

Figures 5 and 6 show the calculated linear Jahn–Teller coupling vibronic energy levels for two different regimes of D_i. Each of them show that, at small values of D_i, oscillations of the energy levels make generalizations about the patterns difficult. However, simple formulae for the limiting cases of very small and very large Jahn–Teller coupling have been derived previously using perturbation theory.

In the limit of small Jahn–Teller coupling, Child [69] used second-order perturbation theory to derive the energy levels of a single Jahn–Teller active mode:

$$E(v_i, l_i) = \omega_{e,i}(v_i + 1) \mp 2D_i\omega_{e,i}(l_i \pm 1). \tag{78}$$

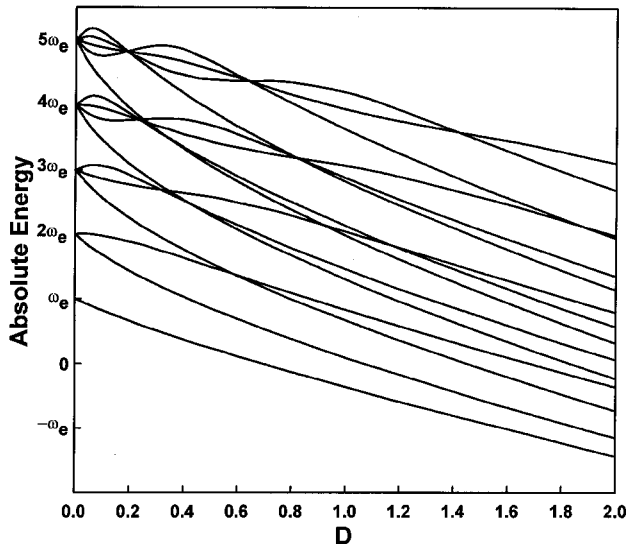

Figure 6. Absolute energies of the vibronic levels for linear Jahn–Teller coupling in a single active mode over the range from $D_i = 0$ to $D_i = 2.0$. The ordinate scale is in units of $\omega_{e,i}$ while the abscissa is the dimensionless linear Jahn–Teller coupling constant D_i.

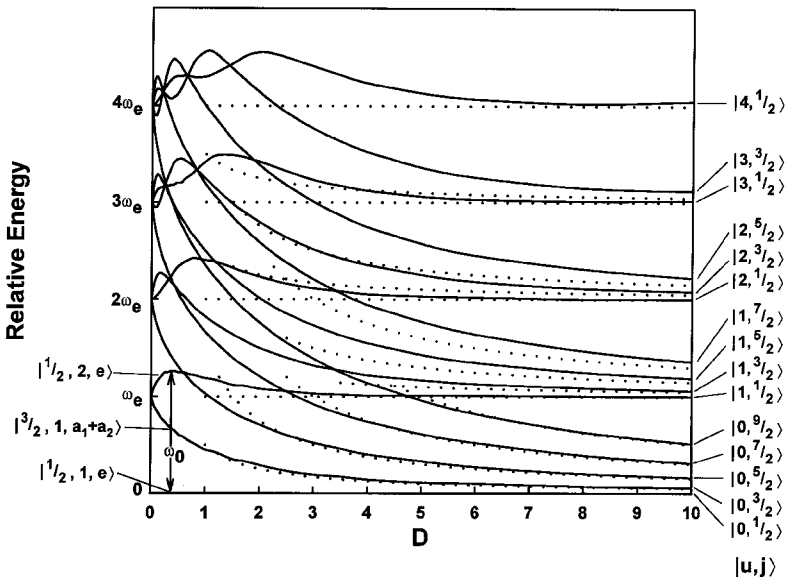

Figure 7. Relative energies of the vibronic levels for linear Jahn–Teller coupling in a single active mode over the range from $D_i = 0$ to $D_i = 10.0$. The ordinate scale is in units of $\omega_{e,i}$ while the abscissa is the dimensionless linear Jahn–Teller coupling constant D_i, with the zero of energy set as the energy of the lowest level. On the right-hand side the energy levels are labelled $|u_i, j\rangle$, equation (79). The dotted lines are the energies calculated via the approximation of equation (79).

Under small Jahn–Teller coupling, the harmonic oscillator energy levels are split according to their values of l_i, with each value of l_i giving rise to two levels, except for $l_i = 0$. Child proposed that this formula is a reasonably good formula up to $D_i \lesssim 0.05$, which is a very small value for a Jahn–Teller coupling constant. In figure 5, we compare the validity of equation (78) against numerical calculations. For the lowest few levels, equation (78) is a reasonably good approximation up to approximately $D_i = 0.1$, while at higher energies the approximation is valid only for smaller values of D_i. Despite its shortcomings, the use of equation (78) may be a good starting point for a more complete analysis even in a system that has a relatively large value of D_i.

Figure 7 shows that, as D_i increases, the vibronic energy levels converge to the strong coupling limit, where ultimately the energies can be described well by the formula [31]

$$E(u_i, j) = -D_i\omega_{e,i} + (u_i + \tfrac{1}{2})\omega_{e,i} + \frac{\omega_{e,i}j^2}{4D_i}, \tag{79}$$

where a new quantum number u_i has been introduced that can take any non-negative integer value, independent of j. From figure 7, it can be seen that this formula holds true only for large values of D_i. Physically this situation corresponds to an uncoupled stretching motion along the radial coordinate ρ_i of equation (12), characterized by the quantum number u_i, while the continuously good quantum number j characterizes the unhindered pseudo-rotation motion in the angular coordinate ϕ_i.

Between these two limits, one must resort to the exact calculation of the energy levels using the complete Hamiltonian and a large basis set, as shown in figures 6 and 7. Figure 7 is a more useful diagram when examining the spectroscopy of these levels. Because the lowest energy vibronic level, denoted $\left|\tfrac{1}{2}, 1, e\right\rangle$ in the notation of equation (75), is the zero-point energy level of the molecule, the differences between its energy and the other energy levels will be the energies measured in spectroscopic experiments. In particular, two common techniques, laser-induced fluorescence (LIF) and infrared absorption, most often observe the second $j = \pm\tfrac{1}{2}$ level ($\left|\tfrac{1}{2}, 2, e\right\rangle$, figure 7). The energy difference between these two levels is the fundamental transition frequency $\omega_{0,i}$ of the vibrational mode. However, as figure 7 shows, this energy difference will be greater than the equilibrium vibrational frequency $\omega_{e,i}$. This holds true even when spin–orbit coupling is included in the calculation, provided that the spin–orbit coupling splitting of the electronic potential is not larger than the harmonic frequency of the vibrational mode. The difference between the two frequencies $\omega_{e,i}$ and $\omega_{0,i}$ is governed by the magnitude of D_i. In many published papers of the spectroscopy of Jahn–Teller active states, $\omega_{0,i}$ is given as the vibrational frequency of the Jahn–Teller active modes. In the limit of very weak Jahn–Teller coupling, $\omega_{0,i}$ and $\omega_{e,i}$ will be comparable with each other, but figure 6 shows that even a relatively small D_i can cause $\omega_{0,i}$ to be greater than $\omega_{e,i}$ by 25% or more. A true description of the vibrational structure of a Jahn–Teller active molecule must include both $\omega_{e,i}$ and D_i. While the value of $\omega_{0,i}$ is useful, by itself it is not an accurate representation of the vibrational potential of the molecule.

3.2.2. *Linear Jahn–Teller coupling with spin–orbit coupling*

Nearly all Jahn–Teller calculations in the literature have added spin–orbit coupling to the linear Jahn–Teller Hamiltonian 'after the fact' via a formula initially derived by Child and Longuet-Higgins [31]. The formula is derived by taking the ex-

pectation value of $\hat{\mathscr{H}}_{\mathrm{SO}}$ for the vibronic eigenfunction, computed without including $\hat{\mathscr{H}}_{\mathrm{SO}}$ in the Hamiltonian:

$$\begin{aligned}
\langle\Sigma|\langle j,n_j,\alpha|\,\hat{\mathscr{H}}_{\mathrm{SO}}\,|j,n_j,\alpha\rangle|\Sigma\rangle &= \langle\Sigma|\langle j,n_j,\alpha|\,a\hat{L}_z\hat{S}_z\,|j,n_j,\alpha\rangle|\Sigma\rangle \\
&= \Sigma\,\langle j,n_j|\,a\hat{L}_z\,|j,n_j\rangle \\
&= \Sigma\sum_i\left(c_{i,n_j}\,\langle\Lambda_i|\prod_{m=1}^{p}\langle v_{m,i},l_{m,i}|\right)a\hat{L}_z \\
&\quad\times\sum_{i'}\left(c_{i',n_j}\,|\Lambda_{i'}\rangle\prod_{m=1}^{p}|v_{m,i'},l_{m,i'}\rangle\right) \\
&= \Sigma\sum_i c_{i,n_j}^2\,\langle\Lambda_i|\,a\hat{L}_z\,|\Lambda_i\rangle \\
&= \Sigma\sum_i a\zeta_e\Lambda_i c_{i,n_j}^2 \\
&= a\zeta_e d_{j,n_j}\Sigma, \qquad (80)
\end{aligned}$$

where $d_{j,n_j} = \sum_i \Lambda_i c_{i,n_j}^2$. The parameter d_{j,n_j} is often called the Ham [29, 59] reduction factor and is usually not given with subscripts. However, because each vibronic level has a unique value of d, we feel that it is appropriate to assign subscripts to this parameter to identify the eigenfunction to which it corresponds. The values that d_{j,n_j} may take range from -1 to $+1$, corresponding respectively to the limits $\Lambda = -1$ and $\Lambda = +1$, and are strongly dependent on the vibrational parameters of the system. These limits are reached for zero Jahn–Teller distortion, because in that case only one c_{i,n_j} is non-zero and hence must be unity. For a large Jahn–Teller effect the sum of the squares of the coefficients for $\Lambda = +1$ will be approximately equal to those for $\Lambda = -1$, and hence d_{j,n_j} approaches zero.

The approximate spin–orbit splitting $\Delta E_{j,n_j}^{\mathrm{SO}}$ of the n_jth energy level of the jth symmetry block is

$$\Delta E_{j,n_j}^{\mathrm{SO}} = E_{j,n_j,\Sigma=+1/2} - E_{j,n_j,\Sigma=-1/2} = a\zeta_e d_{j,n_j}. \qquad (81)$$

There are several key features to be gleaned from equations (80) and (81). First, d_{j,n_j} is always less than unity so that spin–orbit coupling is always quenched to some extent by the presence of linear Jahn–Teller coupling. (However, when there is non-zero quadratic Jahn–Teller coupling, the apparent spin–orbit splitting can appear for some levels to not be quenched, or even enhanced, as will be discussed in the next section.) Second, each and every vibronic energy level has a *different* spin–orbit splitting. While $a\zeta_e$ is the product of two molecular parameters for the given electronic state, d_{j,n_j} is different for each vibronic energy level. In general, as j and n_j increase, the magnitude of d_{j,n_j} decreases and the spin–orbit splitting is quenched. Likewise, as the Jahn–Teller mixing increases, D_i increases and the magnitude of d_{j,n_j} decreases for all the energy levels and the spin–orbit coupling is decreased by Jahn–Teller coupling.

Under linear Jahn–Teller coupling only, every vibronic energy level is doubly degenerate, with the two components differing by the sign of j. The two j components differ in the signs of l_i, Λ and Σ for each basis function (equation (76)) but, because of their degeneracy, they will have identical expansion coefficients $c_{i,n_j,\Sigma} = c_{i,n-j,-\Sigma}$. Therefore, if one component has the quenching parameter d_{j,n_j}, it follows from equation (80) that the quenching parameter $d_{-j,n-j}$, for the other component will be

equal in magnitude but opposite in sign:

$$d_{j,n_j} = -d_{-j,n_{-j}}. \tag{82}$$

Because the degeneracy of the levels is independent of the magnitude of the coupling constants, we shall restrict our discussion to only one of the components of the degenerate energy level and assume j to be positive.

If only a single mode is Jahn–Teller active, the sign of d_{j,n_j} alternates with n_j for a given value of j. (This result follows from the fact that, since $l = j - \Lambda/2$ for C_{3v} symmetry and the allowed values of l change from even to odd with alternating n_j, Λ must change sign to preserve j.) According to equation (81), if d_{j,n_j} changes sign, the spin–orbit splitting $\Delta E_{j,n_j}$ must change sign, as $a\zeta_e$ is a constant, and the spin–orbit doublet will be inverted. Therefore, the sign of d_{j,n_j} is reflected in the ordering of the symmetries of the spin–orbit doublet, that is whether the $e_{1/2}$ component or the $e_{3/2}$ component is lower in energy (figures 3(d) and (b')), consistent with our earlier comment that the ordering of the Ω components alternate with j. Experimentally, the symmetry of each component of the spin–orbit doublet can be determined if the rotational levels have been resolved. The symmetry label $e_{\Omega'}$ (which for the present case is $e_{1/2}$ or $e_{3/2}$) is derived from the value of $\Omega = \Lambda - l_t + \Sigma$ (for the present case, $|\Omega \bmod 3| = \Omega'$). The '$\Omega'$' of $e_{\Omega'}$ is the minimum value that J may have for a given spin–vibronic state (see section 4 for more details about the rotational quantum numbers and energy levels). Simulation of the Q and R branches of a rotationally resolved spectrum will clearly distinguish between the value of J_{min}, and therefore Ω', for the level. (Even when full rotational resolution is not achieved, the 'rotational contours' may suffice to distinguish the $e_{1/2}$ and $e_{3/2}$ components because the Coriolis coupling of the two components may be quite different as well as have distinctive intensity patterns.) Because of the alternation of the sign of d_{j,n_j}, the $v = 0$ spin–orbit doublet will have $e_{1/2}$ lower in energy than the $e_{3/2}$ component for $a > 0$, while the $v = 1$, $j = \frac{1}{2}$ doublet will have the reverse. An example of this inversion of the spin–orbit doublet is the rotationally resolved spectra of the origin and 6^1 bands of the $\tilde{A}\,^2E \leftrightarrow \tilde{X}\,^2A_1$ transition in $MgCH_3$ [70].

In the limit of small linear Jahn–Teller coupling, Child [69] used perturbation theory to derive simple formulae for the estimation of d_{j,n_j} for a single Jahn–Teller active mode:

$$d_{j,n_j} = \mp 1 \pm 4D_i(v_i + 1) \quad \text{for } j = l_i \mp \tfrac{1}{2}. \tag{83}$$

Even at a very small value of $D_i = 0.05$, $d_{1/2,1}$ has already decreased to 0.8 from 1, its value in the absence of Jahn–Teller coupling. This means that molecular spin–orbit coupling has been reduced to 80% of what its value would be in the absence of Jahn–Teller coupling, even though the Jahn–Teller effect has stabilized the molecule by only $0.05\omega_{e,i}$. It should be emphasized that equation (83) is only valid in the limit of small linear Jahn–Teller coupling, and in the absence of any quadratic Jahn–Teller coupling. Nonetheless, it clearly indicates how rapidly even small geometric distortions caused by Jahn–Teller effects can quench the spin–orbit splittings.

With the inclusion of spin–orbit coupling directly in the Hamiltonian, we are now in a position to address the accuracy of equation (81) for the spin–orbit splitting of the vibronic levels of a Jahn–Teller system. Figure 8 shows the calculated energy levels from the diagonalization of the full spin–vibronic Hamiltonian. At relatively small values of $a\zeta_e$, the approximation of equation (81) is reasonably good, as shown by the dotted lines in figure 8. However, as $a\zeta_e$ is increased, the

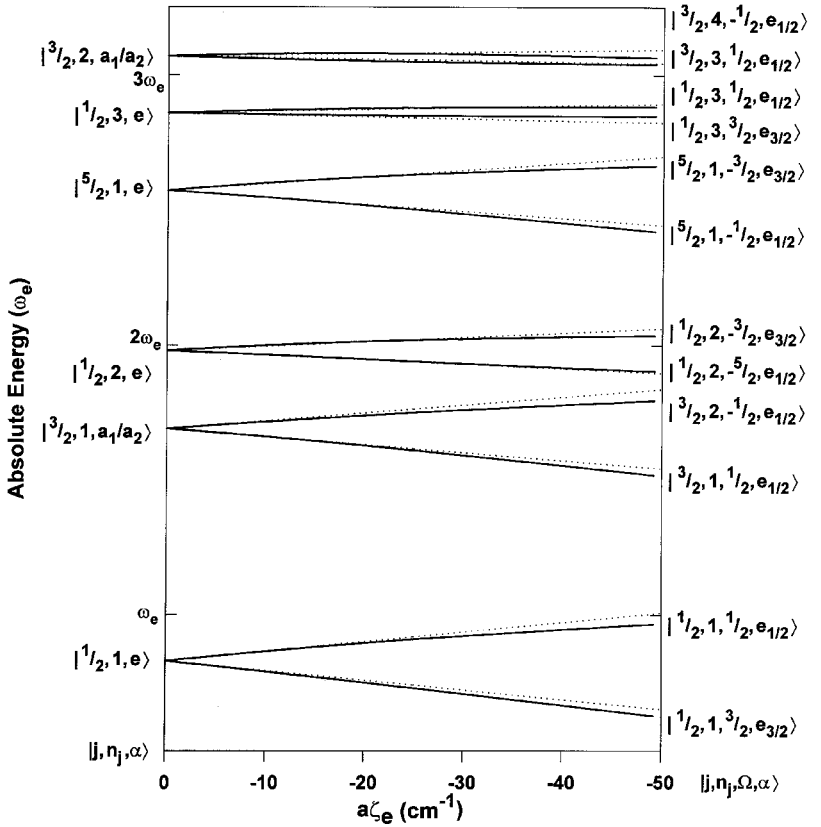

Figure 8. Calculated absolute energy levels for a ^{2}E state of C_{3v} symmetry including linear Jahn–Teller coupling and spin–orbit coupling for a single Jahn–Teller active mode for values of $a\zeta_e < \omega_e$. The solid lines are energy levels calculated including $\hat{\mathscr{H}}_{SO}$ in the Hamiltonian while the dotted lines are those calculated using equation (80). The energy levels were calculated assuming $D_i = 0.25$ and $\omega_{e,i} = 100$ cm^{-1} and varying $a\zeta_e$. Note that if $\Omega \bmod 3 = \pm\frac{1}{2}$, the basis function transforms as $e_{1/2}$, otherwise it transforms as $e_{3/2}$.

necessity of performing the complete calculation becomes clear as the deviations between the approximation and reality become large as figure 9 shows. The reason for the deviation is obvious from figure 9, the addition of spin–orbit coupling to the Hamiltonian properly describes the avoided crossings of states of the same symmetry under the spin double group. As spin–orbit coupling begins to quench the Jahn–Teller coupling (the right-hand side of figure 9), the vibrational spacings of a harmonic oscillator for a pair of $^2E_{3/2}$ and $^2E_{1/2}$ electronic states begin to be recovered. Note, however, that Jahn–Teller coupling still has two significant effects on the energy levels: the vibrational spacing has yet to recover its harmonic value (100 cm^{-1} in this example) and the individual v_i levels are still split according to their l_i values, much as they are in the absence of spin–orbit coupling.

The energy levels are plotted in figure 10 relative to the energy of the lowest level, which makes it a more useful figure for spectroscopy. Figures 9 and 10 clearly show that the quantitative calculation of the spin–vibronic energy levels must be

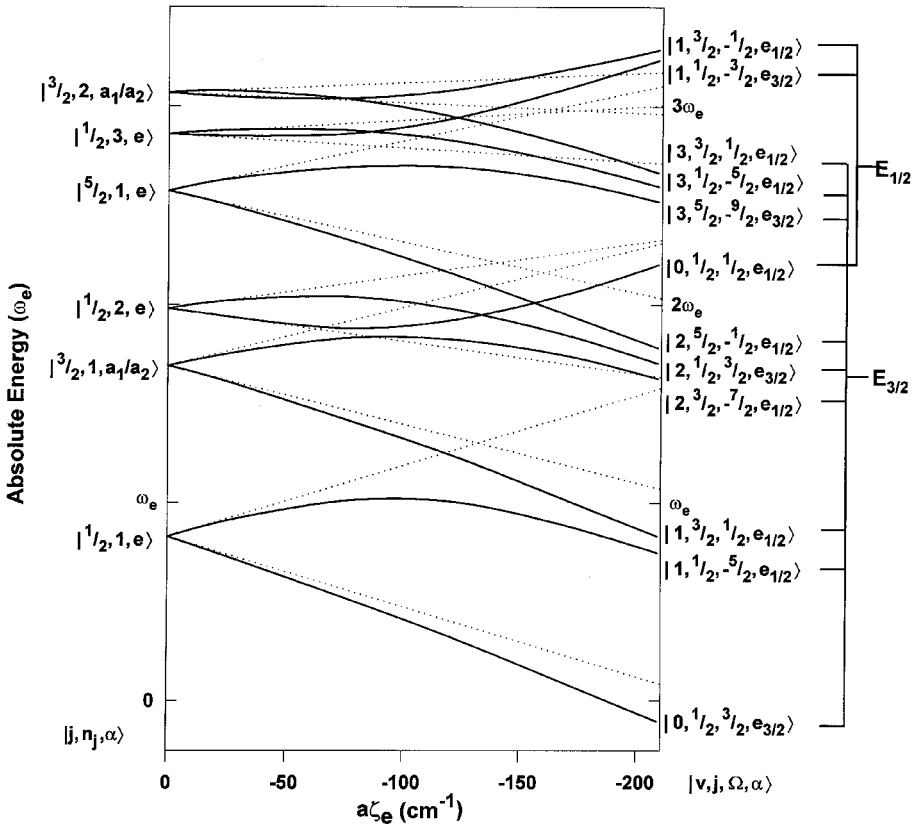

Figure 9. Calculated absolute energy levels for a ^{2}E state of C_{3v} symmetry including linear Jahn–Teller coupling and spin–orbit coupling for a single Jahn–Teller active mode for values of $a\zeta_e < \omega_e$ to $a\zeta_e > \omega_e$. The solid lines are energy levels calculated including $\hat{\mathscr{H}}_{SO}$ in the Hamiltonian while the dotted lines are those calculated using equation (80). The energy levels were calculated assuming $D_i = 0.25$ and $\omega_{e,i} = 100$ cm^{-1} and varying $a\zeta_e$. Note that if $\Omega \bmod 3 = \pm\frac{1}{2}$, the basis function transforms as $e_{1/2}$, otherwise it transforms as $e_{3/2}$.

done with the entire spin–orbit Jahn–Teller Hamiltonian. This also means that the eigenfunction must be calculated using a basis set of the form of equation (74) rather than equation (75). The most important ramification of the change in the wavefunctions is that the two components of a spin–orbit doublet may be significantly different using the basis of equation (74). Figure 11 illustrates how this may happen in the case of linear Jahn–Teller coupling with spin–orbit coupling. Because of the alternation of the symmetry of the levels under the spin-double group, the two spin components will have significantly different Jahn–Teller couplings. Therefore, the spin–vibronic wavefunctions will be quite different. We shall see in later sections that the different vibronic characters of the two spin–orbit components of a level causes intensity variations between them in electronic spectra as well as causing them to have different effective rotational parameters.

In figures 9 and 10, and in all the figures so far, avoided crossings of the levels are a dominant feature. However, there are also a large number of allowed crossings

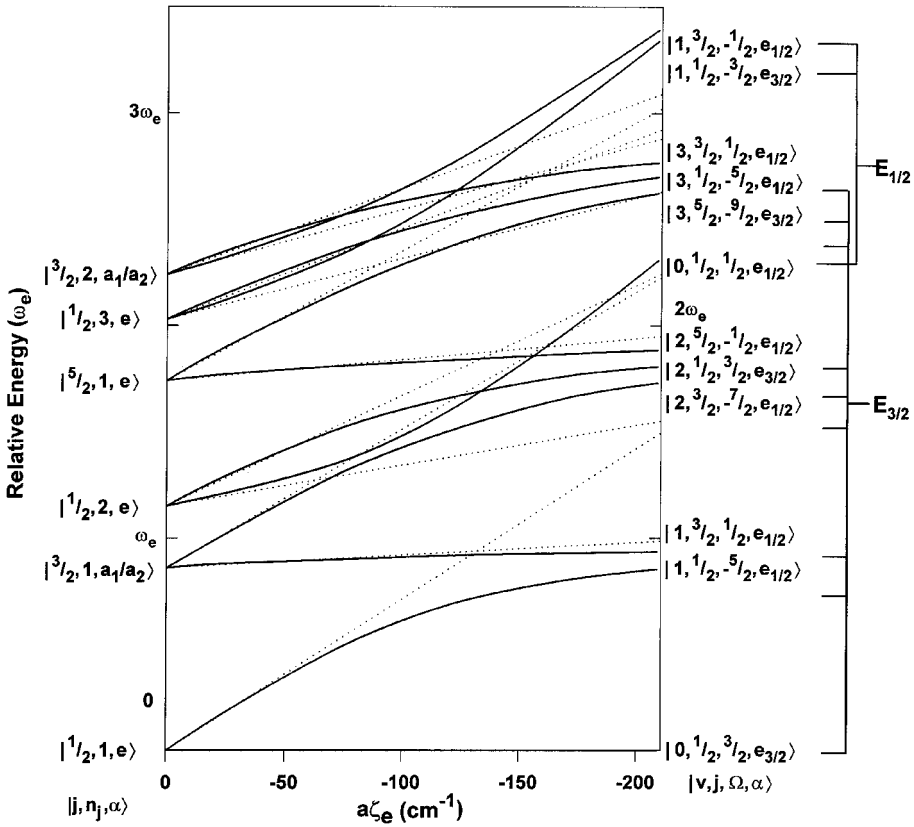

Figure 10. Calculated relative energy levels for a ^{2}E state of C_{3v} symmetry including linear Jahn–Teller coupling and spin–orbit coupling for a single Jahn–Teller active mode. The solid lines are energy levels calculated including $\hat{\mathscr{H}}_{SO}$ in the Hamiltonian while the dotted lines are those calculated using equation (80). The energy levels were calculated assuming $D_i = 0.25$ and $\omega_{e,i} = 100\ \text{cm}^{-1}$ and varying $a\zeta_e$. Note that if $\Omega \bmod 3 = \pm\frac{1}{2}$, the basis function transforms as $e_{1/2}$, otherwise it transforms as $e_{3/2}$.

of the levels. Of significant importance is whether a crossing will be allowed or avoided. In the Hamiltonian, limited to only *linear* Jahn–Teller coupling that we have considered so far, there are two good quantum numbers j and Σ. Two levels will be allowed to cross as long as they differ in at least one of these quantities. When quadratic Jahn–Teller coupling is present, two levels will be allowed to cross as long as they differ in at least one of the quantities (j and $j^{(2)}$) or Σ.

3.2.3. *Quadratic Jahn–Teller coupling with spin–orbit coupling*

As mentioned earlier, modest quadratic Jahn–Teller coupling has a minor effect on most of the levels but a large effect on the $j = \pm\frac{3}{2}$ levels (figure 12). Quadratic Jahn–Teller coupling breaks the degeneracy of the $\pm\frac{3}{2}$ levels into two components, one each of a_1 and a_2 symmetry. Spin–orbit coupling does not further split these, as discussed previously, but instead mixes them together and shifts them (figures 12(*b*) and (*c*)). The amount of mixing can be ascertained by examination of the calculated wavefunctions for each level. In the absence of spin–orbit coupling, the two leading

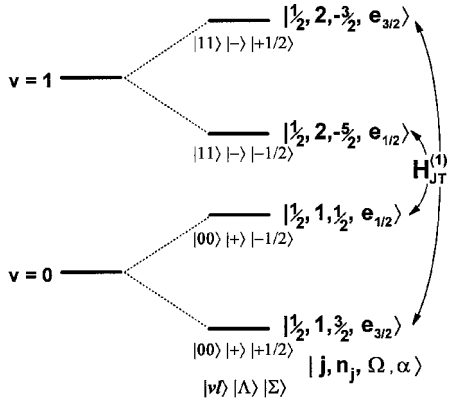

Figure 11. Illustration of the non-vanishing matrix elements of the linear Jahn–Teller Hamiltonian, $\hat{\mathscr{H}}_{\mathrm{JT}}^{(1)}$, when the spin–orbit coupling contribution, $\hat{\mathscr{H}}_{\mathrm{SO}}$, is included. For simplicity, only the $j = +\frac{1}{2}$ levels from $v = 0$ and $v = 1$ are shown and $a\zeta_e$ is assumed to be negative.

terms in the wavefunctions $|j, n_j, \alpha\rangle |\Sigma\rangle$ of the two lowest levels are

$$\left|\tfrac{3}{2}, 1, a_2\right\rangle |\Sigma\rangle = \left[|a_2\rangle = c_1 \{|11\rangle |+\rangle - |1\,-1\rangle |-\rangle\} + c_2 \cdots\right] |\Sigma\rangle \tag{84}$$

and

$$\left|-\tfrac{3}{2}, 1, a_1\right\rangle |\Sigma\rangle = \left[|a_1\rangle = c_1 \{|11\rangle |+\rangle + |1\,-1\rangle |-\rangle\} + c_2 \cdots\right] |\Sigma\rangle. \tag{85}$$

After spin–orbit coupling is introduced, the two wavefunctions can be described to a good approximation by

$$\left|\tfrac{3}{2}, 1\right\rangle |\Sigma\rangle = \left[c_1' |a_2\rangle + c_2' |a_1\rangle\right] |\Sigma\rangle \tag{86}$$

and

$$\left|-\tfrac{3}{2}, 1\right\rangle |\Sigma\rangle = \left[c_1' |a_2\rangle - c_2' |a_1\rangle\right] |\Sigma\rangle. \tag{87}$$

These equations are valid if the mixing is caused by the $\Delta v_i = 0$ perturbation of equation (71) only. If the other two matrix elements of $\hat{\mathscr{H}}_{q_{ii}}$ mix in appreciable amounts of other levels, as will happen with larger values of K_i, then equations (86) and (87) begin to break down. The relative value of the squares of c_1' and c_2', which can be obtained from the computed wavefunction, gives the percentage composition of each of the spin–orbit components of the $\pm\frac{3}{2}$ levels. Figures 12(*b*) and (*c*) show the results of these calculations for an example system. Note that, although the energies of $\left|\frac{3}{2}, 1, \Sigma\right\rangle$ and $\left|-\frac{3}{2}, 1, \Sigma\right\rangle$ levels change as $a\zeta_e$ increases, the difference between their two energies remains relatively constant, but the a_1 and a_2 character of each changes significantly, approaching equal admixtures at large $a\zeta_e$.

3.2.4. *Mode mixing*

While the Jahn–Teller Hamiltonian (13) does not include any off-diagonal matrix elements that are non-diagonal in more than one mode, Jahn–Teller coupling does mix the levels of each active mode with the others. Figure 13 illustrates how, for a two-mode case, the $v_1 = 1$ level is mixed with the $v_2 = 1$ level, even though all matrix elements directly connecting them are zero. They each have non-zero matrix elements with the vibrationless level ($v_1 = v_2 = 0$), and with the $v_1 = v_2 = 1$ level.

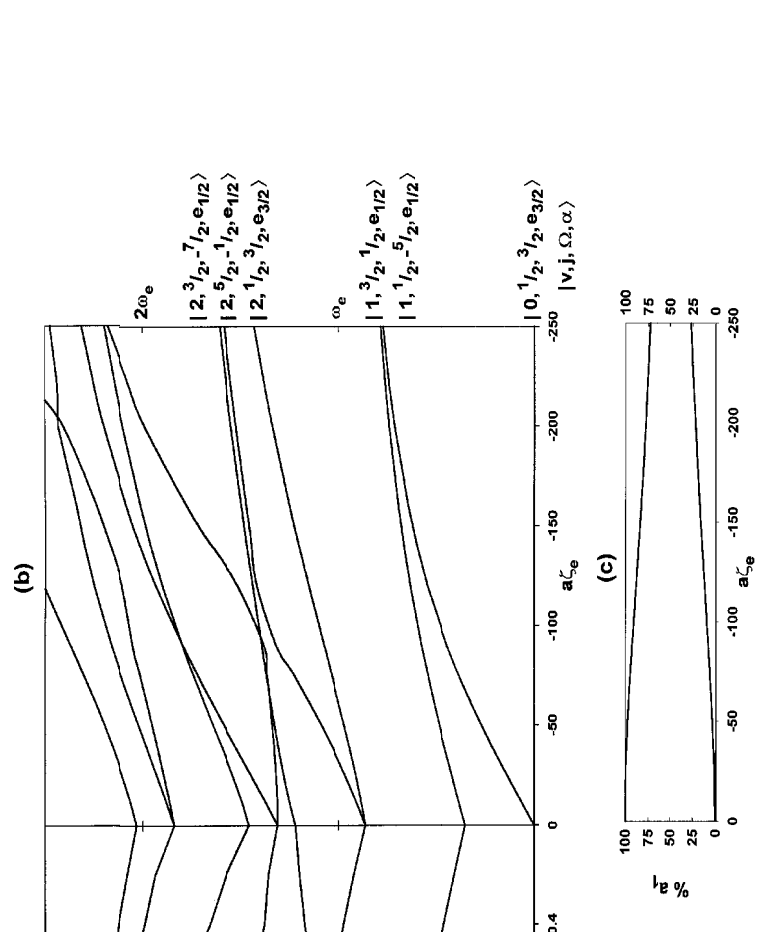

Figure 12. (*a*) Vibronic energy levels including quadratic and linear Jahn–Teller coupling. The levels were calculated for $D_i = 0.1$ and $\omega_{e,i} = 100\ \text{cm}^{-1}$ and varying K_i from 0 to 0.5. (*b*) Vibronic energy levels including quadratic and linear Jahn–Teller coupling and spin–orbit coupling. The curves were calculated for $D_i = 0.1$, $\omega_{e,i} = 100\ \text{cm}^{-1}$, $K_i = 0.5$, and varying $a\zeta_e$ from 0 to $-250\ \text{cm}^{-1}$. The zero of energy for (*a*) and (*b*) is the lowest vibronic energy level. (*c*) Approximate percentage composition ($100c_{a_1}^2$) of the two lowest $j = \pm\frac{3}{2}$ levels, as given by equations (86) and (87).

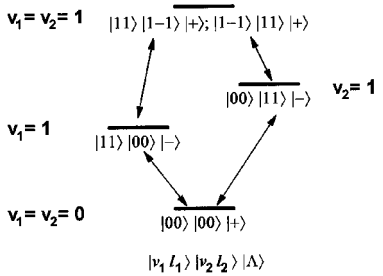

Figure 13. Illustration of the matrix elements, represented by the arrows, that connect the $v_i = 1$ level with $v_{i'} = 1$. The level with $v_i = v_{i'} = 1$ is degenerate and both of its components are shown to illustrate the matrix elements. For convenience, only the $j = \frac{1}{2}$ levels are shown.

Therefore, the Jahn–Teller coupling of one mode indirectly affects the energy of the other level. While this effect has been illustrated for the $v_1 = v_2 = 1$ levels, it exists for all levels.

The impact of mode mixing on the calculation of the vibronic energy levels can be significant for even modest Jahn–Teller effects. Table 4 shows the effects of including two vibrational modes in a single multi-mode calculation. The first two pairs of columns are the results of two independent single-mode calculations, with $\omega_{e,1} = 300\ cm^{-1}$, $D_1 = 0.25$, $\omega_{e,2} = 500\ cm^{-1}$ and $D_2 = 0.25$. The third pair of columns are the energies of these levels from these two calculations and their combinations. For comparison, the final two columns contain the energy levels calculated when both modes are included in the basis set. The most significant result from these calculations is that mode mixing changes the energies enough to necessitate the inclusion of both modes in the calculation simultaneously. As the Jahn–Teller coupling of any of the modes increases, the effects of mode mixing will also increase. In the example in table 4, errors as great as $73\ cm^{-1}$ are seen in the two single-mode calculations compared with the exact two-mode calculation while the rms error is $26\ cm^{-1}$, clearly non-trivial amounts. Therefore, if there is more than one Jahn–Teller active mode in the molecule, one must do a multimode calculation if the energies of the system are to be calculated properly. Furthermore, if spin–orbit coupling is not negligibly small, a multimode calculation including spin–orbit coupling in the Hamiltonian must be performed if spectroscopic accuracy is hoped to be achieved with the calculation.

4. Jahn–Teller effects on the rotational energy levels

Up to this point, we have treated only the spin–vibronic portion of the Hamiltonian and have ignored the rotational energy levels. However, given adequate spectroscopic resolution the vibronic levels may be rotationally resolved, in which case the values of the parameters in the rotational Hamiltonian may give insight to the Jahn–Teller coupling of the molecule. Similarly, Jahn–Teller effects can have rather profound, but generally poorly understood, effects upon the rotational structure.

The rovibronic structure of ^{2}E states has been well studied. Child and Longuet-Higgins [31] laid the theoretical framework, which Child [69, 71] Brown [34], Russell and Radford [72, 73], Endo *et al.* [74], Hougen [35] and Watson [36] elaborated. The last two papers are of particular interest to the current work, as they provide

Table 4. Energy levels, up to 1000 cm^{-1}, for an example two-mode system.[a]

v_1 only		v_2 only		v_1 only + v_2 only		v_1 and v_2 simultaneously	
$\lvert j_1, n_{j_1}, \alpha\rangle$	$E_{j_1,n_{j_1}}$	$\lvert j_2, n_{j_2}, \alpha\rangle$	$E_{j_2,n_{j_2}}$	$\lvert j_1, n_{j_1}, \alpha\rangle + \lvert j_2, n_{j_2}, \alpha\rangle$	$E_{j_1,n_{j_1}} + E_{j_2,n_{j_2}}$	$\lvert j, n_j, \alpha\rangle$	E_{j,n_j}
$\lvert \frac{1}{2}, 1, e\rangle$	0	$\lvert \frac{1}{2}, 1, e\rangle$	0	$\lvert \frac{1}{2}, 1, e\rangle + \lvert \frac{1}{2}, 1, e\rangle$	0	$\lvert \frac{1}{2}, 1, e\rangle$	0
$\lvert \frac{3}{2}, 1, a_1 + a_2\rangle$	222			$\lvert \frac{3}{2}, 1, a_1 + a_2\rangle + \lvert \frac{1}{2}, 1, e\rangle$	222	$\lvert \frac{3}{2}, 1, a_1 + a_2\rangle$	214
$\lvert \frac{1}{2}, 2, e\rangle$	373			$\lvert \frac{1}{2}, 2, e\rangle + \lvert \frac{1}{2}, 1, e\rangle$	373	$\lvert \frac{1}{2}, 2, e\rangle$	335
		$\lvert \frac{3}{2}, 1, a_1 + a_2\rangle$	369	$\lvert \frac{1}{2}, 1, e\rangle + \lvert \frac{3}{2}, 1, a_1 + a_2\rangle$	369	$\lvert \frac{3}{2}, 2, a_1 + a_2\rangle$	423
$\lvert \frac{5}{2}, 1, e\rangle$	460			$\lvert \frac{5}{2}, 1, e\rangle + \lvert \frac{1}{2}, 1, e\rangle$	460	$\lvert \frac{5}{2}, 1, e\rangle$	449
		$\lvert \frac{1}{2}, 2, e\rangle$	621	$\lvert \frac{3}{2}, 1, a_1 + a_2\rangle + \lvert \frac{3}{2}, 1, a_1 + a_2\rangle$	591	$\lvert \frac{1}{2}, 3, e\rangle$	518
$\lvert \frac{1}{2}, 3, e\rangle$	644			$\lvert \frac{1}{2}, 1, e\rangle + \lvert \frac{1}{2}, 2, e\rangle$	621	$\lvert \frac{1}{2}, 4, e\rangle$	619
				$\lvert \frac{1}{2}, 3, e\rangle + \lvert \frac{1}{2}, 1, e\rangle$	644	$\lvert \frac{5}{2}, 2, e\rangle$	651
$\lvert \frac{3}{2}, 2, a_1 + a_2\rangle$	673			$\lvert \frac{3}{2}, 2, a_1 + a_2\rangle + \lvert \frac{1}{2}, 1, e\rangle$	673	$\lvert \frac{3}{2}, 3, a_1 + a_2\rangle$	655
				$\lvert \frac{1}{2}, 2, e\rangle + \lvert \frac{3}{2}, 1, a_1 + a_2\rangle$	742	$\lvert \frac{1}{2}, 5, e\rangle$	748
		$\lvert \frac{5}{2}, 1, e\rangle$	766	$\lvert \frac{1}{2}, 1, e\rangle + \lvert \frac{5}{2}, 1, e\rangle$	766	$\lvert \frac{3}{2}, 4, a_1 + a_2\rangle$	768
				$\lvert \frac{3}{2}, 1, a_1 + a_2\rangle + \lvert \frac{1}{2}, 2, e\rangle$	843	$\lvert \frac{1}{2}, 6, e\rangle$	840
				$\lvert \frac{5}{2}, 1, e\rangle + \lvert \frac{3}{2}, 1, a_1 + a_2\rangle$	849	$\lvert \frac{5}{2}, 3, e\rangle$	848
				$\lvert \frac{5}{2}, 1, e\rangle + \lvert \frac{3}{2}, 1, a_1 + a_2\rangle$	849	$\lvert \frac{3}{2}, 5, a_1 + a_2\rangle$	879
$\lvert \frac{1}{2}, 4, e\rangle$	949			$\lvert \frac{1}{2}, 4, e\rangle + \lvert \frac{1}{2}, 1, e\rangle$	949	$\lvert \frac{1}{2}, 7, e\rangle$	947
$\lvert \frac{5}{2}, 2, e\rangle$	947			$\lvert \frac{5}{2}, 2, e\rangle + \lvert \frac{1}{2}, 1, e\rangle$	947	$\lvert \frac{5}{2}, 4, e\rangle$	948
$\lvert \frac{3}{2}, 3, a_1 + a_2\rangle$	959			$\lvert \frac{3}{2}, 3, a_1 + a_2\rangle + \lvert \frac{1}{2}, 1, e\rangle$	959	$\lvert \frac{3}{2}, 6, a_1 + a_2\rangle$	969

[a]Parameters used in the calculations: $\omega_{e,1} = 300\ cm^{-1}$, $D_1 = 0.25$, $\omega_{e,2} = 500\ cm^{-1}$, $D_2 = 0.25$, $a\zeta_e = 0$, $K_i = 0$.

the most general discussion of the terms directly involving vibronic and electronic angular momentum, which are the properties most affected by Jahn–Teller coupling.

4.1. *Rotational basis set and Hamiltonian*

The total angular momentum of the molecule, excluding nuclear spin, is **J**. It is composed of the electron spin angular momentum **S**, the electronic orbital angular momentum **L**, the vibrational angular momentum **G** and the angular momentum **R** associated with rotation of the molecule as a whole. Both because spin plays a unique role in the problem and because **J** and **S** are conserved vectors, it is useful to define a 'spinless' angular momentum $\mathbf{N} = \mathbf{J} - \mathbf{S}$. The projection of **N** on the z axis is K.

The rovibronic basis set can either include Σ in the vibronic portion or the approximation can be made that both spin components have identical vibronic wavefunctions and Σ is an independent quantum number, which would therefore be included in the rotational basis set. The complete rovibronic basis set, assuming the molecule corresponds to Hund's case (*a*),† is therefore either

$$|\text{spin–vibronic}\rangle\,|\text{rotational}\rangle = |j, n_j, \alpha, \Sigma\rangle\,|J, P, M\rangle, \tag{88}$$

or, if spin–orbit coupling is separated from the Jahn–Teller coupling,

$$|\text{vibronic}\rangle\,|\text{spin}\rangle\,|\text{rotational}\rangle = |j, n_j, \alpha\rangle\,|\Sigma\rangle\,|J, P, M\rangle, \tag{89}$$

where P and M are the projections of J on the molecular and space-fixed z axes respectively. It follows from these definitions that $P = K + \Sigma$.

Equations (88) and (89) are simply the Jahn–Teller eigenfunctions (74) and (75) respectively multiplied by the rotational basis set. In the majority of cases thus far experimentally observed, the assumption has been made that the two spin components have identical PESs and vibronic wavefunctions, and hence equation (89) has been used. As noted in the previous section, none of the terms in the Hamiltonian yet considered raises the degeneracy of the eigenfunction $|j, n_j, \alpha, \Sigma\rangle$ with $|-j, n_{-j}, \alpha, -\Sigma\rangle$ (or $|j, n_j, \alpha\rangle\,|\Sigma\rangle$ with $|-j, n_{-j}, \alpha\rangle\,|-\Sigma\rangle$). To reduce the size of the calculations, it is therefore convenient to take symmetric and antisymmetric combinations of the rovibronic basis set, as in equation (77), and add a parity quantum number. The typical rovibronic basis set for a Jahn–Teller molecule is then either

$$|J, P, \Sigma, \pm\rangle = 2^{-1/2}\left\{|j, n_j, \alpha, \Sigma\rangle\,|J, P, M\rangle \pm (-1)^{J-P+S-\Sigma}\,|-j, n_j, \alpha, -\Sigma\rangle\,|J, -P, M\rangle\right\} \tag{90}$$

or

$$|J, P, \Sigma, \pm\rangle = 2^{-1/2}\left\{|j, n_j, \alpha\rangle\,|\Sigma\rangle\,|J, P, M\rangle \pm (-1)^{J-P+S-\Sigma}\,|-j, n_j, \alpha\rangle\,|-\Sigma\rangle\,|J, -P, M\rangle\right\}. \tag{91}$$

In the two limits of small spin–orbit coupling or large Jahn–Teller coupling, the spin–vibronic wavefunction is identical with the vibronic wavefunction, and the two rovibronic basis set choices become identical. In the situation where neither of these limits is approached, a rovibronic basis set of equation (91) is typically used, even

† A case (*b*) basis can also be proposed in which there is no conserved projection Σ of **S** along the symmetry axis, but instead **N** and **S** are vectorially added. Because most of the experimentally observed molecules have reasonable spin–orbit coupling, case (*a*) is most appropriate. There are numerous discussions in the literature of the rotational coupling cases and we shall not consider case (*b*) further.

though it is not precisely correct to do so. The approximation of equation (91) will have its greatest impact on the interpretation of the vibronic angular momentum.

The total rotational Hamiltonian, $\hat{\mathscr{H}}_{\mathrm{rot}}$, is the sum of a number of terms:

$$\hat{\mathscr{H}}_{\mathrm{rot}} = \hat{\mathscr{H}}_{\mathrm{R}} + \hat{\mathscr{H}}_{L^2} + \hat{\mathscr{H}}_{\mathrm{SR}} + \hat{\mathscr{H}}_{\mathrm{CD}} + \hat{\mathscr{H}}_{\mathrm{HF}}. \tag{92}$$

The first term, $\hat{\mathscr{H}}_{\mathrm{R}}$, is the rotational Hamiltonian for a symmetric top, including the spin uncoupling effects,

$$\hat{\mathscr{H}}_{\mathrm{R}} = B\,(\mathbf{J} - \mathbf{L} - \mathbf{G} - \mathbf{R} - \mathbf{S})^2 + (A - B)\left(\hat{J}_z - \hat{L}_z - \hat{G}_z - \hat{R}_z - \hat{S}_z\right)^2. \tag{93}$$

The parameters A and B are the rotational constants for a prolate symmetric top, defined at the symmetric configuration. (For an oblate top, A and B should be replaced by B and C respectively.) This term describes the simple end-over-end rotation of the nuclei for a symmetric top molecule.

Because of the distortion of the PES caused by Jahn–Teller coupling, a 'correction' term, $\hat{\mathscr{H}}_{L^2}$, is added to the Hamiltonian to account for the molecule's 'asymmetry',

$$\hat{\mathscr{H}}_{L^2} = h_1\left(\hat{\mathscr{S}}^2_{-}\hat{N}^2_{+} + \hat{\mathscr{S}}^2_{+}\hat{N}^2_{-}\right) + h_2\left[\hat{\mathscr{S}}^2_{-}\left(\hat{N}_z\hat{N}_{-} + \hat{N}_{-}\hat{N}_z\right) + \hat{\mathscr{S}}^2_{+}\left(\hat{N}_z\hat{N}_{+} + \hat{N}_{+}\hat{N}_z\right)\right], \tag{94}$$

where $\hat{\mathscr{S}}^2_{+}$ and $\hat{\mathscr{S}}^2_{-}$ are the 'ladder operators' introduced by Hougen [35] to convert one component of the vibronic state into the other. To describe the interaction of the electron spin angular momentum and the rotational angular momentum of the molecule, a spin–rotation term is added to the Hamiltonian:

$$\hat{\mathscr{H}}_{\mathrm{SR}} = \tfrac{1}{2}\sum_{\alpha,\beta}\varepsilon_{\alpha\beta}\left(N_\alpha S_\beta + S_\beta N_\alpha\right). \tag{95}$$

This term will always be present. There are several other possible spin-dependent terms in the rotational Hamiltonian. If Σ is not included in the spin–vibronic basis, the spin–orbit coupling term $\hat{\mathscr{H}}_{\mathrm{SO}}$ must be introduced. If the multiplicity of the state is a triplet or higher, a direct coupling ('spin-spin') term, $\hat{\mathscr{H}}_{\mathrm{SS}}$, must also be included. The terms $\hat{\mathscr{H}}_{\mathrm{CD}}$ and $\hat{\mathscr{H}}_{\mathrm{HF}}$ account for the centrifugal distortion and hyperfine effects and will not be considered further in this review.

Because $\hat{\mathscr{H}}_{L^2}$ is already an 'effective' Hamiltonian operator coupling the degenerate components of the electronic basis, we do not need to simplify it further. However, $\hat{\mathscr{H}}_{\mathrm{R}}$ and $\hat{\mathscr{H}}_{\mathrm{SR}}$ may be simplified. For a symmetric top molecule, only five of the nine possible spin–rotation Cartesian tensor components $\varepsilon_{\alpha\beta}$ are unique, ε_{aa} is the spin–rotation tensor component along the symmetry axis and ε_{bb} (or ε_{cc}) is its counterpart along the axes perpendicular to the symmetry axis. In addition, there are linear combinations, ε_1, ε_{2a} and ε_{2b}, describing spin–rotation coupling between states of $|\Lambda = +1\rangle$ and $|\Lambda = -1\rangle$. Therefore, $\hat{\mathscr{H}}_{\mathrm{SR}}$ reduces to [74]

$$\begin{aligned}\hat{\mathscr{H}}_{\mathrm{SR}} = {} & \varepsilon_{aa}\hat{N}_z\hat{S}_z + \tfrac{1}{2}\varepsilon_{bb}\left(\hat{N}_{+}\hat{S}_{-} + \hat{N}_{-}\hat{S}_{+}\right) + \varepsilon_1\left(\hat{\mathscr{S}}^2_{-}\hat{N}_{+}\hat{S}_{+} + \hat{\mathscr{S}}^2_{+}\hat{N}_{-}\hat{S}_{-}\right) \\ & + \varepsilon_{2a}\left[\hat{\mathscr{S}}^2_{-}\left(\hat{N}_z\hat{S}_{-} + \hat{S}_{-}\hat{N}_z\right) + \hat{\mathscr{S}}^2_{+}\left(\hat{N}_z\hat{S}_{+} + \hat{S}_{+}\hat{N}_z\right)\right] \\ & + \varepsilon_{2b}\left[\hat{\mathscr{S}}^2_{-}\left(\hat{N}_{-}\hat{S}_z + \hat{S}_z\hat{N}_{-}\right) + \hat{\mathscr{S}}^2_{+}\left(\hat{N}_{+}\hat{S}_z + \hat{S}_z\hat{N}_{+}\right)\right].\end{aligned} \tag{96}$$

While, in principle, corrections to $\hat{\mathscr{H}}_{\mathrm{SR}}$ due to distortions are possible, they have in the past always been considered negligibly small. The first term of $\hat{\mathscr{H}}_{\mathrm{SR}}$ is most

important, both because the effective value of ε_{aa} is large and because it alone has non-constant terms diagonal in the fine structure state. However, values for all five parameters have been reported for some molecules.

The first term of $\hat{\mathscr{H}}_{\text{rot}}$ is also complicated. We shall follow the work of others [34–36, 74] and write $\hat{\mathscr{H}}_{\text{R}}$ as the sum of two terms:

$$\hat{\mathscr{H}}_R = B\mathbf{R}^2 + (A-B)\hat{R}_z^2 \tag{97}$$

$$= B(\mathbf{N}-\mathbf{L}-\mathbf{G})^2 + (A-B)\left(\hat{N}_z - \hat{L}_z - \hat{G}_z\right)^2. \tag{98}$$

We can then decompose $\hat{\mathscr{H}}_R$ into three physically meaningful terms:

$$\hat{\mathscr{H}}_{\text{R}} = \hat{\mathscr{H}}_{\text{RD}} + \hat{\mathscr{H}}_{\text{Cor}} + \hat{\mathscr{H}}_{\text{SU}}, \tag{99}$$

where

$$\hat{\mathscr{H}}_{\text{RD}} = A\left(\hat{J}_z - \hat{S}_z\right)^2 + B\left(\hat{J}^2 - \hat{J}_z^2\right), \tag{100}$$

$$\hat{\mathscr{H}}_{\text{Cor}} = -2A\left(\hat{L}_z + \hat{G}_z\right)\hat{N}_z, \tag{101}$$

$$\hat{\mathscr{H}}_{\text{SU}} = -2B\left(\hat{J}_x\hat{S}_x + \hat{J}_y\hat{S}_y\right). \tag{102}$$

These three terms are the rotational operator diagonal in the vibronic basis ($\hat{\mathscr{H}}_{\text{RD}}$), the Coriolis interaction ($\hat{\mathscr{H}}_{\text{Cor}}$), and the spin-uncoupling operator ($\hat{\mathscr{H}}_{\text{SU}}$). In reducing $\hat{\mathscr{H}}_{\text{R}}$ in this fashion a number of steps and assumptions have been employed. The original literature in this area should be consulted for full discussion of these details. We shall mention only some of the most important of these assumptions. To obtain $\hat{\mathscr{H}}_{\text{RD}}$ and $\hat{\mathscr{H}}_{\text{Cor}}$, terms of $\hat{\mathscr{H}}_{\text{R}}$ with only vanishing matrix elements within the electronic state are discarded. Simultaneously a purely vibronic Coriolis term is discarded because its only effect is a very small correction to the rotational constants.

As written, $\hat{\mathscr{H}}_{\text{RD}}$ has only non-vanishing diagonal matrix elements in the vibronic or spin–vibronic basis set, while $\hat{\mathscr{H}}_{\text{SU}}$ has only non-vanishing matrix elements between the different spin components. The Coriolis coupling term $\hat{\mathscr{H}}_{\text{Cor}}$ has both diagonal and off-diagonal matrix elements in the vibronic or spin–vibronic basis set, as does $\hat{\mathscr{H}}_{\text{SO}}$. The matrix elements of all of these terms in the Hamiltonian have been derived elsewhere [74].

Considerable care must be taken with respect to the interpretation of the 'rotational' parameters of the rotational Hamiltonian. In molecules that obey the Born–Oppenheimer approximation, their interpretation in terms of expectation values of operators over the electronic eigenfunction, with at most weak vibrational dependence, is straightforward. Traditionally, in molecules with Jahn–Teller coupling, which is a breakdown of the Born–Oppenheimer approximation, the definition of the rotational parameters would be in terms of the vibronic eigenfunctions, $|j, n_j, \alpha\rangle$. In this case, spin–orbit coupling is considered small compared with 'vibronic' effects and therefore included in $\hat{\mathscr{H}}_{\text{R}}$ with its matrix constructed from the basis set of equation (91). As we have seen, $\hat{\mathscr{H}}_{\text{SO}}$ is often comparable with, or even larger than, the vibronic terms. In this case, the matrix of $\hat{\mathscr{H}}_{\text{R}}$ is constructed using the basis set of equation (90). The 'rotational' parameters then correspond to expectation values over the spin–vibronic eigenfunctions $|j, n_j, \alpha, \Sigma\rangle$. In essence, this amounts to treating the components of each spin multiplet independently. This might appear to be a loss of information with respect to the traditional 'vibronic' approach, which

treats them simultaneously with one set of vibronic parameters. However, as will be shown, when using only one set of vibronic parameters there are often breakdowns in analyses that can only be remedied by considering off-diagonal perturbations in the vibronic basis set. The spin–vibronic approach avoids this problem. Assuming that a complete set of eigenfunctions are available for a 'correct' solution to the eigenvalue problem of the stationary molecule portion of the Hamiltonian, including spin–orbit coupling, both approaches are equivalent.

In addition to the above complexity, it should be remembered that, besides these first-order contributions arising from eigenfunctions within a given electronic state, there are also higher-order effects due to coupling with other electronic states. However, these are generally small corrections and reasonably well documented. More important, but not so well described, are the higher-order effects arising from coupling among the spin vibronic levels of a given electronic state. These effects will be considered below.

4.2. *Coupling of vibronic, rotational and spin angular momenta*

4.2.1. *Coupling using vibronic eigenfunctions*

Critical to the evaluation and interpretation of $\hat{\mathscr{H}}_{\mathrm{rot}}$ is the understanding of the roles that the total vibrational and electronic angular momenta assume in a state perturbed by both Jahn–Teller and spin–orbit coupling. We first examine the situation for the traditional vibronic eigenfunctions, $|j, n_j, \alpha\rangle$.

In equation (101), the operators $\hat{L}_z$ and $\hat{G}_z$ are evaluated over the vibronic portion of the wavefunction. These two operators have the following expectation values for the primitive Jahn–Teller basis functions (8):

$$\prod_{i=1}^{p} \langle v_i, l_i| \langle \Lambda| \hat{G}_z |\Lambda\rangle \prod_{i=1}^{p} |v_i, l_i\rangle = \sum_{i=1}^{p} l_i \zeta_i \tag{103}$$

$$\prod_{i=1}^{p} \langle v_i, l_i| \langle \Lambda| \hat{L}_z |\Lambda\rangle \prod_{i=1}^{p} |v_i, l_i\rangle = \Lambda \zeta_{\mathrm{e}}, \tag{104}$$

where ζ_{e} is the electronic orbital angular momentum, as defined in equation (73), and ζ_i is the Coriolis coupling constant for the ith vibrational mode. With these matrix elements, we can then rewrite $\hat{\mathscr{H}}_{\mathrm{Cor}}$ in terms of the expectation value over the eigenfunction for a given degenerate vibronic level:

$$\hat{\mathscr{H}}_{\mathrm{Cor}} = -2A \langle j, n_j, \alpha = e| \hat{L}_z + \hat{G}_z |j, n_j, \alpha = e\rangle \hat{N}_z \tag{105}$$

$$= -2A \zeta_{\mathrm{t}} \hat{N}_z, \tag{106}$$

where

$$\zeta_t = \sum_i \left[c_{i,n_j}^2 \left(\Lambda_i \zeta_e + \sum_{m=1}^{p} l_{m,i} \zeta_m \right) \right]. \tag{107}$$

The derivation of equation (107) is analogous to that used earlier to obtain the spin–orbit quenching constant (equation (80)). The summation over i in equation (107) runs over all the basis functions in the wavefunction, therefore, the value of ζ_{t} is a complicated function of the Jahn–Teller constants and must be calculated for each set of parameters. Furthermore, this equation shows that each energy level has a distinct value of ζ_{t}, just as each energy level has a unique value of the spin–orbit quenching parameter d_{j,n_j}.

When only a single vibrational mode is active and spin–orbit coupling is small, equation (107) can be simplified, for C_{3v} symmetry, with the aid of equations (46) and (80), to a simpler equation for ζ_t:

$$\zeta_t = \left(\zeta_e - \tfrac{1}{2}\zeta_i\right) d_{j,n_j} + j\,\zeta_i = \zeta_e d_{j,n_j} - \zeta_i \left(\tfrac{1}{2} d_{j,n_j} - j\right). \tag{108}$$

Because j and d_{j,n_j} are signed quantities, ζ_t is also. When d_{j,n_j} is a reasonably good approximation to the spin–orbit quenching by the Jahn–Teller coupling, equation (108) can be combined with equation (83) to deduce the Jahn–Teller coupling constants from the observed Coriolis constants. Later in this article we give several examples of how resolution of the Coriolis coupling for several levels can lead to an accurate evaluation of the spin–orbit and linear Jahn–Teller coupling constants.

We now consider the two limits of no Jahn–Teller coupling ($d_{j,n_j} \to +1$) and strong Jahn–Teller coupling ($d_{j,n_j} \to 0$). When Jahn–Teller coupling vanishes, equation (108) simplifies to

$$\zeta_t = \zeta_e + l_i \zeta_i, \tag{109}$$

which is the normal value for ζ_t of a ^{2}E state, in the absence of any vibronic interactions.

However, when Jahn–Teller coupling is strong, the electronic orbital angular momentum is completely quenched and d_{j,n_j} approaches zero for all levels. Equation (108) then reduces to

$$\zeta_t = j\,\zeta_i. \tag{110}$$

For the vibrationless level, which has only $j = \pm\frac{1}{2}$, this means that the Coriolis coupling constant has changed from ζ_e, its value in the absence of Jahn–Teller coupling, to $\frac{1}{2}\zeta_i$ — a dramatic difference. If Jahn–Teller coupling is strong, the molecule becomes distorted to lower symmetry. How can there be any vibrational angular momentum, which is required to have Coriolis coupling, in a distorted molecule? The answer is that equation (110) has been derived assuming only linear Jahn–Teller coupling and no quadratic coupling. In this case, while the molecule is distorted along ρ_i, there is no distortion along ϕ_i (figures 1(*b*) and 2(*b*)). For the specific case of the 'vibrationless' level, $\left|j = \pm\frac{1}{2},\ n_j = 1\right\rangle$, the eigenfunction is an equal mixture of basis functions with even v_i and $l_i = 0$ and those with odd v_i and $l_i = \mp 1$. Therefore, rather than having zero vibrational angular momentum (the case when there is no vibronic coupling and $l_i = 0$), the 'vibrationless' level has an expectation value of $\langle l_i \rangle = \pm\frac{1}{2}$, and therefore has a Coriolis coupling constant ζ_t of $\pm\frac{1}{2}\zeta_i$. At the further limit of severe quadratic Jahn–Teller coupling, barriers to the pseudo-rotation of the molecule about ϕ_i will be created, vibrational basis functions of higher $|l_i|$ will be mixed into the 'vibrationless' eigenfunction, and l_i will be randomized. At this limit, the molecule is truly distorted and there is then no vibrational angular momentum with which to generate Coriolis coupling. (See also the discussion following equation (79).)

To this point, only the vibronic expectation values of $\hat{\mathscr{H}}_R$ have been considered. If $\hat{\mathscr{H}}_R$ were truly small compared with the terms that determine the vibronic eigenfunctions, no more discussion would be necessary. However, in the vibronic approach, one must consider $\hat{\mathscr{H}}_{SO}$ as contained in $\hat{\mathscr{H}}_R$ and the above assumption is of dubious validity. Indeed, experimental results first prompted the questioning of the validity of neglecting the mixing of the spin components of the vibronic eigenfunctions by terms of $\hat{\mathscr{H}}_R$. In particular, values for ε_{aa} in methoxy and related

radicals were an order of magnitude larger than ε_{bb}. This and related higher order effects were explored for the general case [61] and then applied specifically to the X ^{2}E ground state of CH_3O by Liu *et al.* [46].

Specifically, they considered the second-order effects of two perturbations with non-vanishing matrix elements between different vibronic levels of the same degenerate electronic state. These perturbations were $\hat{\mathscr{H}}_{\mathrm{Cor}}$ (equation (101)) and $\hat{\mathscr{H}}_{\mathrm{SO}}$ (equation (18)). These perturbations give rise to three correction terms. One, involving $|\hat{\mathscr{H}}_{\mathrm{SO}}|^2$, can be viewed as a correction to the spin–spin coupling and vanishes for a doublet state. Another, involving $|\hat{\mathscr{H}}_{\mathrm{Cor}}|^2$, gives a small correction to the A rotational constant. The most interesting correction results from the cross term, $\hat{\mathscr{H}}_{\mathrm{Cor}} \times \hat{\mathscr{H}}_{\mathrm{SO}}$, and gives rise to a correction to the spin–rotation coupling:

$$\hat{\mathscr{H}}'_{\mathrm{SR}} = \varepsilon_{aa}^{2\mathrm{v}} \hat{S}_z \hat{N}_z. \tag{111}$$

Evaluation of the expression for $\varepsilon_{aa}^{2\mathrm{v}}$ showed that it is an order of magnitude larger than the traditional term and conveniently explained the observed value of ε_{aa} in CH_3O. The two spin components of a vibronic level can then be analysed simultaneously with an effective Coriolis and spin–rotation Hamiltonian:

$$\begin{aligned} \left(\hat{\mathscr{H}}_{\mathrm{Cor}} + \hat{\mathscr{H}}_{\mathrm{SR}}\right)_{\mathrm{eff}} &= \hat{\mathscr{H}}_{\mathrm{Cor}} + \hat{\mathscr{H}}_{\mathrm{SR}} + \hat{\mathscr{H}}'_{\mathrm{SR}} \\ &= \left(-2A\zeta_t^0 + \varepsilon_{aa}^{\mathrm{eff}} \hat{S}_z\right) \hat{N}_z + \tfrac{1}{2}\varepsilon_{bb}\left(\hat{N}_+ \hat{S}_- + \hat{N}_- \hat{S}_+\right), \end{aligned} \tag{112}$$

with

$$\varepsilon_{aa}^{\mathrm{eff}} = \varepsilon_{aa}^0 + \varepsilon_{aa}^{2\mathrm{v}}, \tag{113}$$

where ε_{aa}^0 should be viewed as the traditional spin–rotation coupling constant, containing first order contributions from direct coupling of the spin to the magnetic field created by the rotating molecule as well as second order effects involving cross-terms of $\hat{\mathscr{H}}_{\mathrm{rot}}$ and $\hat{\mathscr{H}}_{\mathrm{SO}}$ between different electronic states. It is the form of equation (112) that has been used to analyse experimental spectra and that has yielded anomalously large values of $\varepsilon_{aa}^{\mathrm{eff}}$.

4.2.2. *Coupling using spin–vibronic eigenfunctions*

What happens if the assumption that the two spin components have identical vibronic eigenfunctions is discarded? First, spin–vibronic eigenfunctions instead of vibronic functions must be used to calculate the expectation values of the rotational operators. Because the two spin components no longer have identical vibronic eigenfunctions, they will have different expectation values. In this case, the Coriolis coupling constant for each spin component is

$$\hat{\mathscr{H}}_{\mathrm{Cor}} = -2A \langle j, n_j, \alpha = e, \Sigma | \hat{L}_z + \hat{G}_z | j, n_j, \alpha = e, \Sigma \rangle \hat{N}_z \tag{114}$$

$$= -2A\zeta_t^{\Sigma} \hat{N}_z, \tag{115}$$

where

$$\zeta_t^{\Sigma} = \sum_i \left[c_{i,n_j,\Sigma}^2 \left(\Lambda_i \zeta_e + \sum_{m=1}^{p} l_{m,i} \zeta_m \right) \right]. \tag{116}$$

The addition of a spin–rotation interaction for each fine structure component leads to

$$\hat{\mathscr{H}}_{\mathrm{Cor}} + \hat{\mathscr{H}}_{\mathrm{SR}} = \left(-2A\zeta_t^{\Sigma} + \varepsilon_{aa}^0 \Sigma\right) \hat{N}_z. \tag{117}$$

The difference $\Delta\zeta_t$ between the Coriolis constant for each spin component, is

$$\Delta\zeta_t = \zeta_t^+ - \zeta_t^-, \tag{118}$$

where the signs correspond to the sign of $\Sigma = \pm\frac{1}{2}$. The two Coriolis constants will be approximately related by

$$\zeta_t^{\pm} = \zeta_t^0 \pm \tfrac{1}{2}\Delta\zeta_t, \tag{119}$$

where ζ_t^0 denotes the Coriolis coupling constant that would result if there were no spin–orbit coupling, that is a Coriolis coupling constant corresponding to equation (107).

The two equivalent approaches, equations (112) and (117), must lead to the same expectation value. For the spin component with $\Sigma = \frac{1}{2}$, this reasoning leads to the following equality:

$$-2A\zeta_t^0 + \tfrac{1}{2}\left(\varepsilon_{aa}^0 + \varepsilon_{aa}^{2v}\right) = -2A(\zeta_t^0 + \tfrac{1}{2}\Delta\zeta_t) + \tfrac{1}{2}\varepsilon_{aa}^0. \tag{120}$$

Combining equations (118)–(120) yields the following relationship between the two approaches:

$$\frac{\varepsilon_{aa}^{2v}}{2A} = -\Delta\zeta_t. \tag{121}$$

For the vibrationless level, the sign on $\Delta\zeta_t$ will be the opposite of the sign of $a\zeta_e$ and in the single mode limit its sign will alternate for fixed j with increasing v in the Jahn–Teller active mode. To see why this is true, consider the two components of the vibrationless level of a Jahn–Teller active radical, as shown in figure 11. The component that is higher in energy will, because of its smaller energy difference with the other vibronic energy levels of the state, have a greater amount of mixing with the other levels. This will cause the higher-energy spin component of the vibrationless level always to have its orbital angular momentum quenched to a greater degree. The energy levels of figure 11 are depicted for the case when $a < 0$, which means that the component of the vibrationless level with Λ and Σ of the same sign will be lower in energy, as shown. In this case, ζ_t^+ will be closer to +1 (its value in the absence of Jahn–Teller coupling) than ζ_t^-, and so $\Delta\zeta_t = \zeta_t^+ - \zeta_t^-$ will be positive. If instead a is positive, then the component with $\Sigma = -\frac{1}{2}$ and Λ positive will be lower in energy, and $\Delta\zeta_t$ will be negative.

4.3. *The l-type doubling and Λ-doubling term* $\hat{\mathscr{H}}_{L^2}$

The last contribution to the rotational Hamiltonian that we shall consider in detail is $\hat{\mathscr{H}}_{L^2}$. Our motivation for discussing this term is that it provides an additional means by which experimental data can characterize the Jahn–Teller interaction. The notation $\hat{\mathscr{H}}_{L^2}$ is often written as $\hat{\mathscr{H}}_{JT}$, which is misleading, as it implies that this term is derived exclusively from Jahn–Teller effects. However, each of the parameters h_1 and h_2 in equation (94) contains a contribution from Jahn–Teller coupling as well as from L-uncoupling terms via the interaction of the Jahn–Teller electronic state with other electronic states of the molecule. As both Hougen [35] and Watson [36] have shown, h_1 and h_2 can be broken down into contributions from the two different types of coupling:

$$h_1 = h_1^{JT} + h_1^L, \tag{122}$$

$$h_2 = h_2^{JT} + h_2^L. \tag{123}$$

Here, we follow Hougen [35] in the naming of these parameters as h_1 and h_2, but follow Watson [36] in adding superscripts to denote the source of the coupling. (In Watson's notation, h_1 is $\frac{1}{2}q_0$ and h_2 is $2r_0$.) For some point groups, in particular, D_{3h} and D_{5h}, h_2 may vanish by symmetry.

If h_1 and h_2 are known for only a single isotopomer of a molecule it is impossible to separate the two contributions to each. As both Hougen and Watson showed, h_1^{JT} is proportional to B_0, h_1^L is proportional to B_0^2, h_2^{JT} is proportional to $(A_0B_0)^{1/2}$, and h_2^L is proportional to A_0B_0. Therefore, if h_1 and h_2 are known for more than one isotopomer, the individual contributions from Jahn–Teller and L uncoupling can be extracted.

The Jahn–Teller parameters h_1^{JT} and h_2^{JT} have been shown by Watson [36] to have a clear correlation to the vibronic Jahn–Teller parameters $\omega_{e,i}$ and D_i:

$$h_1^{JT} = \sum_i 2^{1/2} D_i \omega_{e,i} C_i^{xx}, \tag{124}$$

$$h_2^{JT} = \sum_i 2^{1/2} D_i \omega_{e,i} C_i^{xz}, \tag{125}$$

where

$$C_i^{\alpha\beta} = -\frac{1}{\omega_{e,i}} \left(\frac{\partial B_{\alpha\beta}}{\partial q_i} \right) = \frac{a_i^{\alpha\beta}}{2\gamma_i^{3/2} I_\alpha I_\beta},$$

with

$$a_i^{\alpha\beta} = \left(\frac{\partial I_{\alpha\beta}}{\partial Q_i} \right)_0 \qquad \gamma_i = \frac{2\pi c \omega_{e,i}}{\hbar}.$$

In these equations, the $C_i^{\alpha\beta}$ are the inertial derivatives of the ith vibrational mode, which are non-zero for the e modes and the moments $I_{\alpha\beta}$ of inertia are those for the symmetric configuration [75]. It would be quite difficult to determine experimentally all the parameters of equations (124) and (125), particularly for molecules with multiple Jahn–Teller active modes. However, the $C_i^{\alpha\beta}$ are readily calculated from *ab initio* calculations of the vibrational normal modes [76]. These equations may therefore be a point of comparison of *ab initio* calculations with experiment.

In his treatment of the rovibronic problem for Jahn–Teller molecules, Watson made one more key contribution. He showed that the rotational constant tensor for points around the bottom of the moat of the PES can be approximated by

$$\begin{bmatrix} B - h_1^{JT}\cos\phi & h_1^{JT}\sin\phi & -h_2^{JT}\cos\phi \\ h_1^{JT}\sin\phi & B + h_1^{JT}\cos\phi & -h_2^{JT}\sin\phi \\ -h_2^{JT}\cos\phi & -h_2^{JT}\sin\phi & A \end{bmatrix}. \tag{126}$$

This tensor relates the rotational constants at the minimum and maximum, where $\phi = 0$ and π, respectively, with the rotational constants at the symmetric configuration (A and B) and the rotational Jahn–Teller parameters h_1^{JT} and h_2^{JT}. The eigenvalues of equation (126) with $\phi_i = 0$ are the rotational constants of the molecular configuration at the minimum of the moat, which we call A_{min}, B_{min} and C_{min}. (At the bottom of the moat, the configuration is no longer a symmetric top and $B_{min} \neq C_{min}$.) Equations (124)–(126) provide the framework through which the rotational constants A and B, the linear Jahn–Teller parameters $\omega_{e,i}$ and D_i, and the rotational Jahn–Teller parameters h_1^{JT} and h_2^{JT} can all be related to one another.

While experimental determinations of h_1 and h_2 have been made for a number of molecules, relatively few studies have attempted to relate the parameters to the rotational constants, vibronic Jahn–Teller coupling constants and geometric

distortions of the molecule. Herzberg *et al.* [77–79] have analysed the 3p $^2E'$ state of H_3 and D_3 and thereby separated the Jahn–Teller and L-uncoupling contributions. A large amount of data has been collected and analysed for the B $^1E''$ state of NH_3, but no analysis of it has been successful in identifying all the various coupling constants outlined above [80–84]. The microwave work of Endo and co-workers [74, 85, 86] on the methoxy radical has identified the h_1 and h_2 parameters of $^{12}CH_3O$ and $^{13}CH_3O$, but unfortunately a completely analysed spectrum for CD_3O has not yet been published. Lastly, Yu *et al.* [12–14] have rotationally resolved the electronic origin band of the C_5H_5, C_5D_5, C_5H_4D and C_5D_4H radicals, providing a beautiful example of all of the rotational Jahn–Teller coupling constants and their relationship to the geometric distortion of the radical. However, all of their calculations relating the h_1 parameter to the geometric distortion assumed that the radical had only a single Jahn–Teller mode. They were able to make only a relatively crude estimate of the vibronic Jahn–Teller coupling constant D_i for that mode, as there is an absence of supporting Jahn–Teller analysis of the vibronic structure. Thus, a significant amount of work remains in deciphering the Jahn–Teller coupling in the cyclopentadienyl radical.

5. Intensities in electronic spectroscopy

Electronic spectroscopy has been the major tool for the investigation of the Jahn–Teller effect. The examples to be shown later all involve electronic transitions between a $^2A_1$ state and a Jahn–Teller active ^2E state, under C_{3v} symmetry. The intensities of the vibronic progressions in these spectra can be calculated once the eigenvectors are known from the diagonalization of the Hamiltonian matrix. Other types of spectroscopy that have been performed on Jahn–Teller active molecules include microwave, laser magnetic resonance, Raman and infrared. The selection rules and intensities for Raman [31, 52, 87] and infrared [31, 88, 89] transitions of Jahn–Teller active molecules have been developed elsewhere, albeit without the consideration of spin–orbit coupling as we have treated it in this paper.

Before we delve into the transitions to and from the Jahn–Teller state, we shall quickly review the transitions between two states that are described only by harmonic oscillator potentials. In this case, if the molecule begins in the vibrationless level of one state, it will have electronically allowed transitions only to the vibrationless level of the other state, and to any of the totally symmetric modes. The relative intensities of the latter progressions are given by the Franck–Condon factors between the two states. Under the harmonic oscillator potentials, there is zero intensity to the overtones of the degenerate modes (figure 14(*a*)). As originally derived elsewhere [32], Jahn–Teller coupling produces intensity in transitions in the Jahn–Teller active modes that are otherwise dark, and the addition of spin–orbit coupling does not change this fundamental conclusion. As the starting point for the calculation of transition intensities, the wavefunction for the ^2A state is given by

$$\left\langle {}^2\mathrm{A}\right| = \langle \Sigma | \prod_{r=1}^{p} \langle v_r, l_r | \langle \Lambda = 0 |, \tag{127}$$

where the product is over all the vibrational modes of e symmetry that were included in the Jahn–Teller calculation of the corresponding ^2E state. Because there is no electronic orbital angular momentum in the ^2A state, Λ takes on an effective value of zero. It is included in the wavefunction as a quantum number to simplify the

transition dipole matrix elements with the ^{2}E wavefunction. Note the similarity between the basis functions for the ^{2}A state (equation (127)), and the basis functions for the ^{2}E state (equation (8)), for every combination of vibrational quantum numbers, there exists one basis function in the ^{2}A state with $\Lambda = 0$ and two in the ^{2}E state with $\Lambda = \pm 1$. For the following equations, it is immaterial whether the state is of A_1 or A_2 symmetry, as both are electric dipole allowed transitions, but for different symmetry of the non-degenerate state.

The transition dipole intensities I, of an $^2\mathrm{A} \leftrightarrow {}^2\mathrm{E}$ electronic transition are given by

$$I = \left| \left\langle {}^2\mathrm{A} \middle| \hat{T} \middle| {}^2\mathrm{E} \right\rangle \right|^2 = \left| \langle \Sigma' | \prod_{r=1}^{p} \langle v_r', l_r' | \langle \Lambda' = 0 | \hat{T} | j, n_j, \alpha, \Sigma \rangle \right|^2, \tag{128}$$

where $\hat{T}$ is the transition dipole operator. Because these are electric dipole transitions, the spin angular momentum is unaffected by the transition and can be factored out of the intensity calculations. Equation (128) can therefore be combined with equations (127) and (74) and be rewritten as

$$I = \left| \prod_{r=1}^{p} \langle v_r', l_r' | \langle \Lambda' = 0 | \hat{T} \sum_i \left(c_{i,n_j,\Sigma} | \Lambda_i'' \rangle \prod_{m=1}^{p} \left| v_{m,i}'', l_{m,i}'' \right\rangle \right) \right|^2, \tag{129}$$

which after invocation of the Born-Oppenheimer approximation and separation of the nuclear and electronic components becomes

$$I = \left| \sum_i c_{i,n_j,\Sigma} \prod_{r=1}^{p} \langle v_r', l_r' | \prod_{m=1}^{p} \left| v_{m,i}'', l_{m,i}'' \right\rangle \langle \Lambda' = 0 | \hat{T} | \Lambda_i'' \rangle \right|^2. \tag{130}$$

Assuming that the transition dipole matrix element $\langle \Lambda' = 0 | \hat{T} | \Lambda_i'' \rangle$ is constant, the transition probability from a given vibrational level of the ^{2}A state to a given vibronic level of the ^{2}E state becomes equal to a sum of vibrational overlap integrals.

If we make the obviously oversimplified assumption that the Franck–Condon factors are completely diagonal, the only terms in equation (130) that survive are those that have identical vibrational quantum numbers in the two basis functions. The general form of the transition intensity then becomes proportional to the sum of the squares of the expansion coefficients:

$$I = \left| \left\langle {}^2\mathrm{A} \middle| \hat{T} \middle| {}^2\mathrm{E} \right\rangle \right|^2 = \sum_i c_{i,n_j,\Sigma}^2 \prod_{m=1}^{p} \langle v_m', l_m' | v_{m,i}'', l_{m,i}'' \rangle^2. \tag{131}$$

Equation (131) gives a general formula for the transition intensity between a vibrational level of the ^{2}A state and a level of the ^{2}E state of a Jahn–Teller active molecule. In most spectroscopic investigations, especially those performed in free jet expansions and molecular beams, the molecules are prepared in individual vibronic levels and the spectra are obtained from that level. We shall therefore continue to develop these equations for the cases where the molecule is initially in a single vibronic level of either state.

For a given vibronic level of a ^{2}A state, the initial vibrational wavefunction is described by a single set of vibrational quantum numbers. Therefore, the intensity

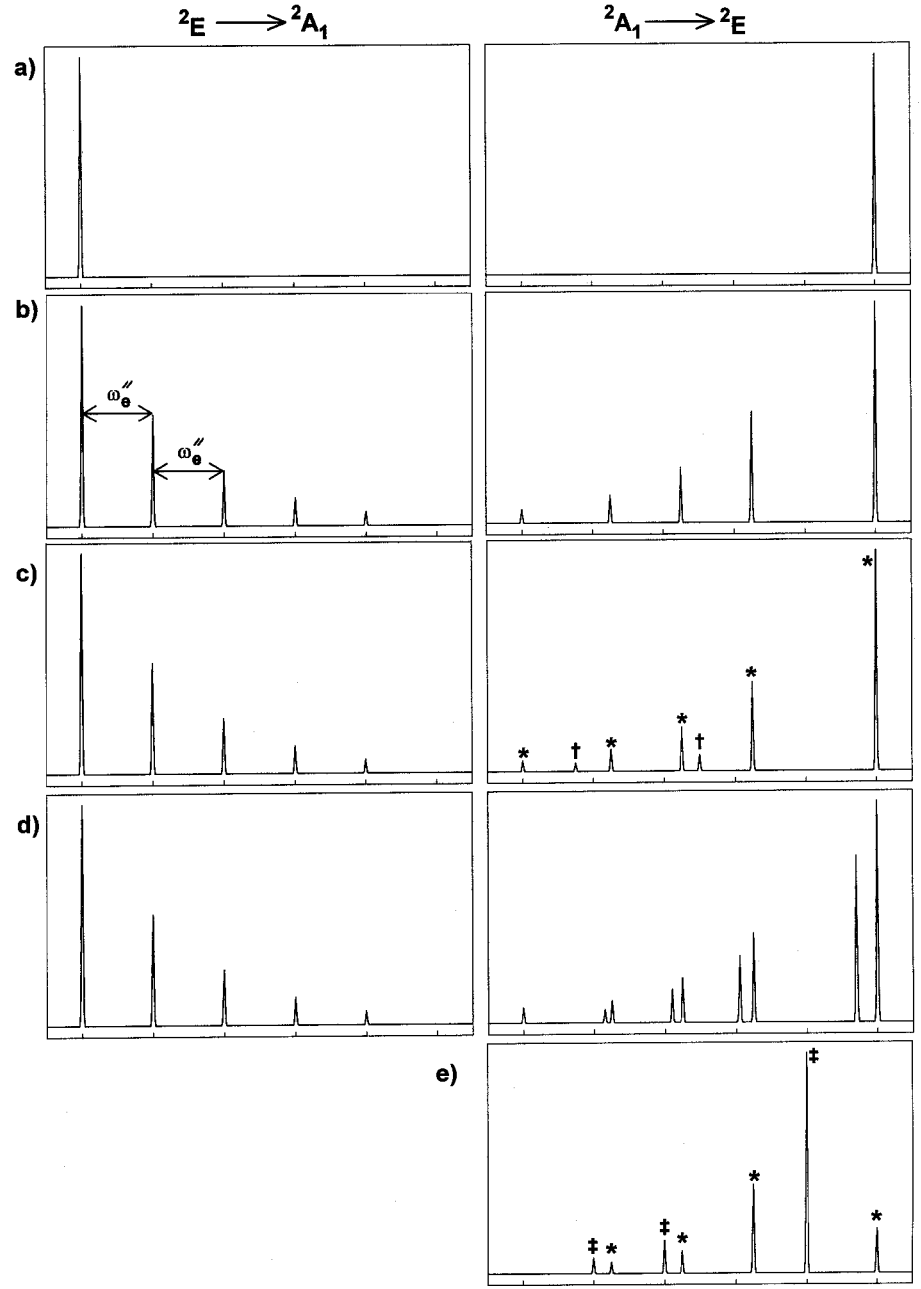

Figure 14. Qualitative electronic spectra for a $\tilde{A}\ ^2A_1 \leftrightarrow \tilde{X}\ ^2E$ transition for a Jahn–Teller active molecule. (*a*)–(*d*) Sample intensities for an excitation spectrum from the lowest energy level of the ^2E state on the left and an emission spectrum from the vibrationless level of the ^2A state on the right, assuming a single Jahn–Teller active mode. The terms in the Hamiltonian included for each spectrum are as follows: (*a*) $\hat{\mathscr{H}}_{h,e}$, (*b*) $\hat{\mathscr{H}}_{h,e} + \hat{\mathscr{H}}_1$, (*c*) $\hat{\mathscr{H}}_{h,e} + \hat{\mathscr{H}}_1 + \hat{\mathscr{H}}_{qii}$, (*d*) $\hat{\mathscr{H}}_{h,e} + \hat{\mathscr{H}}_1 + \hat{\mathscr{H}}_{SO}$. (*e*) A sample transition from the ^2A state with $v' = 1$ to the $\tilde{X}\ ^2E$ state for the case of linear Jahn–Teller coupling only. The lines in the $\tilde{A}\ ^2A_1 \rightarrow \tilde{X}\ ^2E$ spectra are labelled according to their values of j: (★), $\frac{1}{2}$, (‡), $\frac{3}{2}$, (†), $\frac{5}{2}$. The levels in (*a*), (*b*) and (*d*) all correspond to $j = \frac{1}{2}$.

is given by

$$I = \left| \prod_{i=1}^{p} \langle v_i', l_i' | \hat{T} \, | j, n_j, \alpha, \Sigma \rangle \right|^2 = c^2_{i,n_j,\Sigma}. \tag{132}$$

In most experiments, the molecules are prepared in a way such that all the l_i' are populated equally and equation (132) becomes a summation over all possible l_i'.

The intensity of the transitions from the vibronic level of the ^{2}A state to the levels of the ^{2}E state will be proportional to the square of the coefficient in the ^{2}E wavefunction of that basis function (figure 14(*b*)). The energy spacings of the transition are given by the energies of the ^{2}E state, for example, the energy levels of figures 5–10 and 12. Because of the erratic nature of the energy levels, no simple patterns can be generalized, as is done for Franck–Condon progressions of symmetric modes in typical electronic spectra.

The symmetry blocking of the wavefunctions by the half-integer quantum number j has important ramifications in the spectroscopy from a ^{2}A state to a ^{2}E state. For example, if the molecule begins in the vibrationless level of the ^{2}A state, where all $v_i' = 0$, then all l_i' must also be equal to zero. Because of the nature of the vibrational overlap integrals in equation (131), transitions will occur only to those levels in the ^{2}E state that have contributions from basis functions with $v''_{m,i} = l''_{m,i} = 0$. These levels of course have $j = \pm\frac{1}{2}$ and, because j is conserved for linear coupling, all accessible levels must have $j = \pm\frac{1}{2}$. If one vibrational mode is excited to $v_i' = 1$ in the ^{2}A state, then $l_i' = \pm 1$ and j can be $\pm\frac{1}{2}$ or $\pm\frac{3}{2}$. In general, the observable levels in the ^{2}E state will be those with $|j| \leqslant \left|\frac{1}{2} + \sum_i v_i'\right|$. This conclusion plays a key role in the analysis of the spectra. If spectra are obtained from both the $v_i' = 0$ and $v_i' = 1$ levels, then the peaks in the $v_i' = 1$ spectrum that do not appear in the $v_i' = 0$ spectrum must be due to $j = \pm\frac{3}{2}$ levels (compare figures 14(*b*) and (*e*), as well as the dispersed fluorescence spectra of CF_3S, see figure 18 later). The spectra from higher vibrational levels can be compared with those from lower lying states and definite assignments of j can be made.

The intensities of the converse transitions, from a given level of the ^{2}E state, $|j, n_j, \alpha, \Sigma\rangle$, to the levels of the ^{2}A state are also contained in equation (131). Transitions to all a_1 (or a_2) and e vibrational levels of the ^{2}A state are therefore possible, because the true basis set for the ^{2}E state is an infinite set of all possible combinations of vibrational quantum numbers. The relative intensities of the transition to each level in the ^{2}A state is again given by the square of the coefficient of that level's corresponding basis function in the wavefunction of $|j, n_j, \alpha, \Sigma\rangle$. The energy spacings of the spectrum correspond to those of the ^{2}A state, which are the normal spacings of a harmonic oscillator (figure 14(*a*)). For the transition from the ^{2}A state to the ^{2}E state, marked differences appear depending on which level of the ^{2}A state is populated. The transitions from different levels of the ^{2}E state will all go to the same energy levels of the ^{2}A state, just with different intensities.

We mentioned earlier that, when a transition occurs from the $v' = 0$ level of the ^{2}A state to the ^{2}E state, only those levels with $j = \pm\frac{1}{2}$ will be observed. This is true only when quadratic Jahn–Teller coupling is neglected and j is conserved. When quadratic Jahn–Teller coupling is introduced, the $j = \pm\frac{1}{2}$ levels are mixed with the $j = \mp\frac{5}{2}$ levels (figure 3). The levels that are predominantly $j = \pm\frac{5}{2}$ have some $j = \pm\frac{1}{2}$ character mixed in by quadratic coupling and therefore gain intensity

in the transition (figure 14(*c*)). Similar arguments hold true for the intensities of the higher j levels. However, the $j = \pm\frac{3}{2}$ levels will still be dark.

The addition of spin–orbit coupling has several effects on the spectra from the ^{2}E state to the ^{2}A state. For the transitions from the ^{2}A state to the ^{2}E state, spin–orbit coupling has the clearly observable effect of turning nearly all the transitions into doublets. (If the a_1 and a_2 levels have been split by quadratic coupling, they will remain as singlets owing to symmetry (figure 3). If, however, quadratic coupling is absent, the degenerate pair of a_1 and a_2 levels will be split into two levels of $e_{1/2}$ symmetry.) Furthermore, because of the quenching of the spin–orbit coupling by the Jahn–Teller coupling, the splitting is not constant, nor is it a smoothly varying splitting with respect to energy, although in general the splitting is smaller as the internal energy is increased (see the discussion earlier and figures 8–10).

In the absence of any Jahn–Teller coupling, the relative intensities of the two spin–orbit components of a given vibronic level should be 1: 1. However, figure 14(*d*) and the experimental spectra of the methoxy family of radicals (see figures 18 and 19 later) clearly indicate that this is not the case for molecules with significant Jahn–Teller and spin–orbit coupling. The origin of this effect lies in the relative ordering of the spin–orbit components of the vibronic levels. Figure 11 is a schematic representation of the linear Jahn–Teller interactions between the spin–orbit components of the $v = 0$ and $v = 1$ levels. Clearly, the linear Jahn–Teller mixing of the $e_{1/2}$ manifold will be quite different from the $e_{3/2}$ levels, as all the energy separations are different. Because of the different energy separations, the $\left|\frac{1}{2}, 1, e_{1/2}, \Sigma\right\rangle$ wavefunction will have much less $v = 0$ character than the $\left|\frac{1}{2}, 1, e_{3/2}, \Sigma\right\rangle$ wavefunction. Therefore, when a transition from the $v' = 0$ level of a ^{2}A state occurs to the ^{2}E state, the transition to the $\left|\frac{1}{2}, 1, e_{3/2}, \Sigma\right\rangle$ level will be stronger than the one to the $\left|\frac{1}{2}, 1, e_{1/2}, \Sigma\right\rangle$ level. Conversely, when the transition is from the $v' = 1$ level of the ^{2}A state, the transition intensities will be reversed. An excellent example of this mixing is found in the emission spectra of the CF_3S radical, where the relative intensities to the two spin components of the origin are 3 : 1 from the vibrationless level of the ^{2}A state but 1 : 4 from the $v_6' = 1$ level (see figure 18).

Spin–orbit coupling also changes the intensities of the a_1 and a_2 levels. Under the spin double group they are of the same symmetry, $e_{1/2}$. As we discussed in section 3.2.3, this pair of levels are mixed with each other when both quadratic Jahn–Teller coupling and spin–orbit coupling are present (figure 12). In a $^2A_1 \leftrightarrow {}^2E$ perpendicular electronic transition, the a_1 levels of a Jahn–Teller distorted ^{2}E state are allowed from the vibrationless level of the ^{2}A state, whereas the a_2 levels will have zero intensity. The combination of spin–orbit and quadratic Jahn–Teller coupling allows *both* of the levels to be observed, with their intensities given by the amount of a_1 character in each. The best examples of this phenomenon are CH_3O and CF_3O, which have $K_6 = -0.14$ and 0.05 respectively. The spin–orbit coupling in each of these radicals is substantial and mixes the a_1 and a_2 levels of the lowest $j = \pm\frac{3}{2}$ levels quite thoroughly, allowing the two components to have nearly identical intensities in the dispersed fluorescence spectra.

A second spectroscopic implication of quadratic Jahn–Teller coupling on these levels is that the observed splitting of the a_1 and a_2 levels can be greater than the spin–orbit splitting of the origin. This result seems counterintuitive to the statement made earlier that spin–orbit quenching generally increases as the internal energy of the state is increased. However, the splitting of these two levels is actually

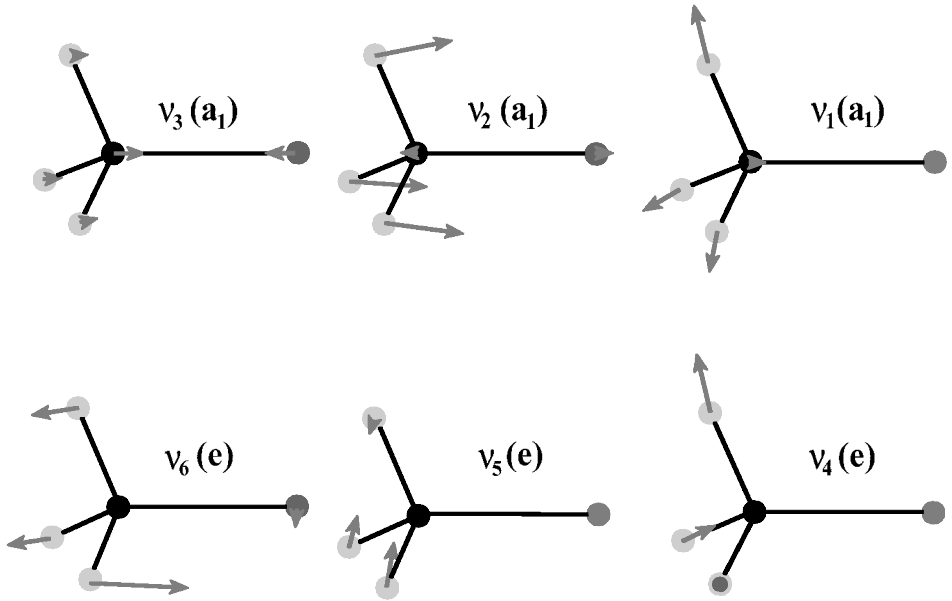

Figure 15. Normal modes of the CX_3Y radicals.

increased by the combination of spin–orbit and quadratic Jahn–Teller coupling. A clear example of this effect is in the spectra of the CF_3O (section 6.2.3) and CH_3O (section 6.2.4) radicals.

6. Examples of the analysis of the spectra involving Jahn–Teller states

In this final section, we shall review the analysis of the electronic spectra of several Jahn–Teller molecules, all of C_{3v} symmetry and all of the general form CX_3Y. This class of molecules offers a wide diversity of phenomena and is probably the best studied experimentally. It includes the $\tilde{X}\,^2E$ states of the methoxy family (CH_3O, CH_3S, CF_3O and CF_3S), as well as the $\tilde{A}\,^2E$ states of the organometallic monomethyl radicals $MgCH_3$, $CaCH_3$, $ZnCH_3$ and $CdCH_3$. These examples will allow us to apply the principles developed in the preceding sections and illustrate the different ways in which molecules yield information about their spin–vibronic coupling and the different approaches that have been developed to decipher this coupling. We shall proceed from perhaps the simplest case, the excited state of the $MgCH_3$ radical, to probably the most complex (but most studied) member of the family, the ground state of CH_3O.

For each radical there are three vibrational normal modes of a_1 symmetry and three potentially Jahn–Teller active modes of e symmetry. The normal modes for CH_3O, calculated at the Hartree–Fock level, are depicted in figure 15. The a_1 modes are nominally the symmetric C–H stretch (ν_1), the O–C–H umbrella motion (ν_2) and the C–O stretch (ν_3). The degenerate modes are the asymmetric C–H stretch (ν_4), the H–C–H scissor motion (ν_5) and the O–C–H rock (ν_6). While the true normal modes of each state of each molecule are linear combinations of these internal coordinate motions, the internal coordinate descriptions are still useful visualizations of the vibrational modes of the molecule.

6.1. *Metal monomethyl radicals*

The organometallic radicals discussed in the next three sections have $^2A_1$ ground states and ^2E first excited states. We shall focus our attention on the LIF excitation spectra, as these experiments yield extensive data about the spin–vibronic coupling in the A ^2E states of these radicals. Other spectroscopic techniques that have been used to investigate these molecules in their A states include optical Stark spectroscopy ($CaCH_3$ [90]) and zero-electron kinetic energy pulsed field ionization (ZEKE-PFI) spectroscopy ($MgCH_3$ [91], $ZnCH_3$ [91] and $CdCH_3$ [92]).

Generally speaking, the experiments have yielded data about both spin components, $^2E_{1/2}$ and $^2E_{3/2}$, of the excited state as well as an overview of the vibrational structure. For the most part, Jahn–Teller activity has been observed in only one mode, v_6. The combination of relatively extensive data and moderately simple spectra make these nearly ideal molecules for discussing the methodology of the analysis of Jahn–Teller molecules, as well as the information that can be extracted from the spectra.

In particular, these molecules nicely illustrate the complementary roles played by the spin–vibronic analysis and the rotational analysis. As we have seen, the spin–vibronic eigenvalues and eigenfunctions are determined by a combination of vibrational, Jahn–Teller and spin–orbit effects. Therefore, the spin–vibronic spectrum determined by these eigenvalues is the direct messenger of information about the Jahn–Teller interaction and spin–orbit coupling.

However, the rotational spectrum is also affected and can produce its own 'messages' about these couplings. As noted earlier, the rotational parameters are expectation values over the spin–vibronic eigenfunctions that are often quite complicated linear combinations of the initial basis set. The expectation values of several parameters (e.g. the rotational constants) vary only slightly among the basis functions. Therefore, their absolute variations and hence sensitivity to the modifications of the eigenfunctions are quite small. On the other hand, some parameters, particularly those related to electronic or vibronic angular momentum, show large variations among the basis functions. Therefore, parameters measuring these angular momenta may be very strongly affected by the mixing of the basis functions and hence efficient messengers of the inherent Jahn–Teller and spin–orbit coupling.

6.1.1. *$MgCH_3$*

The electronic spectra of the $MgCH_3$ radical have been obtained in our laboratory, both at moderate resolution [70] and at higher resolution for the origin band [93]. The moderate resolution spectra of the two spin components of the 2^1 and 6^1 levels are shown in figure 16 together with simulations of the rotational structure. The spin–orbit splitting of the 2^1 levels is clear in figure 16(*a*), with additional rotational structure in each spin component. The fundamental of v_6 (figure 16(*c*)), appears quite different, however.

The A ^2E state of $MgCH_3$ appears to have Jahn–Teller activity in only one mode, v_6, and even this is fairly weak. Additionally, the spin–orbit coupling in $MgCH_3$ is relatively small compared with the vibrational frequency. This state therefore falls into the situation where some of the simple expressions historically developed to describe Jahn–Teller effects are relatively accurate. We can thus manipulate several of the equations from the previous sections to analyse easily the spin–orbit and Jahn–Teller coupling in this state. The partial rotational analyses of the origin (0^0 =

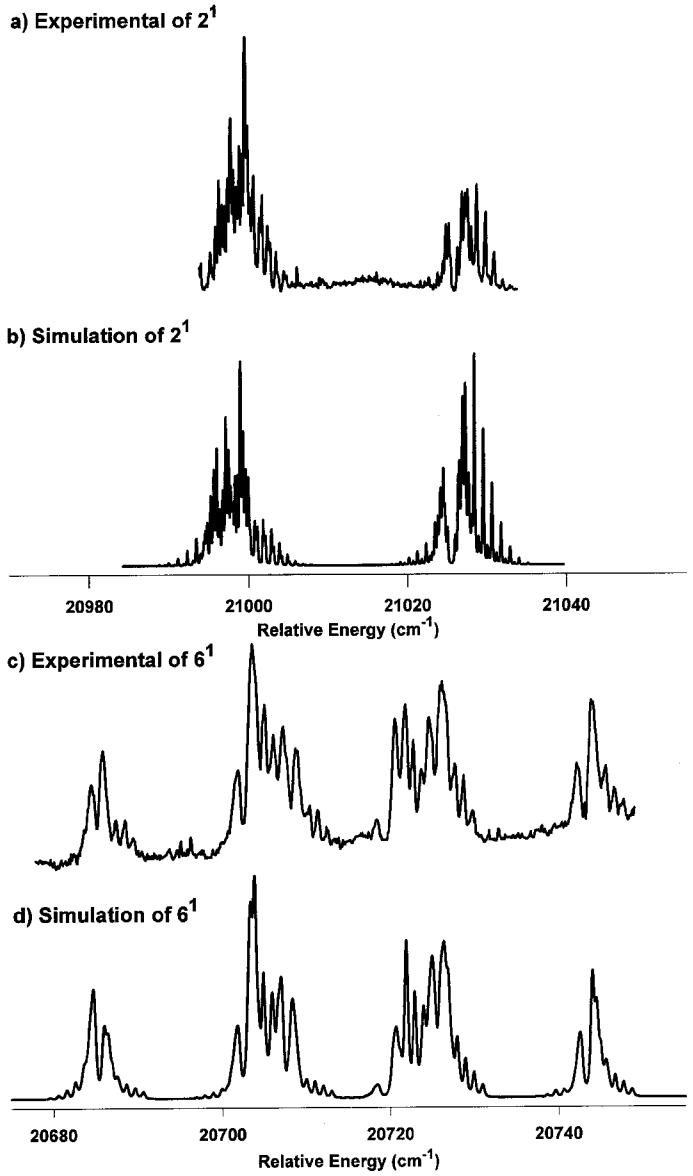

Figure 16. LIF excitation spectra of $MgCH_3$. (Adapted from [70].)

$\left|j = \frac{1}{2}, n_j = 1, \Sigma = \pm\frac{1}{2}\right\rangle$) and the fundamental of v_6 ($6^1 = \left|j = \frac{1}{2}, n_j = 2, \Sigma = \pm\frac{1}{2}\right\rangle$) bands have measured the following parameters: $\omega_{0,6}$, $a\zeta_e d_{1/2,1}$ (the observed spin–orbit splitting of the origin), $a\zeta_e d_{1/2,2}$ (the observed spin–orbit splitting of 6^1), and ζ_t (0^0) and ζ_t (6^1) (table 5). To have a complete description of the Jahn–Teller and spin–orbit coupling in the $\tilde{A}\ ^2E$ state, the following molecular parameters need to be calculated from the experimentally measured quantities: $\omega_{e,6}$, D_6, a, ζ_e (or at least the product $a\zeta_e$), and ζ_6.

Table 5. Rotational parameters experimentally observed for the vibrationless level (0^0) and the level with one quantum of ν_6 excited (6^1) of the $\tilde{A}\,^2E$ states of the organometallic monomethyl radicals.[a]

Parameter	$MgCH_3$	$CaCH_3$	$ZnCH_3$	$CdCH_3$
	0^0			
$a\zeta_e d_{1/2,1}$	28.591	72.709	253.233	1008
A	4.989	5.386	4.946	4.965
$A\zeta_t^0$	4.309	5.360	3.661	4.8
$\varepsilon_{aa}^{\text{eff}}$	0.202	0.013	2.73	
ζ_t^0	0.8637	0.995	0.7402	0.55[b]
T_{00} [c]	20 030.296	14 743.382	24 082.820	23018
Reference	[93]	[90]	[94]	[95]
	6^1			
$a\zeta_e d_{1/2,2}$	−24.95	−67[d]	−189	−736
A	5.04	5.0		
$A\zeta_t^0$	−4.97		−3.1	
ζ_t^0	−0.986		−0.62	
$\omega_{0,6}$ [e]	669	795[d]	825	650
Reference	[70]	[96]	[91]	[95]

[a] All parameters are in cm^{-1}, except ζ_t^0, which is dimensionless.

[b] For $CdCH_3$, ζ_t was not determined by a simultaneous fit to both spin components, as it was for the other radicals. Instead, each spin component was analysed independently. The average of the two values of ζ_t^Σ is given.

[c] Defined as the frequency from the vibrationless level of the ground state to the centre of the two spin components of the origin of the excited state.

[d] Estimated from figure 1 of [96]. In this work, the fundamental of ν_6 is assigned as two quanta of ν_6.

[e] Defined as the frequency from $\left|\tfrac{1}{2}, 1, \Sigma = -\tfrac{1}{2}\right\rangle$ to $\left|\tfrac{1}{2}, 2, \Sigma = +\tfrac{1}{2}\right\rangle$, which are the lower energy spin components of the origin and the fundamental of ν_6 respectively.

If there is only small Jahn–Teller coupling, the approximate energies of the origin and the $j = \frac{1}{2}$ level of the fundamental of ν_6 are given by equation (78):

$$E_{\nu_6=0} = \omega_{e,6} - 2D_6\omega_{e,6} \tag{133}$$

$$E_{\nu_6=1} = 2\omega_{e,6}. \tag{134}$$

The difference between these two levels, the experimentally observed $\omega_{0,6}$, is

$$\omega_{0,6} = \omega_{e,6}(1 + 2D_6). \tag{135}$$

Because each of these levels is split by spin–orbit coupling, we approximate $\omega_{0,6}$ as the difference between the average energies of the two spin components of each level (table 5).

The observed spin–orbit splitting of each level, $a\zeta_e d_{j,n_j}$, is approximated by

equation (83):†

$$a\zeta_e d_{1/2,1} = a\zeta_e (1 - 4D_6), \tag{136}$$

$$a\zeta_e d_{1/2,2} = a\zeta_e (-1 + 8D_6). \tag{137}$$

The left-hand sides of equations (136) and (137) are measured experimentally (table 5) which means that they form a 2×2 set of equations in two unknowns: the product $a\zeta_e$ and D_6. Solving the system leads to

$$D_6 = \frac{a\zeta_e d_{1/2,1} + a\zeta_e d_{1/2,2}}{8a\zeta_e d_{1/2,1} + 4a\zeta_e d_{1/2,2}}, \tag{138}$$

$$a\zeta_e = \frac{a\zeta_e d_{1/2,1}}{1 - 4D_6} = \frac{a\zeta_e d_{1/2,2}}{-1 + 8D_6}. \tag{139}$$

Because $\omega_{0,6}$ is also observed, equation (135) can now be solved for $\omega_{e,6}$. The calculated values of $a\zeta_e$, D_6 and $\omega_{e,6}$ for $MgCH_3$ are listed in table 6. These calculations illustrate how, if the spin–orbit splitting of the origin and the fundamental of a Jahn–Teller active mode are both resolved, values for the spin–orbit and Jahn–Teller coupling constants can be obtained.

If, in addition to the spin–orbit splittings, the Coriolis coupling of the two levels are also resolved, then additional information about the molecule can be obtained. Approximate expressions for the projection of the vibronic angular momentum, in terms of the molecular parameters ζ_e and ζ_6 and the spin–orbit quenching parameters $d_{1/2,1}$ and $d_{1/2,2}$, are given by equation (108):

$$\zeta_{t,0^0} = \zeta_e d_{1/2,1} - \tfrac{1}{2}\zeta_6 \left(d_{1/2,1} - 1\right), \tag{140}$$

$$\zeta_{t,6^1} = \zeta_e d_{1/2,2} - \tfrac{1}{2}\zeta_6 \left(d_{1/2,2} - 1\right). \tag{141}$$

As before, the left-hand sides of equations (140) and (141) are known from the experimental analyses and $d_{1/2,1}$ and $d_{1/2,2}$ have been calculated from the spin–orbit splittings via equations (136) and (137). These two equations are also a 2×2 system of equations in two unknowns: ζ_e and ζ_6. Solving them leads to

$$\zeta_6 = 2\frac{d_{1/2,2}\zeta_{t,0^0} - d_{1/2,1}\zeta_{t,6^1}}{d_{1/2,2} - d_{1/2,1}} \tag{142}$$

$$\zeta_e = \frac{\zeta_{t,0^0} + \tfrac{1}{2}\zeta_6(d_{1/2,1} - 1)}{d_{1/2,1}}. \tag{143}$$

Equation (139) can now be solved for a. The complete set of parameters determined in this fashion for $MgCH_3$ is shown in table 6. Because the calculated values of D_6 are small (about 0.05 or less), the equations given above should be fairly accurate.

† The factor d_{j,n_j} is defined as an expectation value of $\hat{\mathcal{H}}_{SO}$ for the vibronic eigenfunction including Jahn–Teller effects. One might therefore expect that the validity of the quenching parameter is limited to cases where $\hat{\mathcal{H}}_{SO}$ is small compared with Jahn–Teller effects, since for larger values of $\hat{\mathcal{H}}_{SO}$ its non-diagonal matrix elements will also be important. However, as equations (67)–(71) show, $\hat{\mathcal{H}}_{SO}$ has no off-diagonal elements in the original basis. Thus, so long as $\hat{\mathcal{H}}_{SO}$ is small compared with the difference in energies of the original basis set, d_{j,n_j} as defined by equation (80) remains approximately correct. In other words, the spin–orbit splitting will be approximated reasonably well by $a\zeta_e d_{j,n_j}$ so long as $\omega_{e,i} \gg a\zeta_e$, which is a limit of validity of the eigenfunction expansion of equation (80). This latter condition is easily fulfilled for all the MCH_3 radicals except $CdCH_3$.

Table 6. Spin–vibronic constants of the $\tilde{A}\,^2E$ states of the organometallic monomethyl radicals.[a]

Parameter	$MgCH_3$	$CaCH_3$	$ZnCH_3$	$CdCH_3$
	ν_2 and ν_3			
$\omega_{e,2}$	998		1060	1019
$\omega_{e,3}$	464		467	401
	ν_6			
$\omega_{e,6}$	633	767	749	710
D_6	0.0282	0.02	0.05	0.02
	Spin–orbit and Coriolis constants			
$a\zeta_e$	32.23	78	317	950
a	32.56	—	—	—
ζ_e	0.99	—	—	—
ζ_6	−0.25	—	—	—
ε_{total}	18.5	15.2	38.8	14.2
ε^{so}_{total}	15.0	0	0	0
Reference	[70]	[96]	[91]	[95]

[a] Only ν_2, ν_3 and ν_6 have been observed for these radicals.

We have verified the validity of these results by performing the full spin–orbit Jahn–Teller calculation using the parameters calculated via the perturbation equations. As expected, the agreement is quite good.

We can now use the results of table 6 to compute the spin–vibronic eigenfunctions and eigenvalues numerically. As expected and as shown by table 7, the calculated and observed energies agree quite well. However, the calculation also gives us the eigenfunctions, which allows us to directly compute ζ_t^+ and ζ_t^- for each observed level and hence $\Delta\zeta_t$ for each spin doublet. These calculated values are compared with the 'observed' values obtained from equations (119) and (121) and assuming that the observed value of ε_{aa}^{eff} has negligible contributions from ε_{aa}^0. The close agreement between the 'observed' and calculated values lends strong support to the assumption that the 'anomalously' large experimental value of ε_{aa}^{eff} is independent of the direct contribution ε_{aa}^0 to the spin–rotation coupling when one 'allows' for different spatial wavefunctions in the two spin states. As was previously suggested (see equation (111)), the value of ε_{aa}^{eff} can be rationalized in terms of a vibronic contribution, ε_{aa}^{2v}, to the spin–rotation coupling caused by second-order effects of the spin–orbit coupling. Alternatively the effect can be attributed to the different values of ζ_t^+ and ζ_t^- for the vibronic angular momentum in the two spin states.

6.1.2. *$CaCH_3$ and $ZnCH_3$*

The spin–vibronic structure of the excited states of the $CaCH_3$ and $ZnCH_3$ radicals are not very different from that for $MgCH_3$, with the exception that the spin–orbit coupling constants are larger. The perturbation expressions for the energy levels can still be used to a good approximation, as they were for $MgCH_3$. Tables 5 and 6 give the experimentally observed parameters and those calculated from a fit to the perturbation expressions, and the spin–orbit and Jahn–Teller coupling constants derived therefrom. As with $MgCH_3$, the agreement between the experimentally

Table 7. Spin–vibronic energy levels $|j, n_j, \Sigma\rangle$ of the $\tilde{A}\,^2E$ states of the organometallic monomethyl radicals.

		$MgCH_3$		$CaCH_3$		$ZnCH_3$		$CdCH_3$	
		Origin							
Level	Parameter	Observed	Calculated	Observed	Calculated[a]	Observed	Calculated[a]	Observed	Calculated[a]
$\left\|\frac{1}{2}, 1, -\frac{1}{2}\right\rangle$	Energy[b]	0	0	0	0	0	0	0	0
	ζ_t^-	0.8738	0.896	0.995	0.934	0.88	0.89	0.97	0.99
$\left\|\frac{1}{2}, 1, \frac{1}{2}\right\rangle$	Energy	28.6	28.8	73.1	73.4	253.2	260.1	1008	1029
	ζ_t^+	0.8536	0.876	0.957	0.903	0.60	0.58	0.2	0.63
	$\Delta\zeta_t^c$	−0.0202	−0.02	−0.038	−0.031	−0.28	−0.31	−0.77	−0.36
		$v_6 = 1$							
$\left\|\frac{1}{2}, 2, -\frac{1}{2}\right\rangle$	Energy	701.3	702.2	795	793	860	862	650	646
	ζ_t^+	−0.986	−1.01	—	−1.08	—	−0.71	−0.62	−0.86
$\left\|\frac{1}{2}, 2, \frac{1}{2}\right\rangle$	Energy	726.3	727.5	862	861	1045	1050	≈ 1386	1350
	ζ_t^-	−0.986	−1.01	—	−1.08	—	−0.64	—	−0.64
	$\Delta\zeta_t^c$	0.00	0.00	—	0.00	—	0.07	—	0.22

[a] Computed using the value of ζ_e and ζ_6 determined for $MgCH_3$ (table 6).

[b] The energy of the lowest level is set to zero.

[c] The observed values of $\Delta\zeta_t$ are obtained from the experimental value of $\varepsilon_{aa}^{\text{eff}}$, assuming that it is well approximated by ε_{aa}^{2v}. The calculated values of $\Delta\zeta_t$ are the differences in ζ_t^+ and ζ_t^-, calculated from the eigenfunctions.

observed energies and those calculated from exact spin–orbit Jahn–Teller coupling calculations is excellent (table 7). Likewise, the calculated change in the vibronic angular momentum accurately predicts the experimentally observed 'spin–rotation' coupling constant $\varepsilon_{aa}^{\text{eff}}$.

6.1.3. *$CdCH_3$*

The spin–vibronic coupling is quite different for the excited state of $CdCH_3$. For the lighter radicals, the spin–orbit splitting of each vibronic level could easily be discerned by the doublet structure in the electronic excitation spectra. However, for $CdCH_3$, the spin–orbit coupling constant $a\zeta_e$ (about 1000 cm^{-1}) is greater than the vibrational frequency of the degenerate mode. Therefore, the electronic spectra look rather peculiar in comparison with those for $MgCH_3$, $CaCH_3$, and $ZnCH_3$ in that the vibrational structure is smaller than the spin–orbit coupling structure. This also means that the traditional expectations of Jahn–Teller coupling may have to be modified.

As with the others, the spin–orbit splitting of the origin and the relative energies of the fundamentals of v_6 will be the levels that provide the greatest and most readily attainable information about the Jahn–Teller parameters. If the perturbation expressions that were used so successfully for $MgCH_3$, $CaCH_3$ and $ZnCH_3$ are applied, the following constants for $CdCH_3$ are determined: $\omega_{e,6}$ = 588 cm^{-1}, D_6 = 0.053 and $a\zeta_e$ = 1278 cm^{-1}. While the vibrational frequency and linear Jahn–Teller coupling constant are of the same order as those for the other organometallic monomethyl radicals, the spin–orbit coupling constant is quite a bit larger. While this is to be expected, as spin–orbit coupling scales approximately as Z^4, the spin–orbit constant A in the $A\,^2\Pi$ state of CdH is only 1013 cm^{-1} [97]. If anything, the spin–orbit coupling in the $\tilde{A}\,^2E$ state of $CdCH_3$ should be smaller than that in the $A\,^2\Pi$ state of CdH and not larger. Given the much larger spin–orbit interaction, it is not particularly surprising that the perturbation expressions should fail for $CdCH_3$.

However, the parameters obtained from the perturbation analysis can be used as a starting point for an analysis of the spectrum using full spin–orbit Jahn–Teller calculations. The results of this analysis are shown in figure 17, using the parameters listed in table 6. While the Jahn–Teller coupling constant did not change very much, the vibrational frequency and spin–orbit coupling parameter did. Most significantly, the value of $a\zeta_e$ = 950 cm^{-1} is now less than the spin–orbit coupling constant of CdH.

As discussed earlier, the decrease in the spin–orbit constant from CdH to $CdCH_3$ is readily explained by two phenomena. First, it is expected that the addition of three off-axis hydrogen atoms in $CdCH_3$ will decrease ζ_e, which is unity for the diatomic CdH. Secondly, the a constant in $CdCH_3$ will be different from A for CdH, as the electronic wavefunction, which has its major contribution from cadmium, will be slightly more delocalized in the case of $CdCH_3$. Because the atomic spin–orbit parameters for carbon and hydrogen are much smaller than that for cadmium, any delocalization onto these atoms will decrease the molecular spin–orbit coupling constant.

Because the spin–orbit coupling in the $\tilde{A}\,^2E$ state of $CdCH_3$ is larger than the frequency of the Jahn–Teller mode, figure 17 shows that many of the normal generalizations about the vibronic structure do not hold. For example, the observed spin–orbit splitting of the origin is normally smaller than the molecular spin–orbit coupling constant $a\zeta_e$ owing to the quenching of the orbital angular momentum

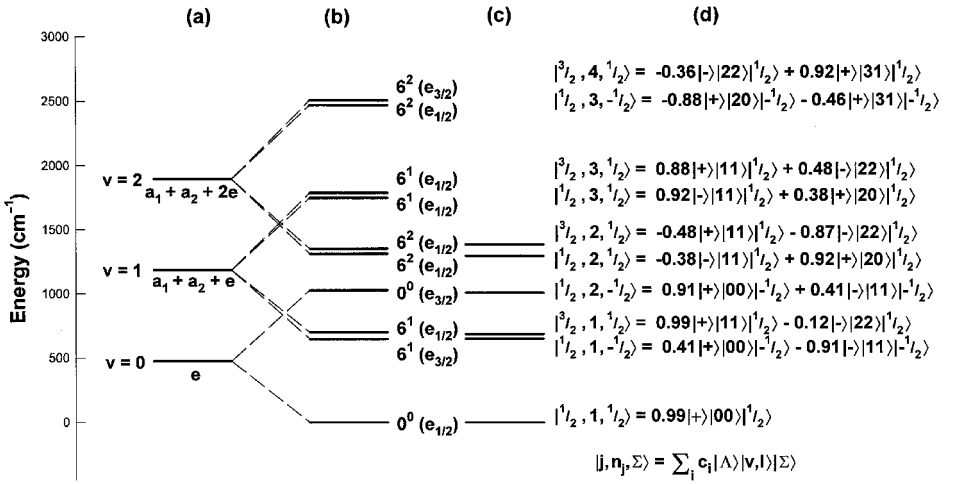

Figure 17. Vibronic energy level diagram for the $\tilde{A}\ ^2E$ state of $CdCH_3$. (*a*) harmonic oscillator energy levels for $v_i \leqslant 2$, (*b*) calculated energy levels using the parameters of table 6, (*c*) experimentally observed energy levels, (*d*) leading terms in the spin–vibronic wavefunction. Only the wavefunctions for $j > 0$ have been shown, for each level there is a second wavefunction with $j < 0$ with identical coefficients, but opposite signs on Λ, l and Σ.

by Jahn–Teller coupling. However, in $CdCH_3$, the observed spin–orbit splitting (1008 cm^{-1}) is actually greater than $a\zeta_e$ (950 cm^{-1}). Additionally, the energy of the 'fundamental' of v_6, 6^1 ($e_{3/2}$) is normally greater than the equilibrium frequency $\omega_{e,6}$. However, in $CdCH_3$ the reverse is true: the lower spin component of v_6 is at 650 cm^{-1} while the equilibrium frequency is 710 cm^{-1}. Both of these effects are caused by the fact that the spin–orbit coupling constant is greater than the vibrational frequency, which places the upper spin component of the origin at higher energy than the fundamental of the vibrational mode. Jahn–Teller coupling mixes these two levels, increasing the difference in energy between them. In the normal case, this decreases the energy of the upper spin component of the origin and increases the energy of the fundamental of the vibrational mode. However, in $CdCH_3$ the $v_6 = 1$ level is decreased in energy and the upper spin component of the origin is increased in energy, leading to the observed energy pattern.

For the lower energy spin component of the origin, the calculated and observed vibronic angular momentum components (table 7) agree very well. However, they do not agree for the upper spin component, although the experimental precision of these numbers is low. The most likely explanation for this disagreement is that v_5 is also active but is not included in the calculation. This explanation would also explain the poor agreement between the calculated and observed intensities in the electronic spectra at higher frequencies [95].

It is useful to conclude this section by clarifying some of the history of the $CdCH_3$ analysis. In the original report of the rotationally resolved LIF excitation spectrum [94], only the lower spin-component of the origin (labelled 0^0 ($e_{1/2}$) in figure 17) and the lower spin component of the fundamental of v_6 (labelled 6^1 ($e_{3/2}$) in figure 17) were observed. (All the other levels, except two totally symmetric modes, are dark and observable only by a fluorescence depletion technique [95].) Because

these were the only two levels observed in the LIF spectrum, they were assigned and analysed as the two spin components of the origin. This misassignment was possible because the upper spin component of the origin will have the same symmetry, $e_{3/2}$ under the spin-double group, and hence a similar rovibronic structure as the lower spin component ($6^1(e_{3/2})$) of the fundamental of the degenerate mode (figure 17). The correct assignment was made possible by a later ZEKE-PFI study, in which the different Franck–Condon factors for ionization for these two levels led to their true identification [92].

In the rotationally resolved LIF experiment, an extremely large spin–rotation constant, $\varepsilon_{aa}^{\text{eff}} = 15.8\ \text{cm}^{-1}$, was reported [94]. The explanation of this phenomenon is not coupling to other electronic states of the molecule, as was speculated in that paper, but rather alteration of the Coriolis coupling constants of the two spin components by simultaneous spin–orbit and Jahn–Teller coupling. Despite the earlier misassignment, the observed value of $\varepsilon_{aa}^{\text{eff}}$ still reflects the difference in the Coriolis coupling constants of the two levels, $\left|\frac{1}{2}, 1, \frac{1}{2}\right\rangle$ and $\left|\frac{1}{2}, 1, -\frac{1}{2}\right\rangle$, that were analysed, since they form a pair of $e_{1/2}$ and $e_{3/2}$ levels. Using equation (121), the observed value of $\varepsilon_{aa}^{\text{eff}}$ of 15.8 cm^{-1} corresponds to $\Delta\zeta_t = 1.59$. The full spin–orbit Jahn–Teller calculation of the eigenfunctions (table 7), allows us to calculate independently a value for $\Delta\zeta_t$ of 1.85. This value is in reasonable agreement with that obtained from the 'spin–rotation' constant. The small discrepancy between them is most probably caused by the neglect of Jahn–Teller activity in ν_5. Finally, we note that the LIF study can be viewed as misassigning the lowest observed level above the $e_{1/2}$ origin to its corresponding spin component. However, given the spin–vibronic eigenfunctions shown in figure 17, a fairer view is that it merely assumed that what in reality was the second most important contribution $|+\rangle|00\rangle\left|-\frac{1}{2}\right\rangle$ to the eigenfunction of the level was actually the most important.

6.1.4. *Summary of the metal monomethyl radicals*

When dealing with the spectroscopy of Jahn–Teller active molecules, several issues must be borne in mind. First, even to begin to assign and analyse the spectrum correctly, one needs to be aware of the spectral patterns that may result from the combined effects of Jahn–Teller and spin–orbit coupling. Then one must be able to use the spectra to obtain detailed quantitative information about a number of molecular parameters that either determine the Jahn–Teller and spin–orbit effects or are in turn clearly affected by them. From these parameters the nature and extent of the Jahn–Teller distortion and stabilization can be determined.

The $\tilde{A}\ ^2E$ states of the MCH_3 radicals have been fairly extensively, although not completely, characterized experimentally. They all fall into the category of small Jahn–Teller effects compared with spin–orbit coupling. Physically this situation exists because the 'unpaired' electron is localized in a metal orbital that is essentially an atomic p orbital. Hence, the orbital is only slightly perturbed by the lowering of the symmetry by the methyl group that ultimately is the source of the Jahn–Teller effect.

Correspondingly, the spectra are fundamentally those of symmetric top molecules with well defined spin–orbit doublets. The Jahn–Teller effect is primarily manifested in the spin–vibronic energy level structure via the partial quenching of the spin–orbit coupling, which in all the radicals, except $CdCH_3$, is well described by the generalized Ham reduction factor d_{j,n_j}. Just as the spin–vibronic eigenvalues are

modified by Jahn–Teller coupling, so are the spin–vibronic eigenfunctions, which determine the vibronic angular momentum $\zeta_t^{\pm}$, which can be measured from the rotational structure of the spin–vibronic levels.

For $MgCH_3$, experimental measurements of the spin–vibronic levels combined with information from this rotational structure allow a rather complete description of the Jahn–Teller coupling. For the other radicals the experimental information is somewhat less extensive, nonetheless, considerable information about the Jahn–Teller effect in these radicals is available. In all cases, there appears to be significant Jahn–Teller activity in only mode, v_6, nominally the metal methyl rock. This is not particularly surprising since the orbital degeneracy is mostly localized on the metal atom, thus the other two e modes, v_4 and v_5, are expected to have little influence on the electron on the metal.

We see that the activity in even the rock mode is slight, with D_i always about 0.05 or less. Nonetheless even such a small Jahn–Teller coupling can cause significant quenching of the spin–orbit interaction. In the vibrationless level (excited v_6 levels have greater quenching) the spin–orbit splitting is reduced by 11%, 7% and 20% respectively, for the series MCH_3 (M = Mg, Ca or Zn). For $CdCH_3$, the spin–orbit splitting of the 'origin' is actually enhanced by 6% because $a\zeta_e$ is greater than $\omega_{e,6}$. From table 7 we also note that the spin–vibronic eigenfunctions predict a substantial effect on the Coriolis coupling from the Jahn–Teller induced modification of the vibronic angular momentum ζ_t. It is indeed a reassuring check on our overall understanding of the system that, for the most part, these predictions are well confirmed by direct measurements of the relevant parameters from the rotationally resolved spectrum.

Finally the spectral analyses give us a relatively clear picture of the distortion of the $\tilde{A}\ ^2E$ PES by the Jahn–Teller effect. In all cases, the hypothetical PESs for the spinless molecules show at least a small minimum at a distorted configuration. However, the more meaningful PES that includes spin–orbit coupling shows that for all the radicals, with the exception of $MgCH_3$, there is no net stabilization and the minimum of the PES remains at the symmetrical C_{3v} configuration for all the normal modes. Thus the correct picture of the PES is provided by figure 2(*h*), where one notes that neither the $^2E_{1/2}$ nor the $^2E_{3/2}$ PES has a minimum other than at the C_{3v} point. However the lower surface (in this case, $^2E_{1/2}$) is much flatter around the symmetrical minimum than it would be if the Jahn–Teller effect were absent. For $MgCH_3$, figure 2(*g*) more appropriately represents the slice of the potential along the v_6 coordinate. However, even here the stabilization is quite small, amounting to only about 15 cm^{-1}.

6.2. *Methoxy radical family*

The methoxy radicals, CH_3O, CH_3S, CF_3O and CF_3S, are all characterized by a $\tilde{X}\ ^2E$ ground state and a lowest excited $\tilde{A}\ ^2A_1$ state. They have all been observed by LIF excitation spectroscopy but its effectiveness in characterizing the spin–vibronic structure of the $\tilde{X}\ ^2E$ state has been limited. In jet-cooled spectra, only the vibrationless level is populated and the information about the Jahn–Teller coupling in the ground state is usually limited to that yielded from the rotational structure. The rotational structure is also provided, often in greater detail, via microwave and laser magnetic resonance (LMR) experiments, which have been performed for CH_3O and CH_3S.

While the rotational information is very valuable, direct information about the

spin–vibronic energy levels is essential. For the most part, this information has been obtained from laser-excited dispersed fluorescence experiments. These experiments, while somewhat limited in resolution, are nonetheless superb for providing an overall picture of the spin–vibronic structure of the $\tilde{X}$ states of the methoxy family. A limited amount of higher resolution stimulated emission pumping data are also available for CH_3O.

6.2.1. *CF_3S*

The dispersed fluorescence spectra from the $\tilde{A}$ state of CF_3S have been obtained in our laboratory and illustrate nicely the analysis of such data [91]. The spectra are dominated by transitions to the totally symmetric modes, just as is the case for the excitation spectrum. The spectra also contain a number of lines that cannot be ascribed to totally symmetric modes and that therefore must be assigned to the Jahn–Teller active modes.

Simulations of the dispersed fluorescence from the origin and from $v_6' = 1$ in the excited state are shown in figure 18. These simulations used the parameters given in table 8. Assignments of several of the bands due to v_6 could be easily made by a comparison between the spectrum from the origin and that from pumping one quantum of v_6 in the excited state. The peaks that are present only in the spectrum from 6^1 must be assigned to the $j = \frac{3}{2}$ levels. Mode 6 accounts for several of the low energy peaks in the spectra, but not all. The rest were identified as predominantly v_5, though there appears to be very little Jahn–Teller coupling in this mode.

As figure 18 shows, linear Jahn–Teller coupling in v_6 and spin–orbit coupling can adequately reproduce the experimental spectra (see also table 8). Because the spin–orbit splitting is so large, quadratic coupling in v_6 would not appear as a splitting in the $j = \frac{3}{2}$ levels but rather as a different splitting from that predicted by just linear Jahn–Teller and spin–orbit coupling. There is no spectral evidence that this is the case. Quadratic Jahn–Teller coupling, if present, must be very small in v_6.

As table 8 shows, there was not enough information available in the dispersed fluorescence spectra for D_5, D_4 and $\omega_{e,4}$ to be determined, even though the fundamental of v_5 is observed in the spectrum. As we shall see for the other methoxy radicals, it is generally the case that v_6 is the mode that carries most of the Jahn–Teller activity, with v_5 and v_4 having smaller Jahn–Teller effects. The spin–orbit coupling constant is in line with that for the diatomic radicals SH and SF (table 8).

The stabilization induced by the Jahn–Teller coupling illustrates the marked difference between an analysis that does not include spin–orbit coupling and one that does (equations (56) and (66), table 8). If the quenching of the stabilization energy by spin–orbit coupling is not included in the calculation, a value of 77 cm^{-1} is obtained. While this value is relatively small, it is not negligible. However, when spin–orbit coupling is included this value drops to exactly zero. Thus, there is no asymmetric minimum in the PES and figure 2(*h*) is an appropriate representation of the potential for the ground state of CF_3S.

Unlike the organometallic radicals, a rotationally resolved spectrum of both spin components of the vibrationless level of the ground state of CF_3S has not been performed, since the upper spin component is not populated in the jet-cooled experiment. Therefore, rotational parameters are available only for the lower energy spin component (table 9) [107]. As such, the values of $A\zeta_t^0$ and ε_{aa}^{eff} could not be determined independently, only the difference $A\zeta_t^0 - \varepsilon_{aa}^{eff}/4$. This means that the rotational information relevant to the Jahn–Teller coupling is quite limited. If we

Table 8. Spin–vibronic constants of the $\widetilde{X}\,^2E$ states of the methoxy family of radicals.

Parameter	CH_3O	CD_3O	CH_3S	CF_3O	CF_3S
	Totally symmetric modes				
$\omega''_{e,1}$			2776	1215	1142
$\omega''_{e,2}$	1359	995	1313	977	765
$\omega_{e,3}$	1050.5	1036	727	527	449
	Degenerate modes				
$\omega''_{e,4}$	2835	2100	—	—	—
D_4	0.02	0.03	—	—	—
K_4	—	—	—	—	—
$\omega''_{e,5}$	1417	1070	—	600	536
D_5	0.075	0.17	—	0.04	< 0.01
K_5	−0.032	−0.03	—	—	—
$\omega''_{e,6}$	1065	825	913[a]	465[b]	320
D_6	0.24	0.20	0.045	0.45	0.24
K_6	−0.14	−0.16	—	0.05	—
$a\zeta_e$	−145	−145	−340	−140	−360
ε_{total}	419	410	41	233	77
ε^{so}_{total}	370	367	0	203	0
	Spin–orbit constants for diatomic radicals				
	OH	OD	SH	OF	SF
A	−139	−139	−377	−196	−398
Reference	[99]	[99]	[99]	[100, 101]	[102, 103]

[a] Fixed at the *ab initio* value [98].
[b] For CF_3O an anharmonicity in v_6 was observed, $\omega_e x_e$ = 8 cm^{-1}.

Table 9. Rotational constants for the $\widetilde{X}\,^2E$ states of the methoxy family of radicals.[a]

Parameter	CH_3O	CH_3S	CF_3O	CF_3S
A''	5.206	5.68	0.1894	0.18886[b]
B''	0.931 682 5	0.449581	0.19754	0.11108
$a\zeta_e d_{1/2,1}$	−61.974	−255.463	−41	−160
$A''\zeta^0_t$	1.773	3.523	—	—
ζ^0_t	0.341	0.620	—	—
ε^{eff}_{aa}	−1.3533	−3.809	−0.08[c]	−0.433[c]
$A''\zeta^0_t - \frac{\varepsilon^{eff}_{aa}}{4}$	2.1113	4.48	0.04961	0.1430
h_1	0.00252	0.000198	⩽ 0.008	⩽ 0.026
h_2	0.0461	0.022	⩽ 0.024	⩽ 0.041
Reference	[104]	[105]	[106, 107]	[107]

[a] The parameters for CH_3O and CH_3S were fit for both spin components of the vibrationless level, whereas only the lower energy spin components of CF_3O and CF_3S were analysed. All parameters are in cm^{-1}, except ζ^0_t, which is dimensionless.
[b] Fixed at the value from an *ab initio* calculation.
[c] Predicted by the spin–orbit Jahn–Teller calculations using the parameters in table 8 and estimates for ζ_e and ζ_6.

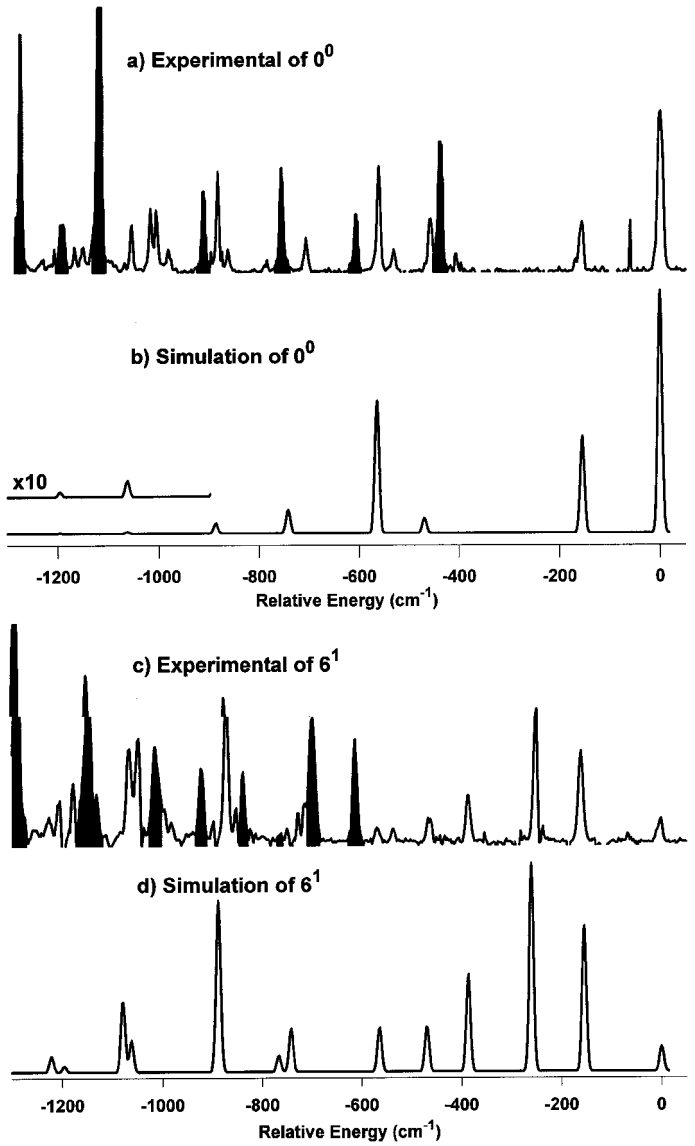

Figure 18. Dispersed fluorescence of the CF_3S radical: (*a*) experimental spectrum from the 0^0 band, (*b*) simulation of the 0^0 spectrum, (*c*) experimental spectrum from the 6^1 band, (*d*) simulation of the 6^1 spectrum. Transitions to the totally symmetric modes (filled) are not included in the simulation.

assume that the Coriolis coupling constant ζ_6 in the ground state is the same as that in the excited state, which has been determined experimentally (table 10) [107], and assume that $\zeta_e = 1$, we can predict a value of $\varepsilon_{aa}^{\text{eff}}$ using the computed spin–vibronic eigenfunction and equation (118). This predicted value is given in table 9.

6.2.2. *CH_3S*

The dispersed fluorescence spectra of the CH_3S and CD_3S radicals were first reported by Suzuki *et al.* [112]. These spectra showed that the spin–orbit splittings

Table 10. Vibrational frequencies of the $\tilde{A}\ ^2A_1$ states of the methoxy family of radicals.[a]

Parameter	CH_3O	CD_3O	CH_3S	CF_3O	CF_3S
T_{00}	31 615	31 5554	26 399	28 531	26 393
	Totally symmetric modes				
$\omega'_{e,1}$	2947.8				998 (3.64)
$\omega'_{e,2}$	1313.2 (7.4)	967	1098		740 (0.50)
$\omega'_{e,3}$	677.2 (4.6)	660	401	635	314.0 (2.40)
	Degenerate modes				
$\omega'_{e,4}$	3077.8	2326			
ζ'_4	0.088				
$\omega'_{e,5}$	1403.0	1045		626	548
ζ'_5	−0.14			−0.39	−0.65
$\omega'_{e,6}$	951 (7)	695	635	426	277 (−0.9)
ζ'_6	0.12			0.037	0.26
References	[108]	[109]	[110]	[107]	[111]

[a] Where available, $\omega_e x_e$ is listed in parentheses. If no value in parentheses is given, insufficient transitions were observed to determine ω_e and $\omega_e x_e$, the value listed is ω_0.

of the origin were −280 and −260 cm^{-1} for CH_3S and CD_3S respectively, in accord with the laser electron photodetachment spectra recorded prior to the LIF spectra [113]. The dispersed fluorescence spectra were vibrationally and rotationally very hot and the spin–orbit splittings of the origin could be determined to an accuracy of only 20 cm^{-1}. The error on the spin–orbit splitting of CH_3S was reduced when microwave [114] and high-resolution LIF [105] spectra were taken. The best experimental value for the spin–orbit splitting of CH_3S is −255.5 cm^{-1}, which was derived from a simultaneous fit of the microwave and high-resolution LIF data [105].

The dispersed fluorescence spectra were later retaken by Lee's group [110], who obtained them in a free-jet expansion rather than a static gas cell. The vibrational and rotational cooling of the free jet meant that much more information about the vibrational modes could be obtained. As usual, the vast majority of the features in the dispersed fluorescence spectra could be assigned to the totally symmetric modes. The spectra showed only marginal intensity to the Jahn–Teller modes, and only the fundamental frequencies could be determined. Jahn–Teller coupling is clearly very small in CH_3S, otherwise greater intensity would be observed in the Jahn–Teller modes.

While for CF_3S and the other methoxy radicals a number of vibronic energy levels owing solely to the Jahn–Teller active modes appear in the dispersed fluorescence spectra, this is not the case for CH_3S. How then is a quantitative determination of the Jahn–Teller and spin–orbit coupling to be made in such a molecule? The answer lies in the experimental determination of the spin–orbit splitting in two isotopomers, CH_3S and CD_3S, by Suzuki *et al.* [112]. Because the masses of the nuclei are different, the frequency of the mode responsible for the Jahn–Teller coupling changes significantly. However, the electronic potential in which these nuclei vibrate is assumed not to change, nor is the spin–orbit coupling parameter $a\zeta_e$ expected to be different between the two isotopomers. The determination of the Jahn–Teller

constants then relies upon a determination of the vibrational frequencies of the Jahn–Teller modes, and which mode or modes are responsible for the Jahn–Teller activity.

The application of this logic to a system where the spin–orbit splitting is known for two isotopomers is readily derived. First, the assumption that the spin–orbit coupling constants $a\zeta_e$ are the same for each isotopomer leads to the following equation:

$$\frac{\left(a\zeta_e d_{1/2,1}\right)^H}{\left(a\zeta_e d_{1/2,1}\right)^D} = \frac{d^H_{1/2,1}}{d^D_{1/2,1}}. \tag{144}$$

The values in parentheses on the left-hand side of equation (144) are the observed spin–orbit splittings of the vibrationless level of each isotopomer, while the parameters on the right-hand side are the spin–orbit quenching parameters of equations (80), (81) and (83). Second, because the Jahn–Teller stabilization energy is independent of the nuclear masses, equation (56) becomes

$$\varepsilon_i = D_i^H \omega_{e,i}^H = D_i^D \omega_{e,i}^D. \tag{145}$$

Assuming that the Jahn–Teller coupling is small, the substitution of $d_{1/2,1} = 1 - 4D_i$ (equation (83)) into equation (144) can be made. Solving the 2x2 system of equations for D_i^H yields

$$D_i^H = \frac{1}{4}\frac{\left(a\zeta_e d_{1/2,1}\right)^H / \left(a\zeta_e d_{1/2,1}\right)^D - 1}{\left(a\zeta_e d_{1/2,1}\right)^H \omega_{e,i}^H / \left(a\zeta_e d_{1/2,1}\right)^D \omega_{e,i}^D - 1}. \tag{146}$$

Thus, if the spin–orbit splitting of the vibrationless level is known for two different isotopomers, and the harmonic oscillator frequencies $\omega_{e,i}^H$ and $\omega_{e,i}^D$, or at least their ratio, can be estimated by another means, than a reasonably accurate determination of the Jahn–Teller constants can be made. The accuracy and precision of the determination depend not only upon the precision of the measured spin–orbit splittings but also on the determination of the oscillator frequencies and on deducing which mode is Jahn–Teller active.

Bent [115] originally applied this logic to CH_3S, though in somewhat different form. He assumed that ν_5 is the Jahn–Teller active mode in CH_3S. He derived oscillator frequencies $\omega_{e,5}^H$ and $\omega_{e,5}^D$ by analogy to the frequencies for CH_3O, CD_3O, CH_3SH and CD_3SH and by invoking the Teller–Redlich product rules for isotopic frequencies [116]. In his calculations, he set $\omega_{e,5}^H$ to 1410 cm^{-1} and $\omega_{e,5}^D$ to 1040 cm^{-1}. Using the values for the spin–orbit splitting from the room temperature LIF spectra [112], he deduced Jahn–Teller coupling constants of $D_5^H = 0.065$, $D_5^D = 0.09$, and a spin–orbit coupling constant $a\zeta_e$ of -356 cm^{-1}. The Jahn–Teller stabilization energy via equation (56) is then approximately 92 cm^{-1}. Invoking equation (66) reduces the real stabilization energy to zero, just as was the case for CF_3S.

Is ν_5 really the mode responsible for the Jahn–Teller coupling and the resultant partial quenching of the spin–orbit coupling? Bent chose ν_5 because, at the time of his publication, it was believed that ν_5 was the mode responsible for the Jahn–Teller coupling in CH_3O. However, the detailed stimulated emission pumping (SEP) spectra of Temps' [109] group have shown that most of the Jahn–Teller coupling in CH_3O is due to ν_6, and not ν_5, and our analysis and *ab initio* calculations [98] support this change. We therefore feel it is necessary to revise Bent's determination of the Jahn–Teller coupling in CH_3S, using ν_6 instead of ν_5.

Rather than derive frequencies from other molecules and from isotopic shift rules, we have calculated the harmonic frequencies via *ab initio* methods [98]. For CH_3S, we calculated $\omega_{e,6}^{H}$ to be 913 cm^{-1} and $\omega_{e,6}^{D}$ to be 688 cm^{-1}. (For comparison with Bent's derivation of the harmonic frequencies for v_5, we calculate $\omega_{e,5}^{H}$ = 1422 cm^{-1} and $\omega_{e,5}^{D}$ = 1029 cm^{-1}, in very good agreement with the values that he estimated.) Using these values for the harmonic frequencies of v_6, we determine D_6^{H} = 0.045, D_6^{D} = 0.062, and $a\zeta_e$ = −341 cm^{-1}. The resultant Jahn–Teller stabilization energy, in the absence of spin–orbit coupling, is only 41 cm^{-1}, compared with Bent's value of 90 cm^{-1}. In either case, the Jahn–Teller distortion is overwhelmed by the spin–orbit coupling so that there is no net Jahn–Teller stabilization for CH_3S.

Information relevant to a decision on which mode accounts for the Jahn–Teller activity in the radical can be obtained from the observed spin–rotation constant (table 9) [105]. While the Coriolis constants for the individual vibrational modes in the ground state of CH_3S have not been determined, the calculated values of $\zeta_t^{\pm}$ depend almost exclusively on the value of ζ_e, with only a minor dependence on the values of ζ_6 or ζ_5. Using Bent's spin–orbit and Jahn–Teller coupling constants, we calculate $\Delta\zeta_t$ = −0.152 while, with our constants, $\Delta\zeta_t$ = −0.225. The experimental value, determined via equation (118), is −0.336. While not a conclusive result, the comparison of these constants supports the assignment of v_6 as the Jahn–Teller active mode in CH_3S. This assignment is also consistent with the observed Jahn–Teller coupling in the other methoxy radicals (table 8).

6.2.3. *CF_3O*

The spectroscopy of the sulphur-centred radicals CF_3S and CH_3S is relatively straightforward to interpret because the spin–orbit coupling is so large in comparison with the Jahn–Teller coupling. The situation is quite different for the oxygen-centred radicals, in which $a\zeta_e$ is only approximately half as large, while the Jahn–Teller coupling probably increases. This means that the approximations of perturbation theory no longer work very well and the only way to analyse the spectra is by the use of complete spin–vibronic calculations.

The LIF spectrum of the CF_3O radical was first observed by Li and Francisco [117] in a static gas cell. The spectrum was recorded in our laboratory using a free jet expansion to cool the radicals vibrationally and rotationally. The rotationally resolved spectra of the origin, 3_0^1, 6_0^1 and 5_0^1 bands were also obtained [106, 107], together with their dispersed fluorescence spectra [118].

The first indication of Jahn–Teller coupling in the ground state of CF_3O is the existence of intensity in the excitation spectrum to the degenerate modes v_6 and v_5, which were rotationally resolved and analysed to support their identification as degenerate vibrations [107]. In the absence of Jahn–Teller coupling, these levels have zero intensity, as only the totally symmetric modes may be observed. Most information about the spin–orbit and Jahn–Teller coupling comes from the dispersed fluorescence spectra [91], which are shown in figure 19.

Transitions to fundamentals and combinations of the totally symmetric modes v_1, v_2 and v_3, can be easily identified in the dispersed fluorescence from $v' = 0$ by their approximately constant spin–orbit splittings. The three totally symmetric modes and one combination of them are observed in the spectra, with an average

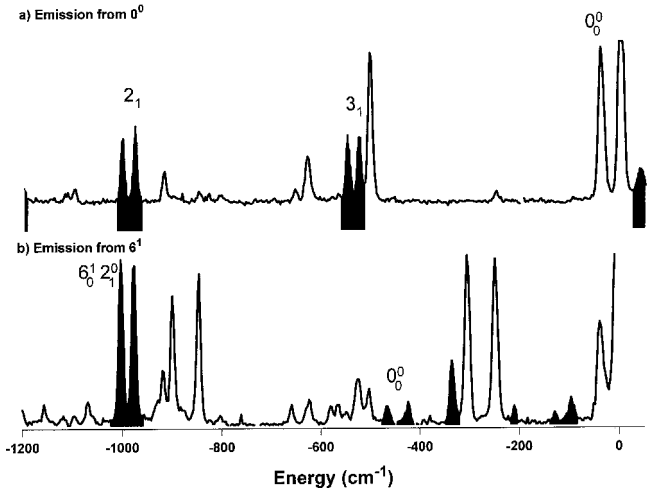

Figure 19. Dispersed fluorescence of the CF_3O radical: (*a*) experimental spectrum from $v' = 0$, (*b*) experimental spectrum from pumping 6^1. The filled peaks either are assigned as totally symmetric modes or are due to emission from species in the expansion that are excited by spontaneous emission from the laser source or to collisional relaxation of the excited state.

splitting of 25 ± 3 cm^{-1}.† Significant insight into the Jahn–Teller coupling in this molecule comes from the comparison of the dispersed fluorescence from the 0^0 and 6^1 bands. As discussed in section 5, only those levels with $j = \pm\frac{1}{2}$ will be observed in the fluorescence from the 0^0 band, whereas both $j = \pm\frac{1}{2}$ *and* $j = \pm\frac{3}{2}$ will be observed in the fluorescence from the 6^1 level. The comparison of these two spectra clearly shows a pair of levels in the 6^1 spectrum, at 249 and 306 cm^{-1}, that are not in the 0^0 spectrum. The splitting of these $j = \pm\frac{3}{2}$ levels is 57 cm^{-1}, which is significantly larger than the splitting of the totally symmetric levels. As we discussed earlier, the only possible way for this to occur is by quadratic Jahn–Teller coupling. The quadratic Jahn–Teller coupling constant K_6 can therefore be deduced by fitting the splitting of these two levels. The other constants can be determined by fitting the position of these two levels relative to the origin.

The spin–orbit and Jahn–Teller coupling constants that have been derived from the analysis of these spectra are given in table 8. The value of $a\zeta_e$ is -140 cm^{-1}, which lies between the values of A in the $X\ ^2\Pi$ states of the OH radical (-139 cm^{-1}) [99] and the OF radical (-196 cm^{-1}) [100, 101]

Lastly, we consider the size of the spin–rotation constant induced by spin–orbit and Jahn–Teller coupling. Because only the lower spin component of the origin has been rotationally resolved [107], only the combination $A\zeta_t^+ - \varepsilon_{aa}^{eff}/4$ was determined (table 9). Given our spin–orbit Jahn–Teller wavefunction, we can predict a value of ε_{aa}^{eff} using equation (118). For this calculation, we must estimate the electronic and

† However, the spin–orbit splitting of the origin was determined to be 41 cm^{-1}. We know of no reason why the spin–orbit splitting should change so dramatically from the origin to the fundamentals of the symmetric modes and suspect that the value for the origin is skewed because of very strong laser scatter on one component in the dispersed fluorescence spectrum. For this reason, we take 25 cm^{-1} as the value for the spin–orbit splitting of the origin.

vibrational Coriolis constants ζ_e and ζ_i (i = 4, 5, 6). We assume a value of ζ_e = 0.95, which is only slightly smaller than unity, its maximum value in the limit of cylindrical symmetry. The vibrational Coriolis constants $\zeta_5 = -0.39$ and $\zeta_6 = 0.037$ have been determined for the excited state of CF_3O [107]. From the calculated spin–vibronic eigenfunction, the following two equations are computed for the Coriolis coupling constants for the two spin components of the origin:

$$\zeta_t^+ = 0.381\zeta_e + 0.285\zeta_6 + 0.023\zeta_5 = 0.36, \quad (147)$$

$$\zeta_t^- = 0.153\zeta_e + 0.393\zeta_6 + 0.027\zeta_5 = 0.15. \quad (148)$$

These two equations illustrate how complex the function that determines the Coriolis constants can be. These calculations predict a value of -0.08 cm^{-1} for ε_{aa}^{2v}, which is much smaller than the values for CH_3S and CH_3O (table 9). The difference is that ε_{aa}^{2v} is proportional to the A rotational constant, which is 27 times smaller for CF_3O. If this scaling is taken into account, the value of ε_{aa}^{2v} induced by spin–orbit and Jahn–Teller coupling is comparable with those in CH_3O and CH_3S.

6.2.4. *CH_3O*

The methoxy radical CH_3O is by far the most exhaustively studied Jahn–Teller radical. Spectroscopic investigations of it include emission [119, 120], LIF, both of the excited state [46, 47, 108, 121] and dispersed fluorescence studies of the ground state [121–123] rotationally resolved LIF [104], SEP studies of the ground state and its isomerization to CH_2OH [124–126], electron spin resonance [127], microwave absorption [74], LMR [72, 73], laser photodetachment of the anion [113], fluorescence depletion of the excited state [128], and fast beam photofragmentation of the excited state [129, 130]. A number of these experiments have also been performed on the isotopomer CD_3O: LIF [120, 121, 131], SEP [109], laser photodetachment of the anion [113], fluorescence depletion [131] and photofragmentation [130]. For the isotopomer $^{13}CH_3O$, the microwave spectrum [85, 86] and dispersed fluorescence spectra [123] have been reported. A more exhaustive list of the earlier investigations of this radical has been given in [120].

The methoxy radical has also served as a benchmark molecule for the evaluation of *ab initio* methods. Most of these calculations have focused on the thermochemistry of the radical and these calculations have been reviewed recently [132]. A few calculations have been reported on the excited states and photochemistry of the methoxy family of radicals [133–135]. One attempt has been made at calculating the Jahn–Teller coupling constants D_i and the Coriolis coupling constants ζ_i (i = 4–6) [136]. The spin–orbit coupling constant [137, 138] and hyperfine coupling constants [139, 140] have also been analysed via *ab initio* calculations. We shall more fully discuss these calculations, and our own *ab initio* calculations, in a subsequent publication [98].

The Jahn–Teller coupling in the $\tilde{X}\,^2E$ state of CH_3O is manifested most strongly in the energies of the degenerate vibrational modes. The energies of these levels are observed in the dispersed fluorescence spectra and the SEP spectra and we shall concentrate on the analysis of these spectra. However, as we saw for the other methoxy radicals and the organometallic monomethyl radicals, the Coriolis coupling constants and spin–rotation constant are also affected by Jahn–Teller coupling, as are the much smaller rotational parameters h_1 and h_2. The methoxy radical is a rare example for which all of these parameters have been obtained,

to quite good accuracy and for several different isotopomers. We shall summarize the experimental data and then discuss the various interpretations of the Jahn–Teller coupling in this radical that have been proposed. We shall first summarize the vibrational results for the $\tilde{A}\ ^2A_1$ excited state, as these vibrational frequencies can be used as a starting point in the Jahn–Teller analyses of the $X\ ^2E$ state.

6.2.4.1. *Vibrational frequencies of the* $\tilde{A}\ ^2A_1$ *state of* CH_3O. A comprehensive experimental investigation and analysis of the vibrational structure of the excited state of the methoxy radical was recently reported [108, 128]. The vibrational frequencies of all six modes were determined (table 10), including a complete analysis of the Fermi resonance between v_2 and $2v_3$. There were several consequences of this work for the Jahn–Teller analysis of the ground state. First, while the C–O bond lengthens significantly, the C–H bond length and O–C–H bond angle do not, which means that the vibrational frequencies of the ground state and excited state should be similar, except for the C–O stretch. Therefore, the values of $\omega''_{e,i}$ (i = 4–6) should not be very different from that of $\omega'_{e,i}$. Secondly, the Coriolis coupling constants for the three degenerate modes in the excited state were determined, thus facilitating the comparison of a calculated spin–rotation constant with that observed experimentally.

The last issue that this study cleared up is the frequency of v_6 in the excited state. In the original report of the jet-cooled LIF spectrum of methoxy [121], a feature was observed at 595 cm^{-1} and assigned to the fundamental of v_6 in the excited state. In the more recent work [108], which included a fixture on the free jet expansion to facilitate vibrational cooling, this feature was shown to belong to a vibrational hot band. The frequency of v_6 was reassigned as 951 cm^{-1}, which was confirmed by its rotational analysis. The incorrectness of the original value of this frequency was independently suggested by Cui and Morokuma [135], whose *ab initio* calculations of the excited state frequencies predicted a value of 1034 cm^{-1}. The reason that this result is important for the interpretation of the ground-state coupling is that the lowest-energy vibronic level in the ground state occurs at 652 cm^{-1}. This level was initially interpreted, in light of an excited state frequency for v_6 of 595 cm^{-1}, as a slightly perturbed v_6 = 1 level. This led to a proposed frequency of $\omega''_{e,6}$ only slightly greater than 650 cm^{-1}. With the reassignment of $\omega'_{e,6}$, the assignment of $\omega''_{e,6}$ needs to be changed. In table 10 we summarize all the $\tilde{A}\ ^2A_1$ state vibrational frequencies and Coriolis constants.

6.2.4.2. *Rotational structure of* $\tilde{X}\ ^2E\ CH_3O$. Before turning to the vibronic structure of $\tilde{X}\ ^2E\ CH_3O$, it will be useful to review the rotational structure of the vibrationless level from which some relevant results can be gleaned for the Jahn–Teller analysis. A number of rotationally resolved experiments have been performed on the vibrationless level of the ground electronic state of CH_3O, including LMR [72, 73], microwave absorption [74, 85, 86] and rotationally resolved LIF [104]. The information obtained from these experiments is summarized in table 11. An important result from table 11 is that the LMR experiment can separate the product $a\zeta_e d_{1/2,1}$ into its components a and $\zeta_e d_{1/2,1}$. This determination of a means that the spin–orbit coupling constant $a\zeta_e$ does not have to be extracted from the vibronic

Table 11. Rotational constants for the $\tilde{X}\,^2E$ state of the methoxy radical.

	LMR	LIF	Microwave	
Parameter	CH_3O	CH_3O	CH_3O	$^{13}CH_3O$
A''	5.3280	5.2059	5.3387	5.3562
B''	0.931 776	0.931 682 5	0.931 639 5	0.910 059 6
$a\zeta_e d_{1/2,1}$	−62.8	−61.974	−62.486	−62.199
a	−142.8	—	—	—
$\zeta_e d_{1/2,1}$	0.4397	—	—	—
$A''\zeta_t^0$	1.79	1.7730	1.7436	1.7199
ζ_t^0	0.3362	0.3406	0.3266	0.3211
$\varepsilon_{aa}^{\text{eff}}$	−1.103	−1.3533	−1.2308	−1.2603
h_1	0.103 30	0.002 511 7	0.002 55	0.002 42
h_2	0.001 44	0.046 05	0.042 72	0.0426
Reference	[73]	[104]	[74, 85]	[85, 86]

structure of the radical but can be assumed to be about $-142\ \text{cm}^{-1}$ or less and to equal $-142\ \text{cm}^{-1}$ as ζ_e approaches unity, which it probably does.

These experiments determined $A''\zeta_t^0$ and A'' quite accurately, yielding a value of $\zeta_t^0 = 0.34$. They also determined the effective spin–rotation constant of the origin to be $-1.353\ \text{cm}^{-1}$. (We use the values from the LIF experiment [104] because its analysis incorporated both the microwave data and the rotationally resolved LIF data.) If one assumes that the observed spin–rotation constant is entirely due to spin–vibronic coupling, then $\Delta\zeta_t^{\pm} = 0.13$. While no Jahn–Teller or spin–orbit coupling constants can be directly determined from this value, it will serve as a useful check of any spin–vibronic analysis.

These methods have also determined the rotational constants h_1 and h_2. As we discussed in section 4.3, these parameters contain contributions both from Jahn–Teller coupling and from mixing with other electronic states. Because the microwave experiments were done on two different isotopomers, $^{12}CH_3O$ and $^{13}CH_3O$, the contributions from these two sources can be separated, owing to their different dependencies on the rotational constants (see section 4.3). Because of these proportionalities, the following pairs of equations can be set up, where the superscripts (JT) and (L) refer to the contributions from Jahn–Teller coupling and L uncoupling, respectively:

$$h_1^{(12)} = k_1^{(\text{JT})}B^{(12)} + k_1^{(L)}(B^{(12)})^2, \tag{149}$$

$$h_1^{(13)} = k_1^{(\text{JT})}B^{(13)} + k_1^{(L)}(B^{(13)})^2, \tag{150}$$

and

$$h_2^{(12)} = k_2^{(\text{JT})}(A^{(12)}B^{(12)})^{1/2} + k_2^{(L)}(A^{(12)}B^{(12)}), \tag{151}$$

$$h_2^{(13)} = k_2^{(\text{JT})}(A^{(13)}B^{(13)})^{1/2} + k_2^{(L)}(A^{(13)}B^{(13)}). \tag{152}$$

From the microwave experiments, all of the parameters of these equations have been determined except the proportionality constants $k_1^{(\text{JT})}$, $k_1^{(L)}$, $k_2^{(\text{JT})}$, and $k_2^{(L)}$. Solving the pairs of 2×2 equations for the proportionality constants leads to the 'decoupled' contributions to h_1 and h_2 (table 12). (While the values for h_1 and h_2 from the combined fit for $^{12}CH_3O$ are probably more precise than the microwave

Table 12. Contributions to h_1 and h_2 in CH_3O from Jahn–Teller and L-uncoupling effects $k_1^{(JT)} = -3.6309 \times 10^{-4}$, $k_2^{(JT)} = 3.5039 \times 10^{-2}$, $k_1^{(L)} = 1.1091 \times 10^{-7}$, $k_2^{(L)} = -2.3757 \times 10^{-7}$.

	$^{12}CH_3O$	$^{13}CH_3O$	$^{12}CD_3O$[a]
h_1	$2.548(3) \times 10^{-3}$	$2.423(2) \times 10^{-3}$	1.55×10^{-3}
h_2	$4.272(18) \times 10^{-2}$	$4.264(17) \times 10^{-2}$	3.58×10^{-2}
h_1^{JT}	$-3.38(3) \times 10^{-4}$	$-3.31(2) \times 10^{-4}$	-2.69×10^{-4}
h_2^{JT}	$7.81(2) \times 10^{-2}$	$7.74(2) \times 10^{-2}$	5.08×10^{-2}
h_1^{L}	$2.886(3) \times 10^{-3}$	$2.754(2) \times 10^{-3}$	1.82×10^{-3}
h_2^{L}	$-3.54(2) \times 10^{-2}$	$-3.49(2) \times 10^{-2}$	-1.50×10^{-2}

[a] Predicted.

values, we use the microwave values in these calculations since only microwave data are available for $^{13}CH_3O$.) From these calculations, it is clear that L uncoupling dominates h_1, while the Jahn–Teller contribution to h_2 is approximately twice the L-uncoupling contribution. For each parameter, the two effects have opposite signs on their contributions. Only a brief report of the rotational constants of CD_3O has been given on the basis of microwave data [85]. From these rotational constants and the scaling factors determined from the $^{12}CH_3O$ and $^{13}CH_3O$, we have made predictions of the h_1 and h_2 terms for CD_3O. An experimental determination of the rotational structure in CD_3O is highly desirable, as the larger change in the rotational constant would increase significantly the precision of the decoupling of the Jahn–Teller and L-uncoupling effects.

As with the Coriolis constants, it would be quite challenging to extract Jahn–Teller coupling constants D_i and $\omega_{e,i}$ from the h_1^{JT} and h_2^{JT} parameters. However, these rotational parameters may serve as a check of the Jahn–Teller constants, via equations (124) and (125). We shall return to this comparison in the next section.

The determination of the parameters h_1^{JT} and h_2^{JT} means that the rotational constants at the minimum and maximum of the PES can be calculated via equation (126). Diagonalizing this matrix with $\phi = 0$ and $\phi = \pi$ yields the following rotational constants for the minimum and maximum respectively, for the $^{12}CH_3O$ isotopomer: $A''_{min} = 5.207\,43\ cm^{-1}$, $B''_{min} = 0.931\,344\ cm^{-1}$, $C''_{min} = 0.930\,594\ cm^{-1}$, $A''_{max} = 5.207\,43\ cm^{-1}$, $B''_{min} = 0.932\,02\ cm^{-1}$, $C''_{min} = 0.929\,918\ cm^{-1}$. These rotational constants are only slightly changed from the rotational constants at the symmetric point, indicating there is only a small change in the geometry upon the distortion. This is generally true of molecules subject to a dynamic Jahn–Teller effect, the geometry does not change significantly, but the spin–vibronic structure changes dramatically.

6.2.4.3. *Vibronic structure of* $\tilde{X}\ ^2E$ *Jahn–Teller coupling of* CH_3O. While the rotational analysis gives some indication of the Jahn–Teller coupling in the ground state of methoxy, it does not quantify it in terms of the Jahn–Teller coupling constants and vibrational frequencies. The greatest amount of information about these parameters comes from the energies of the spin–vibronic levels, which are most readily observed in dispersed fluorescence or SEP experiments. While early dispersed fluorescence experiments were able to identify the vibrational frequencies of the

totally symmetric modes of the ground state, they lacked adequate intensity and spectral resolution to characterize completely the Jahn–Teller coupling [119–123]. Recently, as part of their investigations of the isomerization of CH_3O to CH_2OH, Temps and co-workers [109, 124–126, 141–143] have used rotationally resolved SEP to determine more completely and definitively the Jahn–Teller vibronic energy levels in the ground state of CH_3O.

The rotationally resolved SEP experiments represent a tremendous advance in the spectroscopy of the methoxy radical. In typical dispersed fluorescence spectra, the resolution is not great enough to do any more than resolve different vibronic levels. However, because the $j = \frac{1}{2}$ levels will have a different rotational structure from the $j = \frac{3}{2}$ levels, rotational analyses of the SEP spectra provide the j quantum numbers of the levels, which is an invaluable piece of information to the Jahn–Teller analysis. The SEP experiments also determined the spin–orbit splitting of some doublets that have too small a splitting to be resolved by normal dispersed fluorescence. Lastly, the SEP experiments determined the Coriolis and spin–rotation constants for a number of levels, which provide additional data with which to check a spin–orbit Jahn–Teller analysis.

Temps' group also obtained the dispersed fluorescence from pumping the $3^1 4^1$, $3^1 5^1$ and $3^1 6^1$ levels in CH_3O and CD_3O. These spectra are very valuable in extracting the Jahn–Teller coupling constants. The relative intensities of the ground-state levels between these spectra make the assignment of the ground state levels much easier. For example, the relative intensities of the levels at 652 and 1525 cm^{-1} are 5: 1 from pumping the $3^1 6^1$ level of the excited state, but 1: 6 from the $3^1 5^1$ level. These intensities reflect the vibrational character of the Jahn–Teller mixed states and should be reproduced by a Jahn–Teller analysis.

Because of the wealth of data available for this radical, the Jahn–Teller analysis is fairly straightforward. The large splitting of the $j = \frac{3}{2}$ levels at 652 and 949 cm^{-1}, which have enhanced intensities in the dispersed fluorescence from the $3^1 6^1$ level of the excited states, clearly indicates that ν_6 has a large quadratic coupling constant K_6. The energy of these two levels and the energy of the $j = \frac{1}{2}$ level from $\nu_6 = 1$, which is at 1247 cm^{-1}, depend mostly on D_6 and K_6. A similar set of levels are observed for ν_5 and ν_4. Using the program described in section 2.7 we have combined all this information and obtained a best fit to the spin–vibronic levels. The parameters resulting from this fit are given in table 8. These coupling constants give a total Jahn–Teller stabilization energy of 419 cm^{-1}, which is dominated by distortions along the normal coordinates of ν_5 and ν_6.

Because of the abundance of data for the methoxy radical, a number of consistency checks are available for the Jahn–Teller analysis. For example, a similar but independent analysis has been performed for CD_3O. There are two properties of the radical that change upon isotopic substitution which have a profound effect upon the Jahn–Teller coupling. First, the frequencies of the modes change, most notably the asymmetric C–H stretch ν_4 and to a lesser extent the other modes. Second, the normal modes become different mixtures of the internal coordinate motions. However, what does not change is the electronic PES in which the nuclei vibrate. This means that the Jahn–Teller stabilization energy is a constant, independent of the masses of the nuclei. Because $\varepsilon_{\text{total}}$ is a constant, or nearly so, and the vibrational frequencies and normal modes change, the Jahn–Teller coupling constants D_i and K_i will be quite different for CD_3O. The coupling constants for CD_3O should in

general be larger than those for CH_3O because the vibrational frequencies will be lower, requiring a larger D_i to maintain the same stabilization energy. Table 8 shows that this is the case for D_4 and D_5, although D_6 decreases slightly, presumably because of the change in normal coordinates. However, the overall degrees of Jahn–Teller stabilization of the two isotopomers are the same, within the accuracy of the calculations.

The LMR experiment determined $a = -142\ cm^{-1}$[72, 73]. Dividing the Jahn–Teller simulation value for $a\zeta_e = -145$ by this number yields $\zeta_e = 1.02$. While this value is greater than unity, a reduction in $a\zeta_e$ to $-135\ cm^{-1}$ would yield $\zeta_e = 0.95$. Such a variation in $a\zeta_e$ is probably within the error of the simulations of the Jahn–Teller spin–vibronic analysis.

As a further check on the spin–vibronic parameters, we can calculate the Coriolis coupling constant obtained from the rotational analysis of the origin. This calculation assumes that the individual vibrational mode Coriolis constants ζ_i are the same as those for the excited state, and that $\zeta_e = 0.95$. Given these approximations, the Coriolis constant value of $\Delta\zeta$ from the spin–vibronic analysis is 0.10, which compares well with the value of 0.13 obtained from the rotational analysis.

We can also calculate a value for the rotational parameters $h_1^{(JT)}$ and $h_2^{(JT)}$ using the Jahn–Teller parameters $\omega_{e,i}$ and D_i via equations (124) and (125). These calculations require the rotational constants, which are known experimentally, and the inertial derivatives for the Jahn–Teller active modes, which we have calculated via *ab initio* calculations [98]. Entering all these parameters into equations (124) and (125) yields values for $\left|h_1^{(JT)}\right|$ and $\left|h_2^{(JT)}\right|$ of 3.4×10^{-4} and 4.3×10^{-2} respectively, compared with $3.38(3) \times 10^{-4}$ and $7.81(2) \times 10^{-2}$ from the rotationally resolved experiments. (The *ab initio* calculations of the inertial derivatives are unable to determine the sign of the constants, so only the absolute values should be compared.) The agreement between these constants is quite good, considering that several assumptions are made in the derivations of equations (124) and (125) and that the experimental values are determined using only the isotopic substitution of a ^{13}C atom for a ^{12}C atom.

6.2.4.4. *Spin–orbit splitting in* ν_3. In the development of the Jahn–Teller Hamiltonian and basis set, we made the assumption that the totally symmetric modes of the molecule could be excluded from the calculations. Under this assumption, the energy levels of the symmetric modes should appear with the same spin–orbit splitting as the origin. As part of their investigations, Temps and co-workers [125] obtained the SEP spectra of the progression in ν_3 in methoxy up to $\nu = 10$. They found that the spin–orbit splittings of the lowest few levels ($\nu_3 \leqslant 3$) show little variation from $-62\ cm^{-1}$, while the spin–orbit splitting for $\nu_3 = 4$ is $-50\ cm^{-1}$, and for $\nu_3 > 4$ the spin–orbit splitting is much smaller, varying from -38 to $-30\ cm^{-1}$.

There are several possible explanations for the decrease in the spin–orbit splittings at higher energies. One is that, at higher energies, the density of vibrational levels is much greater, which increases the probability of vibronic interactions between the C–O stretch levels and other levels, including non-totally symmetric ones. Any interaction with a level of e symmetry will reduced the spin–orbit splitting, as observed. A second possibility is that interactions with other electronic states becomes stronger at higher energies, which can alter the spin–orbit splitting, perhaps reducing it.

The third explanation is that, as ν_3 is excited, the C–O bond becomes longer.

The dissociation limit of CH_3O in its ground electronic state along the C–O bond is a CH_3 radical in its ground state $^2A_2''$ (D_{3h}) and an oxygen atom in its ^3P ground state. One might expect, then, that at longer bond lengths the spin–orbit splitting of the atomic oxygen should be eventually recovered. In contrast, the opposite result is observed experimentally. The resolution of this discrepancy again lies in the removal of one of the initial assumptions that we made, that is that the totally symmetric modes are independent of the Jahn–Teller active modes. Under this assumption, all the totally symmetric modes should have a Jahn–Teller structure built on them exactly as the origin does. However, at longer C–O bond lengths, the frequencies of the other vibrational modes will most certainly change. For example, ν_6, which corresponds to a motion of the oxygen atom off the symmetry axis and a concurrent rocking of the CH_3 group, should decrease in frequency as the C–O bond is lengthened, the weaker bond allows the H–C–O bond angle to be more easily distorted. If the same Jahn–Teller stabilization energy is to be obtained, D_6 must be increased, which will in turn decrease the spin–orbit splitting of the levels.

6.2.4.5. *Transition dipole moments.* Up to this point, we have not discussed the intensities of the vibronic levels in the electronic transition in detail. Because the electronic transition is between a $^2A_1$ state and a ^2E state, the transitions are expected to have perpendicular transition dipole moments. However, the excitation and emission spectra of methoxy, and to a lesser extent CF_3O [107] and $CdCH_3$ [95], show unusual intensity patterns. The rotationally resolved excitation spectrum of CH_3O clearly shows both perpendicular and parallel transition moments in the fundamentals of the e modes of the excited state [108]. Furthermore, the SEP spectra of the 6_1 and 3_16_1 levels also contain transitions via both perpendicular and parallel transition dipole moments [124]. While linear Jahn–Teller coupling can account for the intensities of the perpendicular bands, it provides for no intensity to the parallel transitions.

The likely explanation for the observation of parallel transitions in these molecules is that the electronic states are not pure $^2A_1$ or ^2E states. A parallel transition moment will be created if the ground ^2E state is mixed with another state of A_1 symmetry. Such a mixing can give rise to a pseudo-Jahn–Teller effect in the ^2E state. However, the excited $^2A_1$ state can be mixed with other states of E symmetry, thereby inducing a parallel moment. We believe that the latter scenario is probably more important because the ground state is greater than 31 000 cm^{-1} below the nearest excited state, while the A $^2A_1$ state is located very close in energy to several other excited ^2E and ^4E states, including a ^4E state that is responsible for the pre-dissociation observed in the LIF and fluorescence depletion spectra [108, 128, 135].

6.2.5. *Summary of the methoxy family of radicals*

As mentioned when summarizing the metal monomethyl radicals (section 6.1.4), there are a number of aspects when dealing with the spectroscopy of Jahn–Teller active species. First, one has to understand qualitatively the patterns from the various spin–vibronic effects to assign the spectrum and then to extract quantitative information. Once that is accomplished, one can proceed to determining the nature of the Jahn–Teller effect and the resultant PES with its stabilization energy and distortion.

In the metal monomethyl radicals previously discussed, the Jahn–Teller effects

were generally small enough that the traditional approximations provided reasonably accurate spin–vibronic eigenvalues and expectation values. The situation is quite different, with the exception of CH_3S, for the methoxy radicals where Jahn–Teller and spin–orbit effects are comparable. In such cases, the only reliable approach is the direct diagonalization of the Hamiltonian matrix (equations (67)–(71)) to obtain the requisite spin–vibronic eigenvalues and eigenfunctions, the latter of which yields the expectation values relevant to the rotational structure.

Evidence of the significance of both Jahn–Teller and spin–orbit effects on the methoxy family can be gleaned from the quenching of the spin–orbit coupling in the vibrationless level. For CH_3O, CH_3S, CF_3O and CF_3S, the spin–orbit coupling in the vibrationless level is reduced by 61%, 25%, 84% and 56% respectively of the value of $a\zeta_e$. This compares with a maximum reduction of 20% in the metal monomethyls.

We see in analysing the spectra the importance of using all the information available from both the vibronic and the rotational spectrum. For CH_3S, where the Jahn–Teller effect is relatively small compared with spin–orbit coupling, no Jahn–Teller activity in any of the vibrational modes is directly discernible. However, as we have seen, the quenching of the electronic angular momentum is very sensitive to distortion and the comparison of the spin–orbit splittings in two isotopomers of CH_3S allows us to quantify the Jahn–Teller activity.

However, for the remaining methoxy radicals, Jahn–Teller activity is evident in at least two, if not all three, *e* modes. As mentioned above, the comparable magnitudes of the Jahn–Teller and spin–orbit coupling means that the only reliable approach to analysing the spectrum is a fit of the Jahn–Teller and spin–orbit parameters involved in the complete calculation of the spin–vibronic energy levels. For the most part there is sufficient information in the vibronic spectrum to determine these parameters. The expectation values of the spin–vibronic eigenfunctions then can be independently measured from the rotational spectrum. In some cases this check is quite extensive and generally satisfactory.

Particularly in the oxygen-centred radicals, there is clearly measurable activity in all vibrational modes. However, generally speaking it is smallest for ν_4 and ν_5, the modes involving the methyl hydrogen atoms (or fluorine atoms). It is, however, not surprising that all four of the methoxy radicals should exhibit the most Jahn–Teller activity in ν_6, with D_6 being the largest linear Jahn–Teller coupling constant for each radical. The motion of the atoms corresponding to ν_6 is often described as a 'methyl rock'. While this description is fairly accurate, an equivalent description is 'oxygen or sulphur tilt'. Describing the motion as an oxygen or sulphur tilting off the symmetry axis gives a clearer insight into the source of the Jahn–Teller coupling. The ^2E ground state for all these radicals arises from the partial occupation of a $p\pi$ pair of orbitals that are centred on the heteroatom. It is therefore completely consistent with all the Jahn–Teller analyses that the vibrational mode that is most active corresponds to the motion of the heteroatom. The other two modes, the asymmetric C–H(F) stretch (ν_4) and the H–C–H (F–C–F) scissor (ν_5) do not involve the heteroatom nearly as much as ν_6.

From table 8 we note that for the sulphides CH_3S and CF_3S the Jahn–Teller stabilization energy vanishes for the spin–vibronic PES. This means that, like the metal monomethyls (except for $MgCH_3$), the minimum of all normal mode cuts of the PES of both spin components of the ^2E state remains at the C_{3v} configuration, as in figure 2(*h*).

However, for the oxides the situation is quite different. On the lower ($^2E_{3/2}$) PES, there appear to be local potential minima at distorted geometries, as in figure 2(*g*), for *all* three normal coordinate. As table 8 shows, although the D_i values are quite small, the energy stabilizations for v_4 and v_5 are non-negligible. Nonetheless the relatively high frequencies of these modes means that the zero-point energy places even the vibrationless level high above the conical intersection of the PES. Modest distortions in the PES have only small effects on observables, meaning in turn that the experimental spectra determine these distortions with limited precision. The situation is considerably different for v_6, which is relatively low in frequency and is expected to be actively involved in the Jahn–Teller distortion. In this case the Jahn–Teller stabilization energies are determined with higher precision. We see that CF_3O has the largest Jahn–Teller coupling parameter, D_6, which is possibly caused by the relatively large delocalization on to the fluorine atoms of the *e* orbital in which the unpaired electron resides.

7. Conclusions

The purpose of this paper is to review the ramifications of the Jahn–Teller effect on isolated molecular systems. It has been particularly our purpose to provide a guide to experimentalists to analyse and extract correctly the maximum information possible from the rapidly growing number of available spectra. In providing what we hope is a useful account of the available Jahn–Teller theory we have found several shortcomings with respect to applications to real molecular systems.

The most critical shortcoming is the general, although not universal, tendency of the previous literature to treat spin–orbit coupling at best as an afterthought to Jahn–Teller coupling. What is emerging experimentally is that spin–orbit and Jahn–Teller coupling should be treated on a comparable footing, that is a full spin–vibronic calculation. Such an approach will be necessary for almost all molecules involving second-row (and heavier) atoms, with a few notable exceptions such as aromatic hydrocarbons. Finally, when the atoms become heavy enough, spin–orbit coupling will dominate and the appropriate approach may be to treat the Jahn–Teller coupling as the perturbation.

We have tried to outline a comprehensive treatment of the problem combining the effects observable in the spin–vibronic energy level structure with those revealed by rotationally resolved spectroscopy. Our initial treatment is quite general, applicable to molecules conforming to any (non-cubic) symmetry group and includes higher order Jahn–Teller interactions. We have given detailed descriptions of the appropriate Hamiltonian matrices. In addition, we have described how experimental results can be related to the PES of the molecule.

We have taken the simplest Jahn–Teller symmetry, C_{3v}, as an example both to demonstrate the importance of various theoretical interactions as well as to apply the theory to eight Jahn–Teller active molecular states, the $\tilde{A}\ ^2E$ states of the metal monomethyls and the $\tilde{X}\ ^2E$ states of the methoxy radical family, for which copious data have been obtained in recent years.

Theoretically we have provided extensive information about whether traditional approximations made in Jahn–Teller analyses are justified. In the best cases, the recent increase in available computational power often render these approximations superfluous today and in other cases direct computations demonstrate that some traditional approaches are misleading or just simply wrong.

In the molecules whose spectra we have chosen to review, the Jahn–Teller effects

are small to moderate. We have demonstrated that consistent molecular information can be obtained from both vibronic and rotational spectra. We have seen how sensitive the electronic and vibronic angular momenta are to even small Jahn–Teller distortions, which in turn make them sensitive probes of such effects. In contrast, we have seen that even molecules with significant Jahn–Teller activity may have PESs with the global minimum at the symmetrical position.

Overall the consistency and agreement among various experimental observations are rather pleasing for the systems that we have considered. However, it should be pointed out that there still remain minor inconsistencies between theoretical expectations and experiments. Many past approximations have been eliminated owing to the increase in computational power. However, some, like not including the symmetric vibrational modes in the calculation, remain and may be the source of some of the remaining difficulties. However it may also be true that some effects remain inadequately treated by theory at this point.

An area that will be treated in detail elsewhere [98], but has been referred to little in this work, is that of *ab initio* calculations of Jahn–Teller and related effects. One should note that *ab initio* calculations on even open-shell molecules are becoming increasingly accurate and should in the near future provide quantitatively meaningful information about Jahn–Teller effects. The development in this review is in many ways ideally suited to comparison of experiment and such calculations, because in most cases the parameters related to Jahn–Teller coupling that are determined from experiment and that have been developed in this paper are well defined in terms of quantities calculable from electronic wavefunctions.

In conclusion, it is gratifying to note that the Jahn–Teller effect, conceived just over 60 years ago, is still alive and well today. It is alive firstly because symmetry and its breaking lie at the heart of our understanding of the physical universe. However it is also alive because a large number of reactive intermediates in very important chemical reactions have electronic structures satisfying the Jahn–Teller theorem. Understanding the Jahn–Teller effect is an important prerequisite to using their spectra to monitor the chemistry. Most importantly, after over 60 years of nearly continuous effort, the enigma that the Jahn–Teller effect has represented to experimentalists is finally being successfully penetrated. Today there is real hope that this effect, which has often frustrated spectroscopists, is about to be converted into an increasingly useful tool to understand open-shell molecules and their chemistry better.

Acknowledgments

We thank Dr M.-C. Yang and Dr David Powers of The Ohio State University for taking the dispersed fluorescence spectra of CF_3O and CF_3S. We also thank Professor Friedrich Temps (Kiel, Germany) for sharing with us his CH_3O data and analysis prior to publication. We are most grateful to Jon Hougen (National Institute of Standards and Technology) for a careful reading of the manuscript and extensive discussions. We also thank John Brown (Oxford), Sergey Panov (MIT) and Michael Pushkarsky (Ohio State) for useful discussions. We are pleased to acknowledge support of this work by the National Science Foundation in the form of grant CHE-9320909 to T.A.M. and a fellowship to T.A.B., who also thanks the Ohio State University for fellowship support. Finally, we are grateful to the Ohio Supercomputer Center (grant PAS540) for a generous allotment of computer time.

Appendix A: Glossary of symbols used.

Symbol	Description	Equation or section	Units
a	Spin–orbit coupling constant	(18)	cm^{-1}
A	Rotational constant about the z axis for a symmetric prolate top	(93)	cm^{-1}
B	Rotational constant about the x or y axes for a symmetric prolate top	(93)	cm^{-1}
$d_{j,nj}$	Ham reduction factor, spin–orbit coupling quenching parameter	(80)	—
D_i	Linear Jahn–Teller coupling constant for the ith vibrational mode	(59), (70)	—
E_0	Total energy of the symmetric point, expectation value of $\hat{\mathscr{H}}_e$	(67)	kg m^2 s^{-2}
g_{ij}	Second derivative of energy with respect to the ith Jahn–Teller active mode	(16)	kg s^{-2}
G	Vibrational angular momentum	Section 4.1	—
h_1	l-type doubling term for a symmetric top in a degenerate state	(94)	cm^{-1}
h_2	l-type doubling term for a symmetric top in a degenerate state	(94)	cm^{-1}
h_1^{JT}	Jahn–Teller contribution to h_1, proportional to B_0	(122)	cm^{-1}
h_2^{JT}	Jahn–Teller contribution to h_2, proportional to $(A_0B_0)^2$	(123)	cm^{-1}
h_1^L	L-uncoupling contribution to h_1, proportional to B_0^2	(122)	cm^{-1}
h_2^L	L-uncoupling contribution to h_2, proportional to A_0B_0	(123)	cm^{-1}
j	Linear Jahn–Teller quantum number, definition depends on choice of symmetry operations, see section 3.2.2	(46)	—
J	Rotational quantum number	(88)–(91), (93)	—
J	Total angular momentum, excluding nuclear spin	Section 4.1	—
k_i	Derivative of energy with respect to the ith Jahn–Teller active mode	(15)	kg m^{-1} s^{-2}
K_i	Quadratic Jahn–Teller coupling constant for ith vibrational mode	(60), (71)	—
l_i	Quantum number for the vibrational angular momentum of the active mode ith Jahn–Teller	(8)	—
l_t	Total vibrational angular momentum	(5)	—
L	Electronic orbital angular momentum	(73), Section 4.1	—
M	Projection of J on the space-fixed z axis	(88)–(91)	—
M_i	Reduced mass of vibrational mode the ith	(17)	kg
n_j	Index 'quantum number', used to identify the n_jth energy level of a given value of j	(74)	—
N	Total angular momentum, excluding spin	Section 4.1	—
P	Projection of J on the molecular z axis	(88)–(91)	—
$Q_{i,\pm}$	Complex conjugates of Cartesian normal coordinates for the i^{th} Jahn–Teller active mode	(11)	Length
R	Rotational angular momentum	Section 4.1	—
s_e	Symmetry label of electronic state, E_{s_e}	(3)	—
s_v	Symmetry label of vibrational mode, e_{s_v}	(22)	—
s_k	Relative phase between vibrational and electronic phases	(26)	—

Appendix A: continued.

Symbol	Description	Equation or section	Units
S	Spin quantum number of the state	(6)	—
$\mathbf{S}$	Electron spin angular momentum	Section 4.1	—
$\hat{T}$	Transition dipole operator	(128)	—
$U_{i,\pm}$	Function defining the potential energy surface for the i^{th} vibrational mode	(54), (64)	cm^{-1}
u_i	Vibronic quantum number for strong Jahn–Teller coupling	(79)	—
v_i	Principal quantum number for the ith active mode	(8)	—
α	Symmetry label for vibronic energy level	(74)	—
ε_i	Jahn–Teller stabilization energy of ith vibrational mode	(61)	cm^{-1}
ε_i^{so}	Jahn–Teller stabilization energy of ith vibrational mode, calculated with spin–orbit coupling	(66)	cm^{-1}
$\varepsilon_{\text{total}}$	Total Jahn–Teller stabilization energy	(62)	cm^{-1}
$\varepsilon_{\text{total}}^{\text{so}}$	Total Jahn–Teller stabilization energy, calculated with spin–orbit coupling	(66)	cm^{-1}
ε_{aa}	Spin–rotation constant	(95), (96)	cm^{-1}
ζ_e	Electronic orbital angular momentum	(64), (69)	—
ζ_i	Coriolis coupling constant for ith vibrational mode	(109)	—
ζ_t	Coriolis coupling constant for a vibronic level	(103)	—
$\zeta_t^{\pm}$	Coriolis coupling constant for a spin component of a vibronic level	(118), (119)	—
λ_i	Curvature of electronic potential with respect to the ith vibrational mode	(14)	kg s^{-2}
Λ	Quantum number for projection of electronic orbital angular momentum on the symmetry axis	(8)	—
ρ_i	Cylindrical normal coordinate of the ith Jahn–Teller active mode	(12)	Length
Σ	Quantum number for projection of spin angular momentum on the symmetry axis	(8)	—
ϕ_i	Cylindrical normal coordinate of the ith Jahn–Teller active mode	(12)	rad
$\omega_{e,i}$	'Equilibrium' vibrational frequency of the ith vibrational mode	(17), (68)	cm^{-1}
$\omega_{0,i}$	'Fundamental' vibrational frequency of the ith vibrational mode	Section 3.2.1	cm^{-1}
Ω	Total projection of angular momentum on the symmetry axis, excluding nuclear spin, equal to $\Lambda - l_t + \Sigma$	(50)	—

References

[1] JAHN, H. A., and TELLER, E., 1937, *Proc. R. Soc.* A, **161**, 220–235.
[2] BERSUKER, I. B., 1984, *The Jahn–Teller Effect. A Bibliographic Review* New York: Plenum.
[3] LIEHR, A. D., 1963, *J. phys. Chem.*, **67**, 389–471.
[4] LIEHR, A. D., 1963, *J. chem. Phys.*, **67**, 471–494.
[5] LIEHR, A. D., 1963, *A. Rev. phys. Chem.*, **13**, 41–76.
[6] KÖPPEL, H., DOMCKE, W., and CEDERBAUM, L. S., 1984, *Adv. chem. Phys.*, **57**, 59–246.
[7] MILLER, T. A., and BONDYBEY, V. E., 1983, *Molecular Ions: Spectroscopy, Structure, and Chemistry*, edited by T. A. Miller and V. E. Bondybey (Amsterdam: North-Holland).
[8] STURGE, M. D., 1964, *Solid St. Phys.*, **20**, 91–211.
[9] KÖPPEL, H., 1997, *Z. phys. Chem.*, **200**, 3–10.
[10] MILLER, T. A., 1984, *Science*, **223**, 545–553.
[11] ENGELKING, P. C., and LINEBERGER, W. C., 1977, *J. chem. Phys.*, **67**, 1412–1417.
[12] YU, L., FOSTER, S. C., WILLIAMSON, J. M., HEAVEN, M. C., and MILLER, T. A., 1988, *J. phys. Chem.*, **92**, 4263–4266.
[13] YU, L., WILLIAMSON, J. M., AND MILLER, T. A., 1989, *Chem. Phys. Lett.*, **162**, 431–436.
[14] YU, L., CULLIN, D. W., WILLIAMSON, J. M., and MILLER, T. A., 1993 *J. chem. Phys.*, **98**, 2682–2698.
[15] FOSTER, S. C., and MILLER, T. A., 1989 *J. phys. Chem.*, **93**, 5986–5999.
[16] LONG, S. R., MEEK, J. T., and REILLY, J. P. 1983, *J. chem. Phys.*, **79**, 3206–3219.
[17] LINDNER, R., SEKIYA, H., BEYL, B., and MÜLLER-DETHLEFS, K. 1993, *Angew. Chem., Int. Edn Engl.*, **32**, 603–606.
[18] LINDNER, R., MÜLLER-DETHLEFS, K., WEDUM, E., HABER, K., and GRANT, E. R. 1996, *Science*, **271**, 1698–1702.
[19] GOODE, J. G., HOFSTEIN, J. D., and JOHNSON, P. M. 1997, *J. chem. Phys.*, **107**, 1703–1716.
[20] MILLER, T. A., 1994 *Angew. Chem., Int. Edn Engl.*, **33**, 962–964.
[21] (a) OHASHI, N., TSUURA, M., and HOUGEN, J. T., 1995, *J. molec. Spectrosc.*, **173**, 79–99.
[21] (b) MAYER, M., CEDERBAUM, L. S., and KOEPPEL, H., 1996, *J. chem. Phys.*, **104**, 8932–8942.
[21] (c) OHASHI, N., TSUURA, M., and HOUGEN, J. T., 1997, *J. molec. Spectrosc.*, **104**, 22–34.
[21] (d) VITUCCIO, D. T., GOLONZKA, O., and ERNST, W. E., 1997, *J. molec. Spectrosc.*, **184**, 237–249.
[22] (a) MORSE, M. D., HOPKINS, J. B., LANGRIDGE-SMITH, P. R. R., and SMALLEY, R. E. 1983, *J. chem. Phys.*, **79**, 5316–5328.
[22] (b) CRUMLEY, W. H., HAYDEN, J. S., and GOLE, J. L., 1986, *J. chem. Phys.*, **84**, 5250–5261.
[22] (c) ROHLFING, E. A., and VALENTINI, J. J., 1986, *Chem. Phys. Lett.*, **126**, 113–118.
[22] (d) TRUHLAR, D. G., and THOMPSON, T. C., MEAD, C. A., 1986, *Chem. Phys. Lett.*, **127**, 287–291.
[22] (e) ZWANZIGER, J. W., WHETTEN, R. L., and GRANT, E. R., 1986, *J. phys. Chem.*, **90**, 3298–3301.
[22] (f) MORSE, M. D., 1987, *Chem. Phys. Lett.*, **133**, 8–13.
[23] (a) CHENG, P. Y., and DUNCAN, M. A., 1988, *Chem. Phys. Lett.*, **152**, 341–346.
[23] (b) ELLIS, A. M., ROBLES, E. S. J., and MILLER, T. A., 1993, *Chem. Phys. Lett.*, **201**, 132–140.
[23] (c) WEDUM, E. E., GRANT, E. R., CHENG, P. Y., WILLEY, K. F., and DUNCAN, M. A., 1994, *J. chem. Phys.*, **100**, 6312–6317.
[24] BISHEA, G. A., and MORSE, M. D., 1991, *J. chem. Phys.*, **95**, 8779–8792.
[25] SLOANE, C. S., and SILBEY, R., 1972, *J. chem. Phys.*, **56**, 6031–6043.
[26] BALLHAUSEN, C. J., 1965, *Theor. chim. Acta*, **3**, 368–374.
[27] CHAU, F. T., and KARLSSON, L., 1977, *Phys. Scripta*, **16**, 248–257.
[28] CHAU, F. T., and KARLSSON, L., 1977, *Phys. Scripta*, **16**, 258–267.
[29] HAM, F. S., 1972, *Electron Paramagnetic Resonance*, edited by S. Geschwind (New York: Plenum).
[30] KOIZUMI, H., and SUGANO, S., 1995, *J. chem. Phys.*, **102**, 4472–4481.
[31] CHILD, M. S., and LONGUET-HIGGINS, H. C., 1961, *Proc. R. Soc.* A, **245**, 259–294.
[32] LONGUET-HIGGINS, H. C., ÖPIK, U., PRYCE, M. H. L., and SACK, R. A., 1958, *Proc. R. Soc.* A, **244**, 1–16.
[33] LONGUET-HIGGINS, H. C., 1961, *Adv. Spectrosc.*, **2**, 429–472.

[34] Brown, J. M., 1971, *Molec. Phys.* **20**, 817–834.
[35] Hougen, J. T., 1980, *J. molec. Spectrosc.* **81**, 73–92.
[36] Watson, J. K. G., 1984, *J. molec. Spectrosc.* **103**, 125–146.
[37] Herzberg, G., 1966, *Molecular Spectra and Molecular Structure*, Vol. 3 (New York: van Nostrand Reinhold).
[38] Hougen, J. T. 1964, *J. molec. Spectrosc.*, **13**, 149–167.
[39] Moffitt, W., and Thorson, W., 1957, *Phys. Rev.* **108**, 1251–1255.
[40] Bernstein, E. R., and Webb, J. D., 1978, *Mol. Phys.* **4**, 1113–1118.
[41] Child, M. S., 1960, *Mol. Phys.* **3**, 601–603.
[42] Meiswinkel, R., and Köppel, H., 1989 *Chem. Phys.* **129**, 463–476.
[43] Scharf, B. 1983, *Chem. Phys. Lett.* **96**, 89–92.
[44] Scharf, B. 1983, *Chem. Phys. Lett.* **98**, 81–85.
[45] Watson, J. K. G. 1974, *J. mol. Spectrosc.* **50**, 281–285.
[46] Liu, X., Foster, S. C., Williamson, J. M., Yu, L., and Miller, T. A. 1990, *Mol. Phys.* **69**, 357–367.
[47] Liu, X., Yu, L., and Miller, T. A. 1990, *J. mol. Spec.* **140**, 112–125.
[48] Van Vleck, J. H. 1951 *Rev. Mod. Phys.* **23**, 213–227.
[49] Richards, W. G., Trivedi, H. P., and Cooper, D. L. 1981 *Spin–orbit Coupling in Molecules* (Oxford: Clarendon).
[50] Condon, E. U., and Shortley, G. H., 1964, *The Theory of Atomic Spectra* (Cambridge University Press).
[51] Hougen, J. T., 1976, *Interactions Among Electronic, Vibrational, and Rotational Motions*, edited by D. Henderson (New York: Academic Press), chapter 7, pp. 307–348.
[52] Band, Y. B., and Scharf, B., 1983, *J. Chem. Phys.*, **79**, 3175–3180.
[53] Itah, J., Katz, B., and Scharf, B., 1977, *Chem. Phys. Lett.* **48**, 111–114.
[54] Herzberg, G., and Teller, E., 1933, *Z. phys. Chem. B*, **21**, 410–446.
[55] Renner, R., 1934, *Z. Physik*, **92**, 172–193.
[56] Pople, J. A., and Longuet-Higgins, H. C., 1958, *Molec. Phys.*, **1**, 372–383.
[57] Brown, J. M., and Jörgensen, F., 1982, *Molec. Phys.*, **47**, 1065–1086.
[58] Berry, M. V., 1984, *Proc. R. Soc.* A, **392**, 45–57.
[59] Ham, F. S., 1965, *Phys. Rev.* A, **138**, 1727–1740.
[60] Di Lauro, C., 1972, *J. molec. Spectrosc.* **41**, 598–599.
[61] Liu, X., and Miller, T. A., 1992 *Molec. Phys.* **75**, 1237–1258.
[62] Sharf, B., and Jortner, J., 1968 *chem. Phys. Lett.* **2**, 68–70.
[63] Scharf, B., Vitenberg, R., Katz, B., and Band, Y. B., 1982, *J. chem. Phys.*, **77**, 2226–2234.
[64] Eiding, J., and Domcke, W., 1992, *Chem. Phys.* **163**, 133–147.
[65] Lawler, R. G., Bolton, J. R., Fraenkel, G. K., and Brown, T. H., 1964, *J. Am. chem. Soc.* **86**, 520–521.
[66] Carrington, A., Longuet-Higgins, H. C., Moss, R. E., and Todd, P. F., 1965, *Molec. Phys.*, **9**, 187–190.
[67] Barckholtz, T. A., and Miller, T. A., 1998 (*submitted*).
[68] Hougen, J. T., 1963, *J. chem. Phys.*, **38**, 1167–1173.
[69] Child, M. S., 1963, *J. molec. Spectrosc.*, **10**, 357–365.
[70] Salzberg, A., Applegate, B. E., and Miller, T. A., 1998, *J. molec. Spectrosc.* (in the press).
[71] Child, M. S., 1962, *Mol. Phys.*, **5**, 391–396.
[72] Radford, H. E., and Russell, D. K., 1977, *J. chem. Phys.*, **66**, 2222–2224.
[73] Russell, D. K., and Radford, H. E., 1980, *J. chem. Phys.*, **72**, 2750–2759.
[74] Endo, Y., Saito, S., and Hirota, E., 1984, *J. chem. Phys.*, **81**, 122–135.
[75] Watson, J. K. G., 1968, *Molec. Phys.* **15**, 479–490.
[76] Hedberg, L., and Mills, I. M., 1993, *J. molec. Spectrosc.*, **160**, 117–142.
[77] Herzberg, G., and Watson, J. K. G., 1980, *Can. J. Phys.*, **58**, 1250–1258.
[78] Herzberg, G., Lew, H., Sloan, J. J., and Watson, J. K. G., 1981, *Can. J. Phys.*, **59**, 428–440.
[79] Herzberg, G., Hougen, J. T., and Watson, J. K. G., 1982, *Can. J. Phys.*, **60**, 1261–1284.
[80] Child, M. S., and Strauss, H. L., 1965, *J. chem. Phys.* **42**, 2283–2292.
[81] Douglas, A. E. 1963, *Discuss. Faraday Soc.* **35**, 158–174.

[82] ASHFOLD, M. N. R., DIXON, R. N., STICKLAND, R. J., and WESTERN, C. M., 1987, *Chem. Phys. Lett.*, **138**, 201–208.
[83] ASHFOLD, M. N. R., DIXON, R. N., LITTLE, N., STICKLAND, R. J., and WESTERN, C. M., 1988, *J. chem. Phys.* **89**, 1754–1761.
[84] ALLEN, J. M., ASHFOLD, M. N. R., STICKLAND, R. J., and WESTERN, C. M., 1991, *Molec. Phys.*, **74**, 49–60.
[85] MOMOSE, T., ENDO, Y., HIROTA, E., and SHIDA, T., 1988, *J. chem. Phys.*, **88**, 5338–5343.
[86] MOMOSE, T., ENDO, Y., and HIROTA, E., 1989, *J. chem. Phys.*, **90**, 4636–4637.
[87] SCHARF, B. E., and MILLER, T. A., 1987, *J. molec. Spectrosc.*, **122**, 196–220.
[88] SCHARF, B., and MILLER, T. A., 1986, *J. chem. Phys.* **84**, 561–576.
[89] WATSON, J. K. G., 1986, *Mol. Phys.* **59**, 127–140.
[90] MARR, A. J., GRIEMAN, F., and STEIMLE, T. C., 1996, *J. chem. Phys.* **105**, 3930–3937.
[91] BARCKHOLTZ, T. A., POWERS, D. E., MILLER, T. A., and BURSTEN, B. E., 1998, *J. Am. chem. Soc.*, (in the press).
[92] PANOV, S. I., POWERS, D. E., and MILLER, T. A., 1998, *J. chem. Phys.*, **108**, 1335–1346.
[93] RUBINO, R., WILLIAMSON, J. M., and MILLER, T. A., 1995, *J. chem. Phys.*, **103**, 5964–5969.
[94] CERNY, T. M., TAN, X. Q., WILLIAMSON, J. M., ROBLES, E. S. J., ELLIS, A. M., and MILLER, T. A., 1993, *J. chem. Phys.* **99**, 9376–9388.
[95] PUSHKARSKY, M.,BARCKHOLTZ, T. A., and MILLER, T. A., 1998, *J. chem. Phys.* (in the press).
[96] BRAZIER, C. R., and BERNATH, P. F., 1987, *J. chem. Phys.*, **86**, 5918–5922.
[97] TAN, X. Q., CERNY, T. M., WILLIAMSON, J. M., and MILLER, T. A., 1994, *J. chem. Phys.*, **101**, 6396–6404.
[98] BARCKHOLTZ, T. A., and MILLER, T. A., 1998 *J. phys. Chem.* (*submitted*).
[99] HUBER, K. P., and HERZBERG, G., 1979, *Molecular Spectra and Molecular Structure IV: Constants of Diatomic Molecules* (New York: Van Nostrand).
[100] HAMMER, P. D., SINHA, A., BURKHOLDER, J. B., and HOWARD, C. J., 1988, *J. mol. Spectrosc.*, **129**, 99–1188.
[101] TAMASSIA, F., BROWN, J. M., and EVENSON, K. M., 1998 *53rd Ohio State University International Symposium on Molecular Spectroscopy*, talk MG14.
[102] CARRINGTON, A., CURRIE, G. N., DYER, P. N., LEVY, D. H., and MILLER, T. A., 1967, *Chem. Commun.*, **13**, 641–642.
[103] CARRINGTON, A., CURRIE, G. N., LEVY, D. H., and MILLER, T. A., 1969, *J. chem. Phys.* **50**, 2726–2732.
[104] LIU, X., DAMO, C., LIN, T.-Y. D., FOSTER, S. C., MISRA, P., YU, L., and MILLER, T. A., 1989, *J. phys. Chem.* **93**, 2266–2275.
[105] HSU, Y.-C., LIU, X., and MILLER, T. A., 1989, *J. chem. Phys.*, **90**, 6852–6857.
[106] TAN, X.-Q., YANG, M.-C., CARTER, C. C., WILLIAMSON, J. M., MILLER, T. A., MLSNA, T. E., ANDERSON, J. D. O., and DESMARTEAU, D. D., 1994, *J. phys. Chem.*, **98**, 2732–2734.
[107] YANG, M.-C., WILLIAMSON, J. M., and MILLER, T. A., 1997, *J. mol. Spectrosc.*, **186**, 1–14.
[108] POWERS, D. E., PUSHKARSKY, M., and MILLER, T. A., 1997, *J. chem. Phys.* **106**, 6863–6877.
[109] TEMPS, F., private communication.
[110] CHIANG, S.-Y., and LEE, Y.-P., 1991, *J. chem. Phys.*, **95**, 66–72.
[111] POWERS, D. E., PUSHKARSKY, M. B., YANG, M.-C., and MILLER, T. A., 1997, *J. phys. Chem.* A, **101**, 9846–9853.
[112] SUZUKI, M., INOUE, G., and AKIMOTO, H. 1984, *J. chem. Phys.* **81**, 5405–5412.
[113] ENGELKING, P. C., ELLISON, G. B., and LINEBERGER, W. C., 1978, *J. chem. Phys.*, **69**, 1826–1832.
[114] ENDO, Y., SAITO, S., and HIROTA, E., 1986, *J. chem. Phys.* **85**, 1770–1777.
[115] BENT, G. D., 1988, *J. chem. Phys.*, **89**, 7298–7300.
[116] HERZBERG, G., 1950, *Molecular Spectra and Molecular Structure*, Vol. 2 (New York: Van Nostrand Reinhold).
[117] LI, Z., and FRANCISCO, J. S., 1991, *Chem. Phys. Lett.* **186**, 336–342.
[118] YANG, M.-C., 1997, PhD Dissertation, The Ohio State University.
[119] CARRICK, P. G., BROSSARD, S. D., and ENGELKING, P. C., 1985, *J. chem. Phys.*, **83**, 1995–1996.
[120] BROSSARD, S. D., CARRICK, P. G., CHAPPELL, E. L., HULEGAARD, S. C., and ENGELKING, P. C. 1986, *J. chem. Phys.* **84**, 2459–2465.

[121] Foster, S. C., Misra, P., Lin, T.-Y. D., Damo, C. P., Carter, C. C., and Miller, T. A., 1988, *J. phys. Chem.*, **92**, 5914–5921.
[122] Inoue, G., Akimoto, H., and Okuda, M., 1979, *Chem. Phys. Lett.*, **63**, 213–216.
[123] Lee, Y.-Y., Wann, G.-H., and Lee, Y.-P., 1993, *J. chem. Phys.*, **99**, 9465–9471.
[124] Geers, A., Kappert, J., Temps, F., and Sears, T. J., 1993, *J. chem. Phys.* **98**, 4297–4300.
[125] Geers, A., Kappert, J., Temps, F., and Webrecht, J. W., 1994, *J. chem. Phys.*, **101**, 3618–3633.
[126] Geers, A., Kappert, J., Temps, F., and Webrecht, J. W., 1994, *J. chem. Phys.*, **101**, 3634–3648.
[127] Iwasaki, M., and Toryama, K., 1978, *J. Am. chem. Soc.*, **100**, 1964–1965.
[128] Powers, D. E., Pushkarsky, M., and Miller, T. A., 1997, *J. chem. Phys.*, **106**, 6878–6884.
[129] Osborn, D. L., Leahy, D. J., Ross, E. M., and Neumark, D. M., 1995, *Chem. Phys. Lett.*, **235**, 484–489.
[130] Osborn, D. L., Leahy, D. J., and Neumark, D. M., 1997, *J. phys. Chem.* A **101**, 6583–6592.
[131] Pushkarsky, M. B., Applegate, B., and Miller, T. A., 1998 to be published.
[132] Carter, J. T., and Cook, D. B., 1991, *Theochem* **83**, 111–122.
[133] Jackels, C. F., 1982, *J. chem. Phys.*, **76**, 505–515.
[134] Jackels, C. F., 1985, *J. chem. Phys.*, **82**, 311–322.
[135] Cui, Q., and Morokuma, K., 1996, *Chem. Phys. Lett.*, **263**, 54–62.
[136] Bent, G. D., Adams, G. F., Bartram, R. H., Purvis, G. D., and Bartlett, R. J. 1982, *J. chem. Phys.* **76**, 4144–4156.
[137] Bent, G. D., Bertram, R. H., and Rossi, A., 1984, *Molec. Phys.* **51**, 1487–1491.
[138] Cooper, D. L., 1982, *J. chem. Phys.*, **76**, 2765–2766.
[139] Momose, T., Nakatsuji, H., and Shida, T. 1988, *J. chem. Phys.*, **89**, 4185–4192.
[140] Bent, G. D., 1994, *J. chem. Phys.*, **100**, 8219–8232.
[141] Temps, F., 1995 *Adv. Ser. Phys. Chem.*, **4**, 375–431.
[142] Dertinger, S., Geers, A., Kappert, J., Wiebrecht, J., and Temps, F., 1995, *Discuss. Faraday Soc.* **102**, 31–52.
[143] Geers, A. 1993, PhD Dissertation, Universität Göttingen.